To the Graduate Council:

I am submitting herewith a thesis written by Kevin M. Fuller entitled "The Separation Dynamics of the COMET FreeFlyer and an Upper Stage STAR-48V Rocket Motor". I have examined the final copy of this thesis for form and content and recommend that it be accepted in partial fulfillment of the requirements for the degree of Master of Science, with a major in Aerospace Engineering.

R. Engels

Dr. Remi Engels, Major Professor

We have read this thesis and
recommend its acceptance:

George Hanson

Gary A. Chandler

Accepted for the Council:

Carolyn Mitchell

Associate Vice Chancellor and Dean
of the Graduate School

Statement of Permission to Use

In presenting this thesis in partial fulfillment of the requirements for a Master's degree at The University of Tennessee, Knoxville, I agree that the Library shall make it available to borrowers under rules of the Library. Brief quotations from this thesis are allowable without special permission, provided that accurate acknowledgment of the source is made.

Permission for extensive quotation from or reproduction of this thesis may be granted by my major professor, or in his absence, by the Head of Interlibrary Services when, in the opinion of either, the proposed use of the material is for scholarly purposes. Any copying or use of the material in this thesis for financial gain shall not be allowed without my written permission.

Signature _____

Date April 29, 1994

Requests for permission for extensive quotation from or reproduction of this thesis in whole or in parts may be granted by the copyright holder.

The Separation Dynamics of the COMET FreeFlyer and an Upper Stage STAR-48V Rocket Motor

A Thesis Presented for the
Master of Science Degree

The University of Tennessee Space Institute, Tullahoma

Kevin M. Fuller
May, 1994

Dedication

This thesis is dedicated to my parents,

Mr. Willard L. Fuller

and

Mrs. Dorothy A. Fuller

who have given me invaluable educational opportunities and who have encouraged my every decision. It is because of their love and guidance that I have been as successful as I have in my chosen academic pursuits. Without them, none of this could have been accomplished. Thanks.

Acknowledgments

I would like to thank my major professor, Dr. Remi Engels, for his guidance and patient understanding during the writing of this thesis. I would also like to thank the other committee members, Dr. Gary Flandro, and Dr. George Garrison, for their assistance and their constructive criticism over the past year. Without their encouragement I do not think that this thesis could have been produced. I would especially like to thank Mr. Joe Pawlick of CSTAR for giving me the opportunity to study real-world problems during my stay at CSTAR. This opportunity has given me invaluable experience that I believe will be very beneficial to me in the years to come. I would also like to thank my "Bubba's", Mr. Carter Myers and Mr. Bert Allee, for their daily interaction and for helping me through my many problems during my stay at CSTAR. Without these two individuals I would have had a very difficult time finishing my projects at both UTSI and CSTAR. I finally would like to thank my family for their ever continuing support, especially my sister Lisa, for giving me several study breaks both in Bowling Green and in Florida. None of this work could have been accomplished without any of you.

Abstract

An investigation into the separation dynamics between the COMET FreeFlyer and a STAR-48V solid rocket motor is performed in this thesis. This is accomplished by first determining the time histories of the forces and moments that are applied to the STAR-48V and the FreeFlyer. Since there is difficulty in determining these forces and moments in an inertial coordinate system, a body-fixed coordinate system is chosen so that the time histories of the forces and moments can be determined and so that the principal moments of inertia will be constant in this coordinate system. These results, as determined in the body-fixed coordinate system, are then placed into the equations of motion as described in a rotating reference frame.

The differential equations of motion for each body are then numerically integrated using a fourth order Runge-Kutta numerical integration scheme. This integration provides the translational velocity vector and the angular velocity vector of both the STAR-48V and the FreeFlyer as described in the body-fixed coordinate system. In order to determine the separation distances between the center of mass of the STAR-48V and the center of mass of the FreeFlyer, both the translational and the angular velocity vectors of both bodies are transformed into an inertial coordinate system. This is accomplished by determining the Euler angles used in a 3-1-3 Euler angle transformation and then applying this transformation to these vectors. Once this is determined, the velocity vectors, as described in an inertial reference frame, are integrated, thus providing the separation distances between the STAR-48V and the COMET FreeFlyer. From these separation distances, it can be determined if the two

bodies will collide with each other after the separation process has been initiated.

From this analysis, and some basic assumptions about the initial conditions of the STAR-48V/FreeFlyer vehicle, it is concluded that the STAR-48V will not collide with the FreeFlyer if the separation occurs at the presently designed separation delay time of 180 seconds. In fact, this separation delay time could be shorter. However, it is recommended that this separation delay time be as large as possible in order to reduce the possibility of collision.

In addition, a parametric study of the effects that different configuration variables have upon the success of the separation is conducted. From this investigation, it is concluded that the probability of any one of these variables causing a significant effect upon the success of the separation between the STAR-48V and the COMET FreeFlyer will be minimal.

With this in mind, it is concluded that the STAR-48V, as presently designed for the COMET mission, will not collide with the COMET FreeFlyer as long as a separation delay time of 180 seconds is used and as long as the STAR-48V nozzle can be gimbaled by at least 4° from its primary axis.

Table of Contents

Chapter **Page**

1. Introduction 1

    1.1 COMET Background 1

    1.2 Thesis Synopsis 7

2. The Equations of Motion for the STAR-48V and the COMET FreeFlyer 9

    2.1 Determination of Collision Distance 9

    2.2 Determination of Applied Forces 12

    2.3 Equations of Motion 19

    2.4 Assumptions for the STAR-48V/FreeFlyer Separation 22

3. Results for Current Separation Design 26

    3.1 Separation Results Using Thrust Curve Designed by Dr. Reiss in Reference #15 26

    3.2 Separation Results Using the STAR-48 #1 Thrust Curve ... 34

    3.3 Separation Results Using the STAR-48 #2 Thrust Curve ... 36

    3.4 Separation Results Using the STAR-48 #3 Thrust Curve ... 40

4. Effect on the Separation of Altering Certain Configuration Variables 46

    4.1 Effect of Separation Delay Time 46

    4.2 Effect of Nozzle Gimbal Angle 54

4.3 Effect of Roll Rate 56

4.4 Effect of Initial Wobble Rates 58

5. Conclusions 79

Bibliography 82

Appendices 85

Appendix 1 The Equations of Motion for a Rigid Body 86

Appendix 2 STAR-48 Tail-off Thrust Test Data 90

Appendix 3 Runge-Kutta Program 106

Vita 120

List of Tables

Table		Page
2.1	Mass Properties of the STAR-48V and the FreeFlyer	21
A2.1	STAR-48 #1 Test Data	92
A2.2	STAR-48 #2 Test Data	96
A2.3	STAR-48 #3 Test Data	99
A2.4	Data Developed by Dr. Reiss in Reference #15	103

List of Figures

Figure		Page
1.1	COMET Conestoga Launch Vehicle	3
1.2	COMET FreeFlyer	4
1.3	STAR-48V, PAF, and COMET FreeFlyer Vehicle Combination	6
2.1	Separation of STAR-48V/PAF with COMET FreeFlyer	10
2.2	Initial Separation Forces	14
3.1	STAR-48V Inertial Velocity With Thrust Curve Developed by Dr. Reiss in Reference #15	28
3.2	FreeFlyer Inertial Velocity With Thrust Curve Developed by Dr. Reiss in Reference #15	29
3.3	STAR-48V Inertial Angular Velocity With Thrust Curve Developed by Dr. Reiss in Reference #15	30
3.4	FreeFlyer Inertial Angular Velocity With Thrust Curve Developed by Dr. Reiss in Reference #15	31
3.5	Inertial Separation Distance With Thrust Curve Developed by Dr. Reiss in Reference #15	32
3.6	Total Inertial Separation Distance With Thrust Curve Developed by Dr. Reiss in Reference # 15	33
3.7	STAR-48V Inertial Velocity With Thrust #1 Curve	35
3.8	STAR-48V Inertial Angular Velocity With Thrust #1 Curve	37
3.9	Inertial Separation Distance With Thrust #1 Curve	38
3.10	Total Inertial Separation Distance With Thrust #1 Curve	39

3.11 Inertial Separation Distance With Thrust #2 Curve 41

3.12 Total Inertial Separation Distance With Thrust #2 Curve 42

3.13 Inertial Separation Distance With Thrust #3 Curve 43

3.14 Total Inertial Separation Distance With Thrust #3 Curve 44

4.1 Inertial Separation Distance for 180 s Separation Delay 47

4.2 Total Inertial Separation Distance for 180 s Separation Delay 48

4.3 Inertial Separation Distance for 140 s Separation Delay 50

4.4 Total Inertial Separation Distance for 140 s Separation Delay 51

4.5 Inertial Separation Distance for 100 s Separation Delay 52

4.6 Total Inertial Separation Distance for 100 s Separation Delay 53

4.7 Total Inertial Separation Distance With Variable Gimbal Angle 55

4.8 Total Inertial Separation Distance With Variable Initial Roll Rate 57

4.9 Inertial Separation Distance With Initial Wobble Rates of 0.01°/s and 0.01°/s 59

4.10 Inertial Angular Velocity of STAR-48V With Initial Wobble Rates of 0.01°/s and 0.01°/s 61

4.11 Inertial Angular Velocity of FreeFlyer With Initial Wobble Rates of 0.01°/s and 0.01°/s 62

4.12 Total Inertial Separation Distance With Initial Wobble Rates of 0.01°/s and 0.01°/s 63

4.13 Inertial Separation Distance With Initial Wobble Rates of 0.1°/s and 0.25°/s 64

4.14 Inertial Angular Velocity of STAR-48V With Initial Wobble Rates of 0.1°/s and 0.25°/s 66

4.15 Inertial Angular Velocity of FreeFlyer With Initial Wobble Rates of 0.1°/s and 0.25°/s 67

4.16 Total Inertial Separation Distance With Initial Wobble Rates of 0.1°/s and 0.25°/s 68

4.17 Inertial Separation Distance With Initial Wobble Rates of 1.0°/s and 0.9°/s 69

4.18 Inertial Angular Velocity of STAR-48V With Initial Wobble Rates of 1.0°/s and 0.9°/s 70

4.19 Inertial Angular Velocity of FreeFlyer With Initial Wobble Rates of 1.0°/s and 0.9°/s 71

4.20 Total Inertial Separation Distance With Initial Wobble Rates of 1.0°/s and 0.5°/s 72

4.21 Inertial Separation Distance With Initial Wobble Rates of -10.0°/s and 5.0°/s 74

4.22 Inertial Angular Velocity of STAR-48V With Initial Wobble Rates of -10.0°/s and 5.0°/s 75

4.23 Inertial Angular Velocity of FreeFlyer With Initial Wobble Rates of -10.0°/s and 5.0°/s 76

4.24 Total Inertial Separation Distance With Initial Wobble Rates of -10.0°/s and 5.0°/s 77

A1.1 Arbitrary Rigid body in Space 87

A2.1 STAR-48 #1 Test Data 95

A2.2 STAR-48 #2 Test Data 98

A2.3 STAR-48 #3 Test Data 102

A2.4 Thrust Curve as Designed by Dr. Reiss in Reference #15 105

Nomenclature

Arabic Symbols	Definition
B	An arbitrarily shaped body.
C	Cosine of the angle that follows this symbol.
c	The origin of the body-fixed coordinate system.
C_{48}	The maximum collision distance on the STAR-48V.
C_{ff}	The maximum collision distance on the FreeFlyer.
C_{Prog}	The minimum separation distance between the center of mass of the STAR-48V and the center of mass of the FreeFlyer when using the Runge-Kutta program data.
C_{tot}	The sum of the maximum collision distances of the STAR-48V and the FreeFlyer.
d	The moment arm of the thrust moment. This distance is measured from the STAR-48V nozzle pivot point to the center of mass of the STAR-48V.
d_c	The effective electrical connector distance.
d_s	The separation spring effective stroke length.
d_{sep}	The separation distance between the center of mass of the STAR-48V and the center of mass of the FreeFlyer.
$d( )/dt$	The time derivative of the variable within the parentheses.
$d^2( )/dt^2$	The second time derivative of the variable within the parentheses.

$\mathbf{F}$	The force vector applied to the arbitrary body.
F_c	The magnitude of the electrical connector force.
F_x, F_y, F_z	The components of the force vector in the **i**, **j**, **k** directions, respectively, as projected upon the body-fixed coordinate system.
$\mathbf{I}$	The mass moment of inertia matrix.
I, J, K	The unit vectors in the inertial coordinate system in the X, Y, and Z directions, respectively.
i, j, k	The unit vectors in the body-fixed coordinate system in the x, y, and z directions, respectively.
I_{xx}, I_{yy}, I_{zz}	The principal moments of inertia of an arbitrary body about the x, y, and z axes, respectively, as described in the body-fixed coordinate system.
K_s	The separation spring constant.
m	The total mass of an arbitrary body.
m_{48}	The total mass of the STAR-48V and the PAF vehicle combination.
m_{ff}	The mass of the COMET FreeFlyer.
m_{PAF}	The mass of the PAF.
m_{STAR}	The mass of the STAR-48V without attachments.
n	The number of separation springs.
$\mathbf{N}_c$	The moment vector about the center of mass of an arbitrary body, B.
N_{cx}, N_{cy}, N_{cz}	The components of the applied moment vector.

O	The origin of the inertial Cartesian coordinate system.
P	A point of the arbitrary body, B.
R	The inertial position vector of the arbitrary point, P.
r	The body-fixed position vector of arbitrary point, P.
R (ϕ, θ, ψ)	The 3-1-3 Euler angle transformation matrix.
$\mathbf{R}_c$	The inertial position vector of the center of mass of the arbitrary body, B.
S	Sine of the angle that follows this symbol.
t	The time after nominal burnout of the STAR-48V rocket motor.
u	Any arbitrary vector.
u_X, u_Y, u_Z	The inertial components of the arbitrary vector, **u**.
u_x, u_y, u_z	The body-fixed components of the arbitrary vector, **u**.
$\mathbf{V}_c$	The inertial velocity vector of the center of mass of the arbitrary body, B.
V_{cx}, V_{cy}, V_{cz}	The inertial components of the velocity vector, $\mathbf{V}_c$.
X, Y, Z	The inertial Cartesian coordinates of the arbitrary point, P.
x, y, z	The body-fixed Cartesian coordinates of the arbitrary point, P.

Greek Symbols	Definition
γ	The STAR-48V nozzle gimbal angle.
θ	The second Euler angle for a 3-1-3 Euler Transformation.
ψ	The third Euler angle for a 3-1-3 Euler transformation.
ϕ	The first Euler angle for a 3-1-3 Euler transformation.
ω	The angular velocity vector of an arbitrary body, B.
ω_x, ω_y, ω_z	The components of the angular velocity vector, ω.

Chapter 1: Introduction

1.1 COMET Background

The COMmercial Experiment Transporter (COMET) is a commercial space transportation and recovery system developed by a team of contractors and managers from both the private sector and NASA's Center for the Commercial Development of Space (CCDS) program. The COMET program is managed by one of the 17 different CCDS's, namely, the Center for Space Transportation and Applied Research (CSTAR) which is located at the University of Tennessee Space Institute in Tullahoma, TN. The main goal of the COMET program is to provide both reliable and cost-effective space transportation services to private industry, to the U.S. government, and also to academic research institutions (CSTAR, 1992).

The COMET FreeFlyer spacecraft, also referred to interchangeably as simply the FreeFlyer, is intended to carry experiments to a circular, low-Earth orbit and return a portion of these experiments back to Earth in the Recovery Module. The FreeFlyer has the capability of maintaining a microgravity environment for non-recoverable experiments (experiments that do not need to be returned to Earth) for up to 130 days using the Service Module. This dual capability makes the COMET FreeFlyer a unique space vehicle since it can both return experiments back to earth after a 30 day microgravity exposure period as well as expose additional experiments to the microgravity of space for an extended period of up to 130 days, all within the same

mission. With its first planned launch in the Summer of 1994, the COMET FreeFlyer will become a significant asset to the United States space community.

The COMET FreeFlyer is to be launched from the newly designed launch pad on Wallops Island in Virginia aboard the specially designed Conestoga 1620 small expendable launch vehicle. This launch vehicle was designed to place small, 1800 lb payloads into a 300 nautical-mile, low-Earth orbit for as low a cost as possible by EER Systems Corporation located in Vienna, VA. This four stage launch vehicle consists of two Castor IVA's and two Castor IVB's in the first stage, two Castor IVB's in the second stage, and a Castor IVB in the third stage. The final fourth stage consists of the payload and a STAR-48V solid rocket motor, which is used as a kick motor to circularize the intended orbit. A diagram of the Conestoga launch vehicle can be seen in Figure 1.1 and a diagram of the COMET FreeFlyer (without the STAR-48V) can be seen in Figure 1.2.

The STAR-48V solid rocket motor is a uniquely designed motor that has a thrust vectoring control system that allows the flight software and nozzle actuators to gimbal the motor nozzle in order to control the STAR-48V/FreeFlyer combination vehicle during the motor burn without the requirement of spin stabilization. Thus, the STAR-48V/FreeFlyer combination vehicle does not have to endure the rigors of spin stabilization as it is boosted into its designated orbit. This STAR-48V motor is attached to a fastening bracket known as the Payload Attach Fitting (PAF) so that it can be easily integrated with the COMET FreeFlyer. The PAF is then fastened to the FreeFlyer by the use of several explosive bolts. This connection area between the PAF

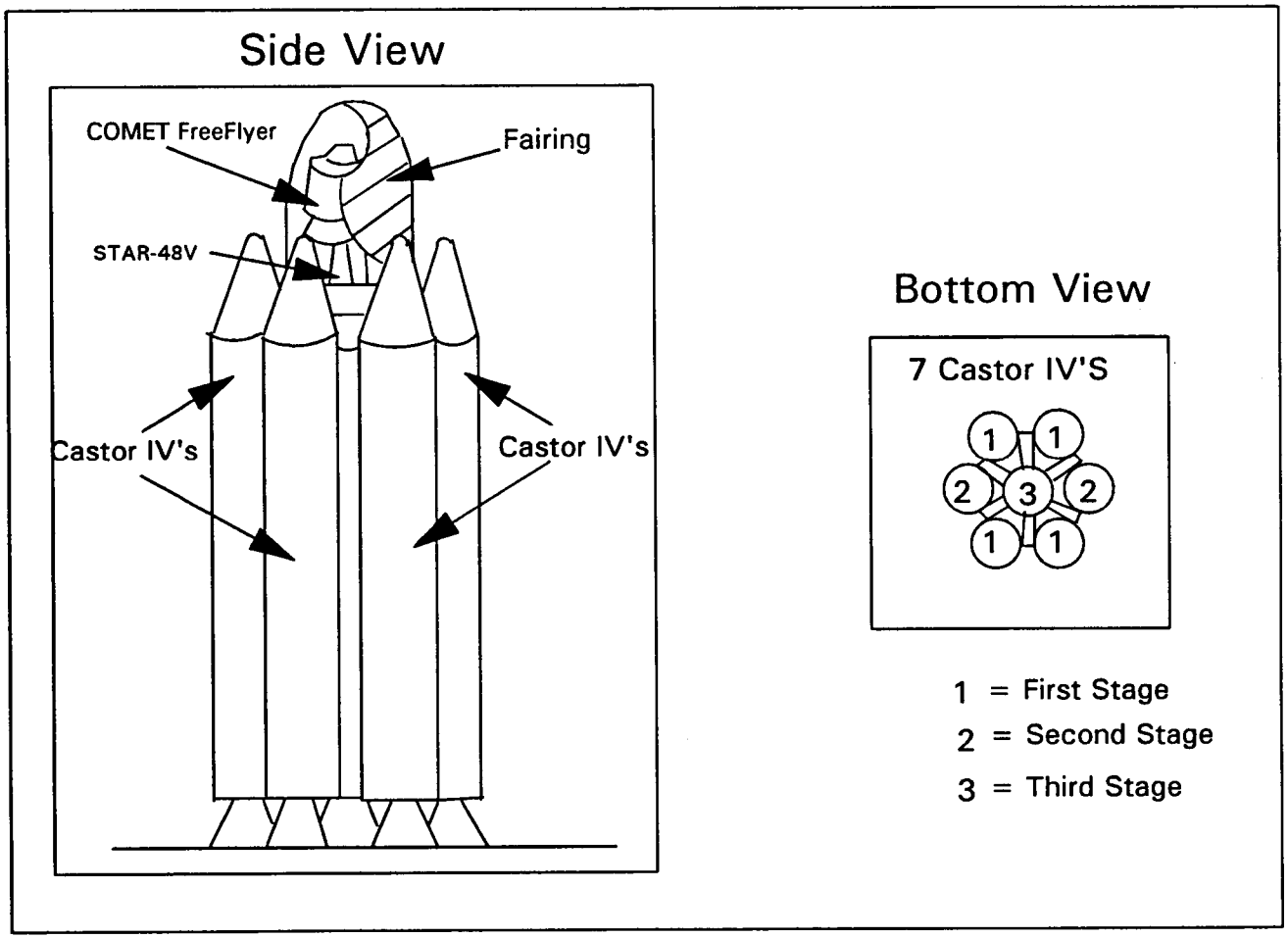


Figure 1.1 COMET Conestoga Launch Vehicle

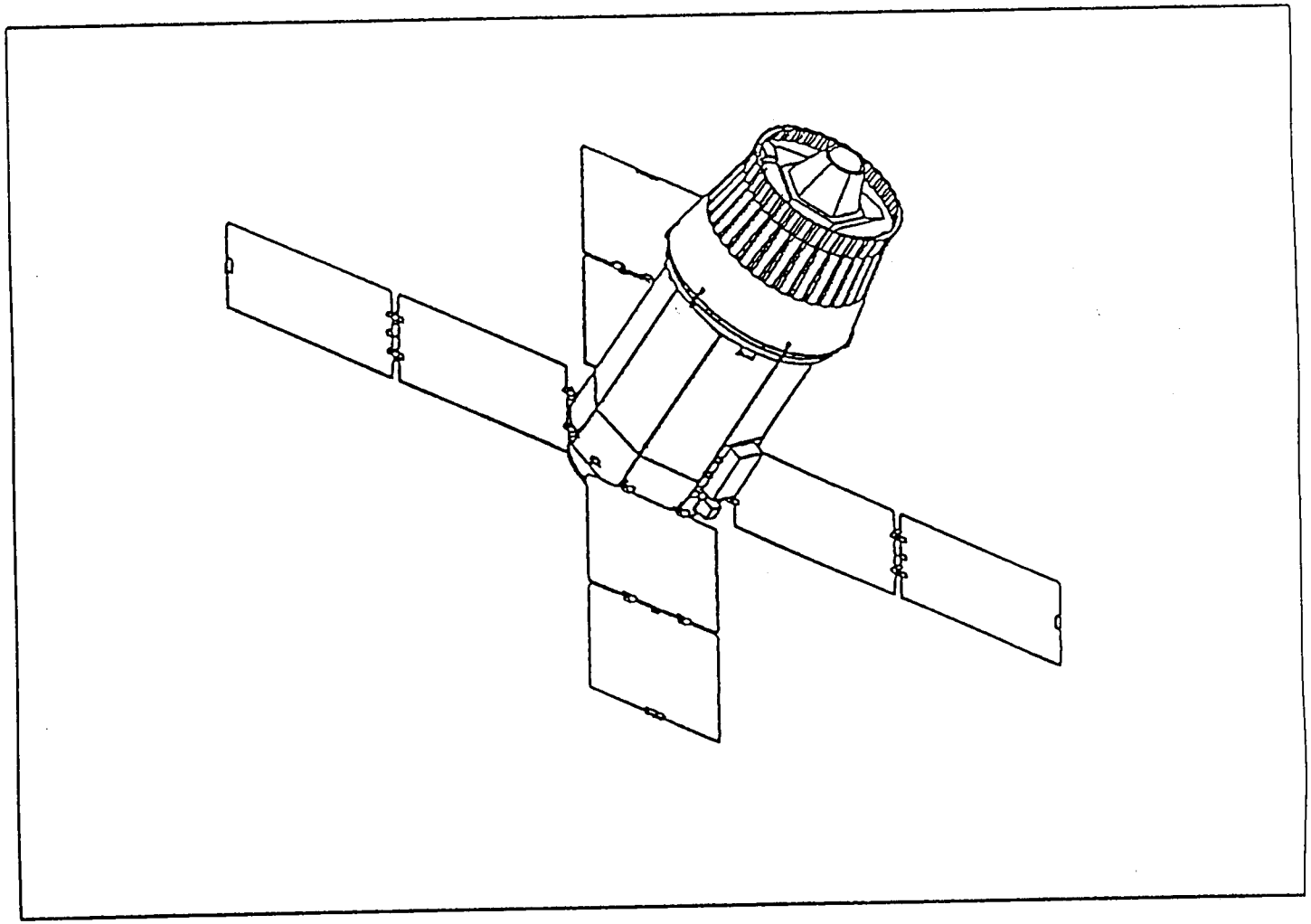


Figure 1.2 COMET FreeFlyer

(CSTAR, 1992)

and the FreeFlyer contains eight compressed separation springs that are designed to provide the necessary force to separate the STAR-48V and the PAF from the FreeFlyer once the nominal burnout time of the STAR-48V has been reached. At separation, both the STAR-48V and the COMET FreeFlyer have achieved a 250 nautical-mile, circular orbit. When the explosive bolts are fired by the flight computer at the designated time, the compressed springs uncoil and force the STAR-48V to separate from the COMET FreeFlyer. It is this situation that is to be analyzed in this thesis. A diagram of the STAR-48V, the COMET FreeFlyer, and the PAF can be seen in Figure 1.3.

At first glance this separation seems fairly straight forward. But there are two conditions that make this simple separation much more complex. The first condition, discovered during static testing of the motor, is that there is still some residual thrust being produced by the STAR-48V after the designed nominal burnout time of the motor. This unwanted thrust acts to offset the separation force provided by the springs and causes the situation where the STAR-48V now has a chance to collide with the COMET FreeFlyer. The easiest solution to this problem is to wait for all the residual fuel in the STAR-48V to burn up before initiating separation. But this cannot be done because of a time constraint created by a second condition. This second condition requires that the separation must occur no later than 180 seconds after the nominal burnout of the STAR-48V. This is due to the limited life span of the power system on-board the STAR-48V that provides power to the vehicle during this phase of the orbit. With a larger redesigned power system (and therefore a reduction in payload) the separation delay time could be increased long enough for all the propellant within the

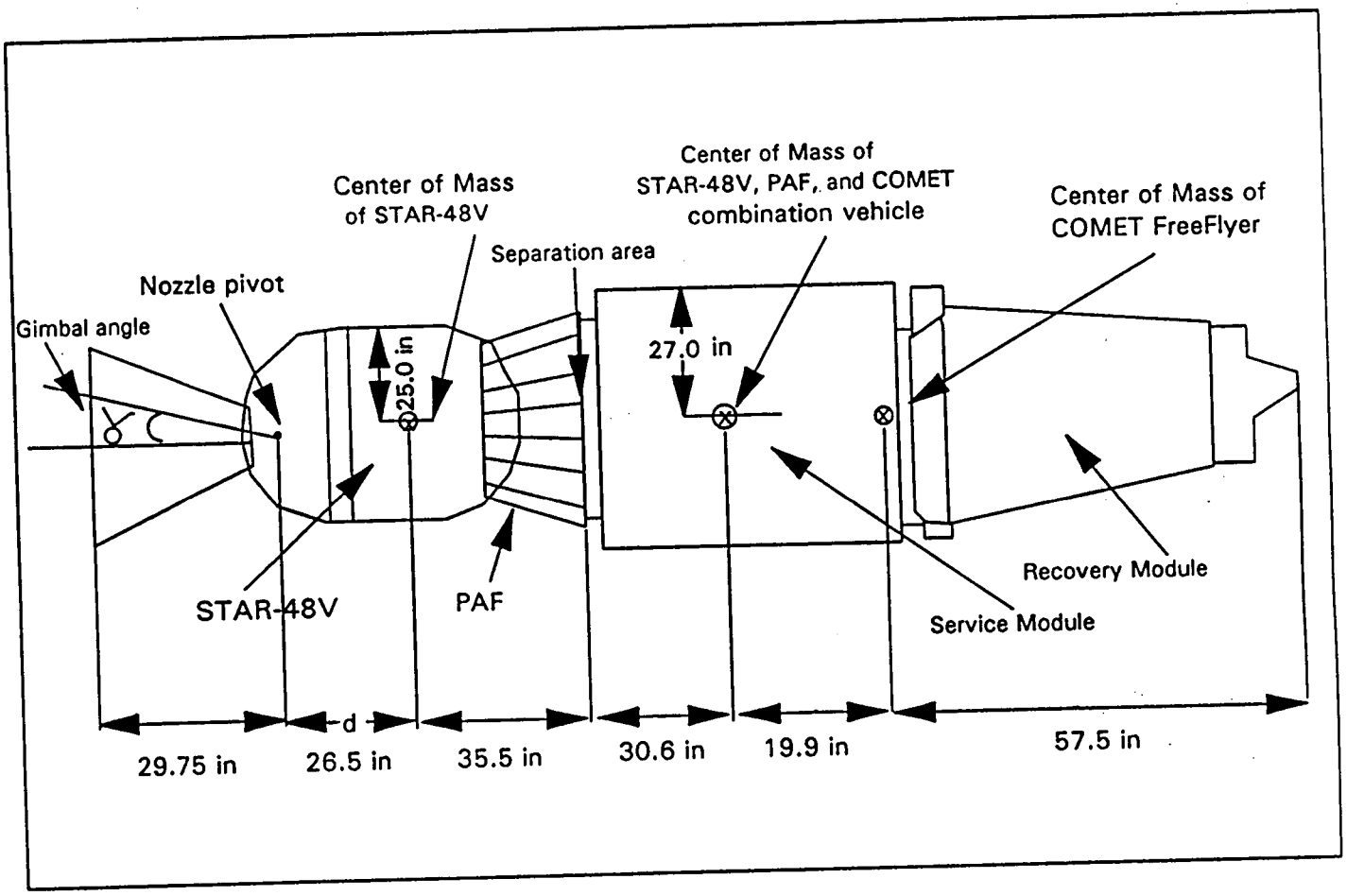


Figure 1.3 STAR-48V, PAF, and COMET FreeFlyer Vehicle Combination

STAR-48V to be consumed. But this solution is unacceptable due to the significant reduction in payload capability.

One more variable plays a significant role in the separation between the STAR-48V and the COMET FreeFlyer. That variable is the thrust vectoring capability of the motor nozzle on the STAR-48V. This thrust vectoring might be large enough to start the STAR-48V into a pin-wheeling, tumbling motion that could reduce the possibility of a collision. But if the STAR-48V acquires a large enough residual roll rate, the STAR-48V could become spin stabilized and the effects of the gimbaled nozzle might be offset. It is apparent from these circumstances that further investigation into the dynamics between these two separating bodies must be undertaken in order to determine if the STAR-48V will collide with the COMET FreeFlyer during the on-orbit separation maneuver. It is this deduction that motivates the following analysis in this thesis.

1.2 Thesis Synopsis

In Chapter 2 the basic equations listed in Appendix 1 are applied to the STAR-48V and the COMET FreeFlyer. First in Section 2.1, a minimum allowable distance between the center of mass of the STAR-48V and the center of mass of the COMET FreeFlyer is developed to determine the minimum separation distance required to insure a safe separation between these two bodies. Next, in Section 2.2, the components of the forces and moments that act upon both the STAR-48V and the FreeFlyer are determined relative to a body-fixed coordinate system. In Section 2.3, the equations of motion relative to a body-fixed coordinate system are then integrated using a fourth

order Runge-Kutta numerical integration scheme. This results in the time histories of both the translational and the angular velocities of the center of mass for both the FreeFlyer and the STAR-48V relative to the body-fixed coordinate system. The corresponding FORTRAN program is listed in Appendix 3. Also, some basic assumptions regarding the separation analysis are discussed in Section 2.4.

Chapter 3 gives the results of the separation analysis between the STAR-48V and the FreeFlyer using the nominal conditions of the COMET mission as presently designed. Also, the determination of which thrust curve to use in order to simulate the tail-off thrust characteristics of the STAR-48V motor is developed throughout this chapter. Plots of the separation are also given to show the tumbling nature of the STAR-48V during the separation. In Chapter 4, selected configuration variables are altered to determine their effects upon the success of the separation. Section 4.1 looks at the effect of the separation delay time upon the success of the separation, while Section 4.2 investigates the effect the gimbal angle of the nozzle on the STAR-48V has upon the success of the separation. Also, Section 4.3 investigates the effect the initial roll rate has upon the separation and Section 4.4 shows the effect that an initial wobble rate might have upon the separation. Finally, the conclusions obtained from this analysis are presented in Chapter 5.

Chapter 2: The Equations of Motion for the STAR-48V and the COMET FreeFlyer

2.1 Determination of Collision Distance

The mathematical model will now be formulated so that the differential equations of motion can be determined. These equations of motion will then be solved using a Runge-Kutta numerical integration scheme with appropriate boundary conditions. The system under consideration is the COMET FreeFlyer (with its experimental payloads), the Payload Attach Fitting (PAF), and a STAR-48V solid rocket motor as shown in Figure 1.3. At the starting point of this analysis, the STAR-48V is attached to the PAF, which is in turn attached to the COMET FreeFlyer by pyrotechnic bolts. This entire system is at the orbit injection point of its intended 250 nautical-mile, circular orbit where the STAR-48V has just achieved nominal burnout.

After orbit insertion, there is a delay period between the time of the STAR-48V nominal burnout and the time of the separation between the STAR-48V (along with the PAF) and the COMET FreeFlyer. A diagram of this separation is shown in Figure 2.1. The separation delay time is presently designed to be 180 seconds for the current COMET mission, but other delay times will be investigated later in Chapter 4 and the effect the separation delay time has upon the separation will be evaluated. After the separation process has been initiated, it then must be determined whether or not the STAR-48V will collide with the COMET FreeFlyer. This is done by tracking the center of mass of both the FreeFlyer and the STAR-48V and determining if these two

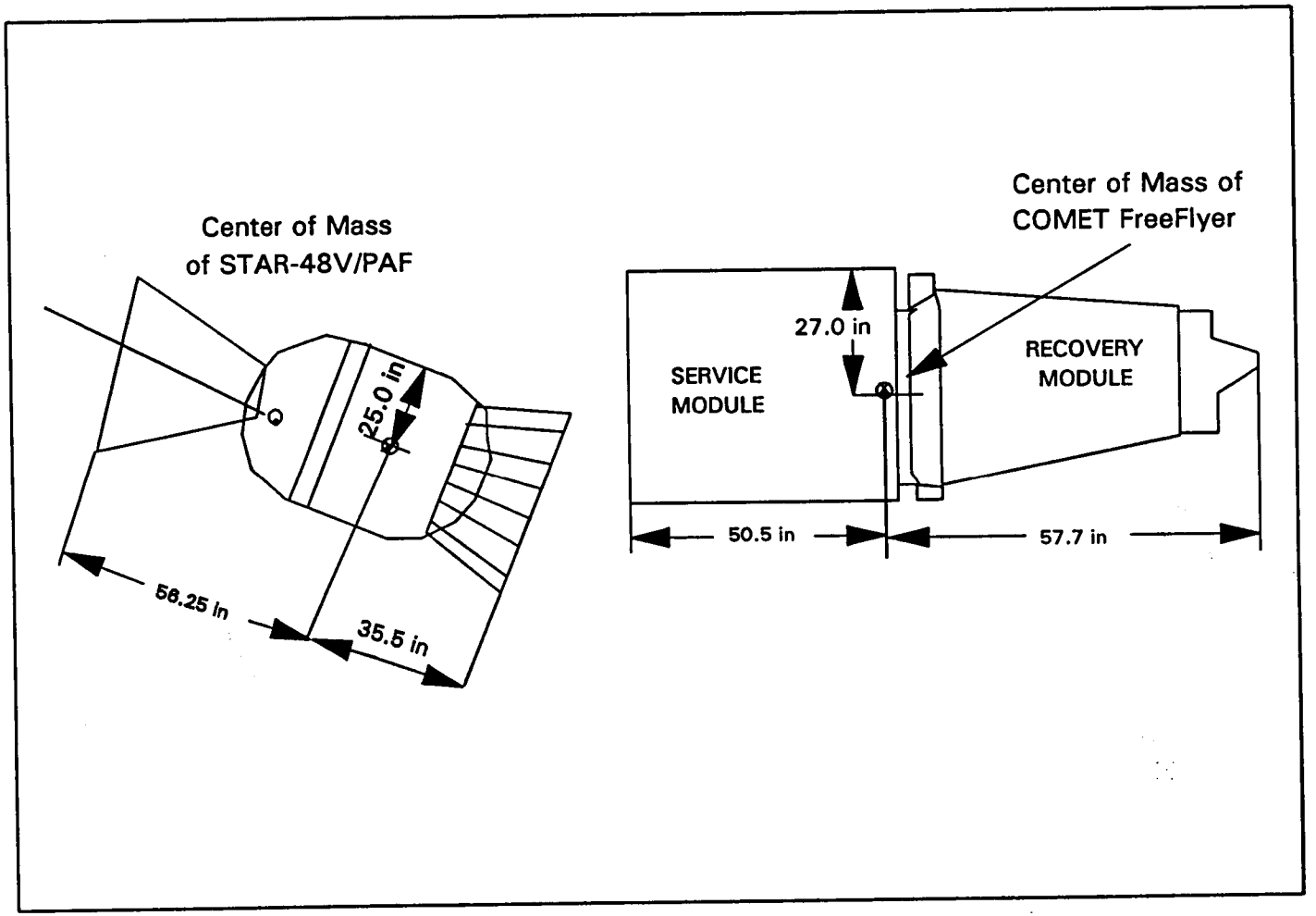


Figure 2.1 Separation of STAR-48V/PAF With COMET FreeFlyer

bodies will approach each other too closely or not. If they do, it can be assumed that there is a collision between the STAR-48V and the FreeFlyer and that the separation is not successful.

To collide, the outer surfaces of the two bodies must actually come in contact with each other. The solution of the equations of motion determine the positions of the center of mass of the STAR-48V and the COMET FreeFlyer individually. It does not determine the position of all points on either the STAR-48V or the FreeFlyer. Thus, a worst case approach will be taken as a minimum distance for collision. Since the STAR-48V spins about its center of mass, the worst case distance for determining the minimum collision distance would be the largest distance from the center of mass of the STAR-48V. By taking the largest dimension in all three directions for the STAR-48V, a very conservative measure for the collision distance of the STAR-48V can be determined. Since the STAR-48V is symmetric about the X-axis and from the dimensions as seen in Figure 2.1, the maximum collision radius can be seen to be

$$C_{48} = 56.25\ \mathbf{I} + 25.0\ \mathbf{J} + 25.0\ \mathbf{K}\ \text{(inches)}. \tag{2.1}$$

The resultant collision distance for the STAR-48V is then determined to be

$$C_{48} = 66.4\ \text{inches} = 5.54\ \text{feet}. \tag{2.2}$$

Similarly for the COMET FreeFlyer, the worst case collision distance can be determined from the dimensions of the FreeFlyer as seen in Figure 2.1. Again taking a very conservative approach and knowing that the FreeFlyer is symmetric about the X-axis, the maximum collision radius can be seen to be

$$C_{ff} = 57.7\ \mathbf{I} + 27.0\ \mathbf{J} + 27.0\ \mathbf{K}\ \text{(inches)}. \tag{2.3}$$

The resultant collision distance for the FreeFlyer is then determined to be

$$C_{ff} = 69.2 \text{ inches} = 5.77 \text{ feet.} \quad (2.4)$$

Thus the minimum allowable distance between the STAR-48V and the FreeFlyer is the sum of these two collision distances, which is

$$C_{tot} = 66.4 + 69.2 = 135.6 \text{ inches} = 11.3 \text{ feet.} \quad (2.5)$$

From Figure 2.1, it can be seen that the initial distance between the center of mass of the STAR-48V and the FreeFlyer is 86.0 inches. For convenience in the Runge-Kutta position tracking program, it is assumed that the initial distance between the center of mass of these two bodies is 0. Thus the minimum collision distance for the data determined in this Runge-Kutta program will be 86.0 inches less than C_{tot}. That is

$$C_{Prog} = 135.6 - 86.0 = 49.6 \text{ inches} = 4.13 \text{ feet} \approx 5 \text{ feet.} \quad (2.6)$$

This means that the center of mass of the STAR-48V must remain at least 5 feet from the center of mass of the FreeFlyer (as determined using the Runge- Kutta numerical scheme) at all times after the initial separation has begun in order for there to be a safe separation. This value for C_{Prog} will be the value used when determining whether or not there is a collision between the STAR-48V and the FreeFlyer throughout the remainder of this thesis.

2.2 Determination of Applied Forces

In order to determine the positions of the center of mass of both the STAR-48V and the FreeFlyer, the forces that act upon each body must be determined as a function

of time. The forces and moments that act upon the STAR-48V and the FreeFlyer initially during the separation is shown in Figure 2.2. There are three forces and one moment that act upon the STAR-48V, but there are only two forces that act upon the FreeFlyer. The forces on the STAR-48V are due to the separation spring system that contains eight separation springs, a male-female electrical connector that must be pulled apart, and the tail-off thrust of the STAR-48V. When the nozzle on the STAR-48V is gimbaled, the thrust force acts both in the +x direction and the -y direction initially as seen in a body-fixed coordinate system. The separation spring force acts over a limited distance in the -x direction and forces the STAR-48V away from the FreeFlyer, while the electrical connector force acts in the +x direction on the FreeFlyer over a different, but very similar, limited distance. There also is an additional moment caused by the off-axis thrust force once the nozzle on the STAR-48V has been gimbaled. This moment causes the STAR-48V to pin-wheel around the z-axis of the body-fixed coordinate system.

Furthermore, there also will be an initial roll rate for both the STAR-48V and the FreeFlyer so that the direction of the gimbaled nozzle is not constant as seen in an inertial frame. It has been determined by Mr. Mark Daniels of EER Corporation located in Vienna, VA, that the maximum expected initial roll rate of the STAR-48V/FreeFlyer combination is 0.5 °/s. This is the value that will be used as a baseline roll rate, but others will be looked at in Chapter 5 and the effect the initial roll rate has upon the separation between the FreeFlyer and the STAR-48V will be determined. This initial roll and the gimbaled nozzle causes the STAR-48V to spin out of the XY

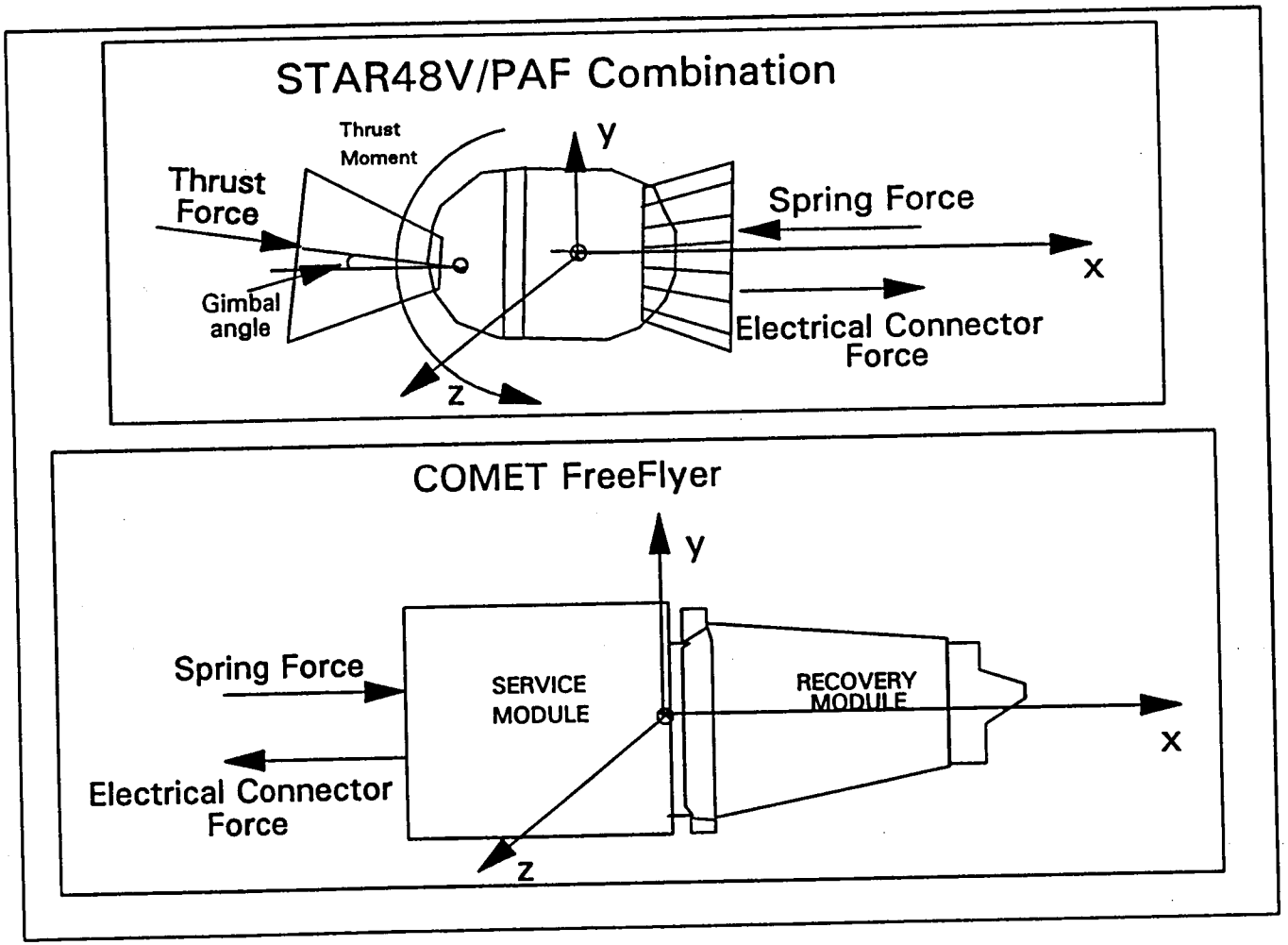


Figure 2.2 Initial Separation Forces

plane and this causes a tumble to be initiated. It can be seen that neither the thrust force nor the thrust moment can be described in the inertial coordinate system as one steps forward in time due to this tumble. As an alternative, it is simple to describe both the thrust force and the thrust moment in the body-fixed coordinate system, cxyz, as described in Appendix 1.

From the force diagram in Figure 2.2, it can be seen that the forces on the COMET FreeFlyer are much simpler than on the STAR-48V and it can be seen that there is no induced moment. The two forces on the FreeFlyer are due to the eight separation springs and the male-female electrical connector. There is no problem describing these forces in either an inertial coordinate system or a body-fixed coordinate system. But it is the thrust force on the STAR-48V that determines the best coordinate system in which to describe the applied forces and moments. Since the forces on the STAR-48V are more easily described in a body-fixed coordinate system, the forces acting on the FreeFlyer will also be described in the body-fixed coordinates. The equations used to determine the values for the spring and the connector forces were determined by Dr. Keith Reiss of EER Corporation located in Vienna, Virginia and are listed below (Reiss, 1992).

$$\text{Spring force} \quad \begin{cases} = n K_s (d_s - d_{sep}) & \text{for } d_{sep} < d_s \\ = 0 & \text{for } d_{sep} > d_s \end{cases} \tag{2.7}$$

$$\text{Connector force} \quad \begin{cases} = F_c & \text{for } d_{sep} > d_c \\ = 0 & \text{for } d_{sep} < d_c. \end{cases} \tag{2.8}$$

In these equations, n is the number of separation springs, K_s is the separation spring constant, d_s is the separation spring effective stroke length, d_{sep} is the separation

distance between the STAR-48V and the FreeFlyer, F_c is the electrical connector force, and d_c is the electrical connector length. From experimentation performed by Dr. Keith Reiss, F_c was found to be 20 lbs, and d_c was found to be 0.2 inches (Reiss, 1992). Once the separation distance between the STAR-48V and the FreeFlyer is greater than the electrical connector action distance, d_c, there is no longer a connector force acting upon either the STAR-48V or the FreeFlyer. A similar situation arises in the spring force where there is no longer a spring force acting upon either body once the STAR-48V has separated a distance greater than the spring effective stroke length, d_s. This spring effective stroke length, d_s, is 1.3 inches for each of the eight separation springs placed symmetrically around the ring attachment of the PAF. Also, the spring constant for each of these springs, K_s, is 180 lbf/in. These forces act in equal and opposite directions along the x-axis during the initial separation. Thus the spring force acts in the -x direction on the STAR-48V and it acts in the +x direction on the FreeFlyer. The electrical connector force acts in the +x direction on the STAR-48V and it acts in the -x direction on the FreeFlyer. This can be seen in the free-body diagram in Figure 2.2. In this situation, the spring force acts to separate the two bodies and the connector force acts to hinder the separation between these two bodies.

The final applied force in this separation situation is the thrust force of the STAR-48V. This thrust force acts throughout the entire time frame of the separation under consideration, but it only acts upon the STAR-48V. Again, this can be observed in Figure 2.2. At the instant the pyrotechnic bolts are fired and the separation process has been initiated, the actuators on the STAR-48V gimbal the nozzle from its nominal

burnout position of 0° to its separation position of 4°. This causes the thrust of the STAR-48V to no longer act only in the +x direction. Instead, there is an additional force that initially acts in the -y direction and this thrust force also produces a moment about the z-axis that eventually causes the STAR-48V to pin-wheel about its center of mass.

There has been much discussion as to the equation that will accurately predict the tail-off characteristics of the STAR-48V. Thus several different equations for the tail-off thrust will be used to model the thrust in this thesis. The first equation that will be investigated is the equation developed by Dr. Keith Reiss of EER Corporation from the STAR-48V static test data (Reiss, 1992),

$$\text{Thrust force \#1} = 44.275\, e^{-0.020932\, t} \tag{2.9}$$

where t is the time since the nominal burnout of the STAR-48V in seconds.

Since the STAR-48V motor is very similar to the regular STAR-48 motor, the tail-off pressures of three different static test firings at Arnold Engineering Development Center, (AEDC) located in Tullahoma, Tennessee were collected by Mr. Billy Philpott of AEDC. From this data, the tail-off thrust characteristics of the STAR-48V could be determined assuming that the tail-off pressure of the STAR-48 is very similar to the tail-off pressure of the STAR-48V, which is a reasonable deduction since the only difference between these two motors is the thrust vectoring control system on-board the STAR-48V. This data can be observed in Appendix 2 along with the curve fits that were used to obtain the following equations. Equation (2.10) is the resulting thrust equation using the STAR-48 #1 test motor data, equation (2.11) is the resulting

thrust equation using the STAR-48 #2 test motor data, and equation (2.12) is the resulting thrust equation using the STAR-48 #3 test motor data.

$$\text{Thrust force \#1} = 55.051\, e^{-0.010880\, t} \tag{2.10}$$

$$\text{Thrust force \#2} = 107.97\, e^{-0.019271\, t} \tag{2.11}$$

$$\text{Thrust force \#3} = 79.449\, e^{-0.015189\, t} \tag{2.12}$$

The effects of the uncertainty of the tail-off thrust equation on the separation between the STAR-48V and the FreeFlyer is discussed later in Chapter 3 where all four equations are used to simulate the tail-off thrust of the STAR-48V motor. At this point, it is sufficient to assume that the STAR-48V produces an exponentially decaying thrust at the time of the initial separation.

Because the nozzle on the STAR-48V is gimbaled, this thrust force is broken up into component form as determined by the gimbal angle, γ, of the nozzle. Thus the thrust force acting in the +x direction (as described in body-fixed coordinates) is given by equation (2.13) and the thrust force acting in the -y direction is given by equation (2.14).

$$\text{Thrust}_x = \text{Thrust force x Cos } \gamma. \tag{2.13}$$

$$\text{Thrust}_y = \text{-Thrust force x Sin } \gamma. \tag{2.14}$$

This thrust force also causes a moment once the nozzle has been gimbaled. From Figure 1.3, it can be observed that the moment arm of the thrust force is the distance from the nozzle pivot point to the center of mass of the STAR-48V. This distance is given by d and it is equal to 26.5 inches Thus the equation for the thrust moment about the z-axis is given by equation (2.15).

$$\text{Thrust Moment} = d \times \text{Thrust force} \times \sin\gamma. \tag{2.15}$$

It is assumed that these are the only forces acting upon the STAR-48V and the FreeFlyer throughout the analysis in this thesis.

2.3 Equations of Motion

Now that the applied forces and moments acting upon the STAR-48V and the FreeFlyer are determined, they can be integrated via a Runge-Kutta numerical integration scheme to determine the position of the center of mass of each body. Equations (A1.1) and (A1.2) of Appendix 1 are repeated here.

$$\mathbf{F} = m\, d^2(\mathbf{R}_c)/dt^2 \tag{A1.1}$$

$$\mathbf{N}_c = \mathbf{I}\, d(\omega)/dt + \omega \times \mathbf{I}\omega \tag{A1.2}$$

These equations can be used to describe the motion of both the STAR-48V and the COMET FreeFlyer. The first step is to project the vector equation (A1.2) onto the body-fixed axes, cxyz,

$$\begin{aligned} N_{cx} &= I_{xx}\, d(\omega_x)/dt + (I_{zz} - I_{yy})\, \omega_y\omega_z \\ N_{cy} &= I_{yy}\, d(\omega_y)/dt + (I_{xx} - I_{zz})\, \omega_z\omega_x \\ N_{cz} &= I_{zz}\, d(\omega_z)/dt + (I_{yy} - I_{xx})\, \omega_x\omega_y. \end{aligned} \tag{2.16}$$

For the STAR-48V these equations become

$$\begin{aligned} d(\omega_x)/dt &= ((I_{yy} - I_{zz}) / I_{xx})\, \omega_y\omega_z \\ d(\omega_y)/dt &= ((I_{zz} - I_{xx}) / I_{yy})\, \omega_z\omega_x \\ d(\omega_z)/dt &= ((I_{xx} - I_{yy}) / I_{zz})\, \omega_x\omega_y + \text{Thrust moment} / I_{zz} \end{aligned} \tag{2.17}$$

and for the COMET FreeFlyer, equation (2.16) becomes

$$d(\omega_x)/dt = ((I_{yy} - I_{zz}) / I_{xx})\ \omega_y\omega_z$$

$$d(\omega_y)/dt = ((I_{zz} - I_{xx}) / I_{yy})\ \omega_z\omega_x \qquad (2.18)$$

$$d(\omega_z)/dt = ((I_{xx} - I_{yy}) / I_{zz})\ \omega_x\omega_y.$$

The appropriate principal moments of inertia for both the STAR-48V and the COMET FreeFlyer can be found in Table 1. Equation (2.17) and equation (2.18) can now be integrated via a Runge-Kutta routine to yield the time history of the angular velocity vector, ω, for both the STAR-48V and the COMET FreeFlyer.

Now consider equation (A1.1), which can be written as

$$\mathbf{F} = m\ d(\mathbf{V}_c)/dt, \qquad \mathbf{V}_c = d(\mathbf{R}_c)/dt \qquad (2.19)$$

where $\mathbf{V}_c$ is the absolute velocity vector of the center of mass, c. Because the force, F, is expressible only in the body-fixed system, it is necessary to project equation (2.19) onto the body-fixed axes. Therefore, the absolute velocity vector also must be projected onto the body axes.

$$\mathbf{V}_c = V_{cx}\,\mathbf{i} + V_{cy}\,\mathbf{j} + V_{cz}\,\mathbf{k} \qquad (2.20)$$

Thus, the time rate of change, $d(\mathbf{V}_c)/dt$, of $\mathbf{V}_c$ as seen by an absolute observer but with $\mathbf{V}_c$ expressed in body-fixed coordinates is

$$\{d(\mathbf{V}_c)/dt\}_A = \{d(\mathbf{V}_c)/dt\}_R + \omega \times \mathbf{V}_c \qquad (2.21)$$

where $\{d(\mathbf{V}_c)/dt\}_R$ is the time rate of change of the absolute velocity, $\mathbf{V}_c$, as seen by a relative observer attached to the body-fixed axes. Thus equation (A1.1) becomes

$$\{d(\mathbf{V}_c)/dt\}_R = \mathbf{F}/m - \omega \times \mathbf{V}_c \qquad (2.22)$$

Projecting equation (2.22) onto cxyz yields

Table 2.1 Mass Properties of the STAR-48V and the FreeFlyer

Parameter		Symbol	Value	Units
STAR-48V	Mass	m_{STAR}	10.88	Slugs
	Roll Inertia	I_{xx}	22.02	Slug*ft^2
	Pitch Inertia	I_{yy}	35.49	Slug*ft^2
	Yaw Inertia	I_{zz}	35.51	Slug*ft^2
PAF	Mass	m_{PAF}	6.98	Slugs
	Roll Inertia	I_{xx}	15.00	Slug*ft^2
	Pitch Inertia	I_{yy}	24.10	Slug*ft^2
	Yaw Inertia	I_{zz}	22.00	Slug*ft^2
STAR-48V/ PAF Combination	Mass	m_{48}	17.86	Slugs
	Roll Inertia	I_{xx}	37.02	Slug*ft^2
	Pitch Inertia	I_{yy}	59.59	Slug*ft^2
	Yaw Inertia	I_{zz}	57.51	Slug*ft^2
COMET FreeFlyer	Mass	m_{ff}	59.82	Slugs
	Roll Inertia	I_{xx}	142.84	Slug*ft^2
	Pitch Inertia	I_{yy}	550.76	Slug*ft^2
	Yaw Inertia	I_{zz}	550.17	Slug*ft^2

$$d(V_{cx})/dt = F_x/m - \omega_y V_{cz} + \omega_z V_{cy}$$
$$d(V_{cy})/dt = F_y/m - \omega_z V_{cx} + \omega_x V_{cz} \quad (2.23)$$
$$d(V_{cz})/dt = F_z/m - \omega_x V_{cy} + \omega_y V_{cx}$$

These equations are now applied to both the STAR-48V and the COMET FreeFlyer. From the solution of equation (2.18) and equation (2.23), both the translational velocity and the angular velocity of both the STAR-48V and the FreeFlyer, as projected upon the body-fixed coordinate system, are known. In order to determine the separation distance between the center of mass of the STAR-48V and the center of mass of the FreeFlyer, the translational velocity vector and the angular velocity vector of both the STAR-48V and the FreeFlyer need to be projected onto the inertial coordinate system. This transformation is accomplished using the transpose of equation (A1.6) as shown in Appendix 1. Once these velocity vectors are known relative to the inertial coordinate system, they can be integrated to determine the position vector of both the center of mass of the STAR-48V and the center of mass of the FreeFlyer as described in the inertial coordinate system. From this position vector, it can be determined if there will be a collision between the COMET FreeFlyer and the STAR-48V.

2.4 Assumptions for the STAR-48V/FreeFlyer Separation

But before this potential collision can be investigated, there are a few assumptions that must be made in order to start the above analysis. One of the assumptions used in this thesis is that the nozzle on the STAR-48V can be initially gimbaled in an upwards direction aligned with the body-fixed y axis by at least 4°. It

has been determined by the manufacturers of the STAR-48V, Thiokol Corporation, that the maximum gimbal angle the nozzle on the STAR-48V can achieve is 4° in any direction. The initial direction alignment along the y axis is needed in order to give the nozzle gimbal an initial orientation. Also, the gimballing of the nozzle is assumed to occur instantaneously after the STAR-48V and the FreeFlyer are no longer in contact and they have moved a safe distance away from each other in order to avoid re-contact due to the pin-wheeling STAR-48V. This safe distance for separation can be determined from the geometry of both the STAR-48V and the FreeFlyer. From Figure 2.1, it can be seen that this distance is the x distance from the center of mass of the STAR-48V to the outer most portion of the PAF, subtracted from the radial distance from the center of mass of the STAR-48V to the outer most portion of the PAF. This is given in equation (2.24)

$$\text{Safe Distance} = 43.4 - 35.5 = 7.9 \text{ inches} = 0.658 \text{ feet} \qquad (2.24)$$

Under normal separation conditions, the thrust moment is relatively small as compared to the moment required to quickly spin the STAR-48V. Thus the separation distance between the STAR-48V and the FreeFlyer will be much larger than 7.9 inches before the thrust moment can cause the STAR-48V to pin-wheel about its z axis and bump into the FreeFlyer immediately after the pyrotechnic bolts are fired. Only for very large gimbal angles or for very short separation delay times would this "initial bumping" problem need further investigation.

The mass properties of both the STAR-48V and the FreeFlyer are also assumed to be constant throughout the entire separation time frame under consideration. It can

be seen in Appendix 2 that this is not entirely true since about 5 lbs of propellant is burned up in the STAR-48V motor during the time frame under consideration. But this change in mass is relatively small in comparison to the total mass of 377 lbs for the STAR-48V, as was seen in Table 2.1. Thus it was determined that this assumption would lead to very small errors that are not worth considering in the analysis presented in this thesis. Also, the position of the center of mass of the STAR-48V is assumed to be constant throughout the analysis. Again, this change is so small that it will have a very small effect on the separation between the STAR-48V and the FreeFlyer.

For the present analysis, it has been assumed that there are 8 separation springs and that each of these springs has an effective stroke length of 1.3 inches It is also assumed that the energy imparted to the STAR-48V due to the separation springs will be half of the total potential energy stored in the separation spring system. Likewise, the energy imparted to the FreeFlyer, due to the separation springs, will also be half of the total potential energy stored in the separation spring system. The value used for the spring force is determined from the theoretical linear spring equation. Since a real spring does not adhere exactly to this equation and to account for friction and imbalance irregularities due to the spring housing, a spring multiplier, SM, of 0.9 was used for the force of the separation springs used in this thesis. Thus, only 90% of the expected separation force due to the separation springs system will be used in this analysis. This acts as a factor of safety and by using this spring multiplier in the theoretical analysis, a greater assurance of a safe separation for the actual mission can be achieved.

Finally, it is also assumed that the initial pitch and yaw rates of both the STAR-48V and the FreeFlyer are 0. This may not be the case due to the unsymmetrical forces that are inevitably applied to both the STAR-48V and the FreeFlyer by the separation spring system. While it is expected that these wobble rates will be small at separation, arbitrarily large rates will be analyzed in Chapter 4 in order to observe their effect upon the success of the separation.

Chapter 3: Results for Current Separation Design

3.1 Separation Results Using Thrust Curve Designed by Dr. Reiss in Reference #15

It is apparent from the previous discussion in Chapter 3 that the separation between the STAR-48V and the COMET FreeFlyer needs a more in-depth study. It would be best to wait until the STAR-48V is no longer producing thrust before initiating the separation, but this is not possible due to the limited life of the on-board power system attached within the security of the PAF. The power system as currently designed allows for only a 180 second delay after the STAR-48V has reached its nominal burnout. This power system must power the avionics of the launch vehicle and this system is operated continuously from the time of launch until the designated separation time. Thus the analysis presented in this thesis will target this separation delay time, knowing that if the separation is successful for this delay time, that a longer delay time, if a larger power source was to be provided, would also be successful due to the exponentially decaying thrust characteristics of the STAR-48V. A configuration with a 4° nozzle gimbal angle and an initial roll rate of 0.5 deg/s will be used as the baseline configuration as discussed in Section 3.4.

First, it is necessary to determine which of the four thrust curves to use as a baseline configuration. That will be accomplished by using each of the thrust curves in the solution algorithm and determining which one gives a worse case separation scenario. The first thrust curve to be investigated is the one developed by Dr. Reiss

and is given by equation (2.9). Figures 3.1 through 3.6 show the results of this separation. Figure 3.1 shows the velocity of the center of mass of the STAR-48V as measured in the inertial coordinate system. This shows that the STAR-48V travels in the -X direction during the entire separation time frame and that it also travels in both the +Y and the +Z directions. Since the velocity of the STAR-48V for this particular thrust curve lies only in the -X direction, there is no possibility for a collision with the FreeFlyer at this separation delay time since there is not enough thrust at separation to offset the initial separation velocity created by the separation spring system. Figure 3.2 shows a similar plot of the velocity of the center of mass of the FreeFlyer. In this diagram it can be observed that the FreeFlyer travels in the +X direction only and that it does not move in either the Y or the Z direction. Since the thrust force does not act upon the FreeFlyer, the separation velocity of the FreeFlyer will not be affected by the magnitude of the thrust force. Thus this curve also acts as the velocity of the center of mass of the FreeFlyer for all of the thrust curves that will be investigated later in this chapter.

Figure 3.3 shows the angular velocity of the STAR-48V as measured in the inertial coordinate system. From this figure, the tumbling nature of the STAR-48V can be observed. The FreeFlyer, on the other hand, experiences only the initial roll rate and does not go through this tumbling motion. This can be observed in Figure 3.4. Again, the thrust force has no effect on the angular velocity of the FreeFlyer and therefore Figure 3.4 acts as the angular velocity of the FreeFlyer for all of the thrust curves that will be investigated later in this chapter.

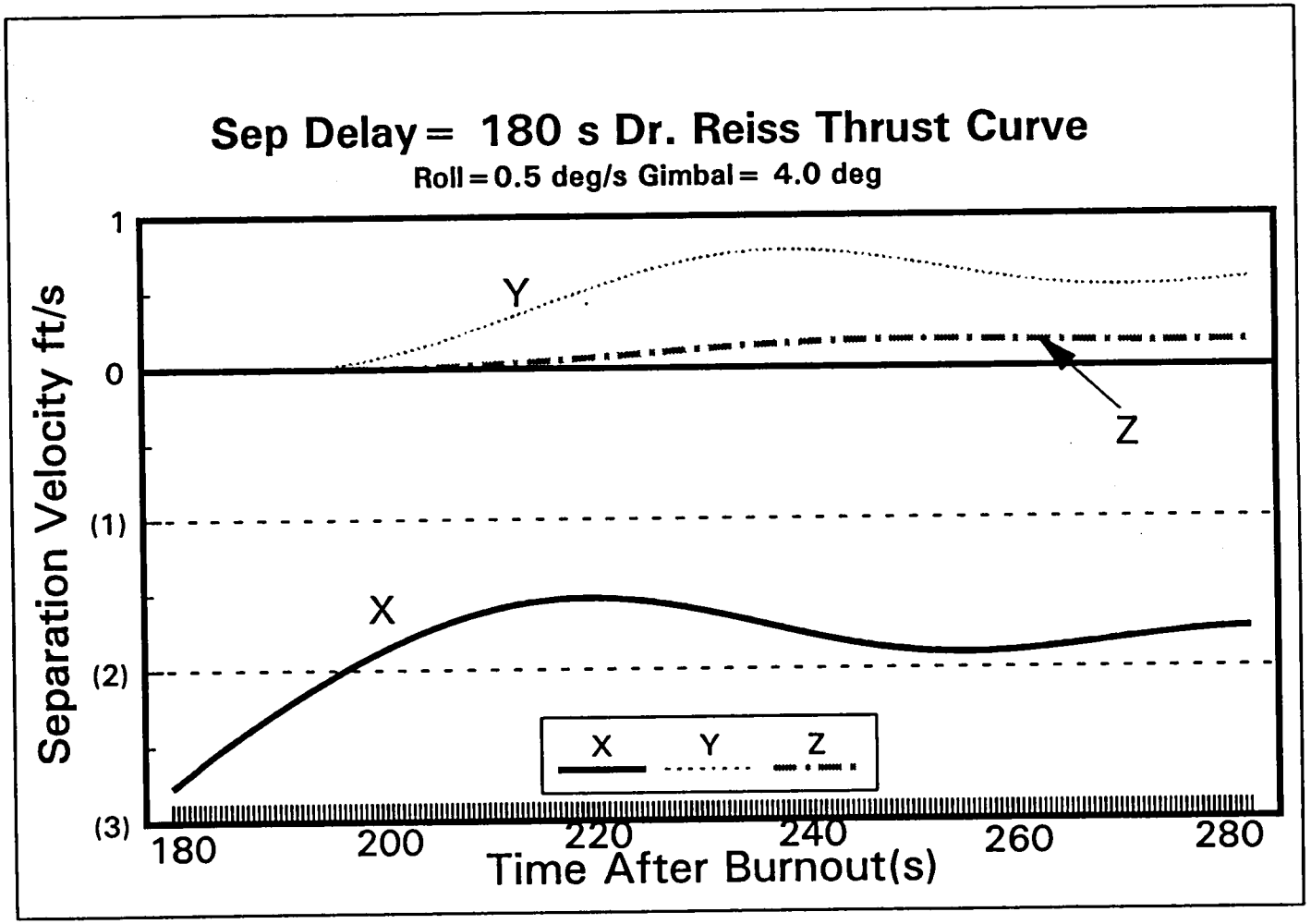


Figure 3.1 STAR-48V Inertial Velocity With Thrust Curve Developed by Dr. Reiss in Reference #15

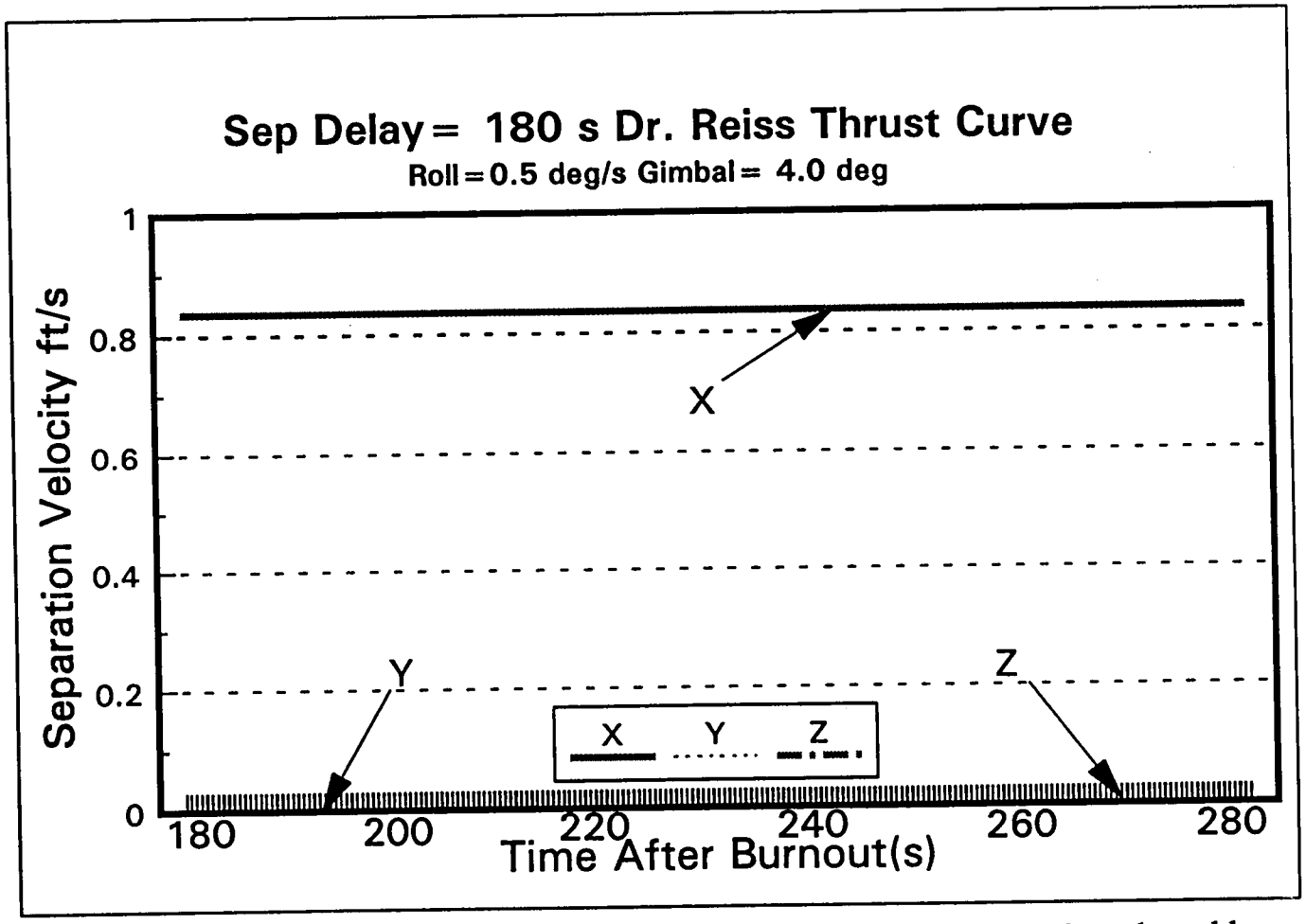


Figure 3.2 FreeFlyer Inertial Velocity With Thrust Curve Developed by Dr. Reiss in Reference #15

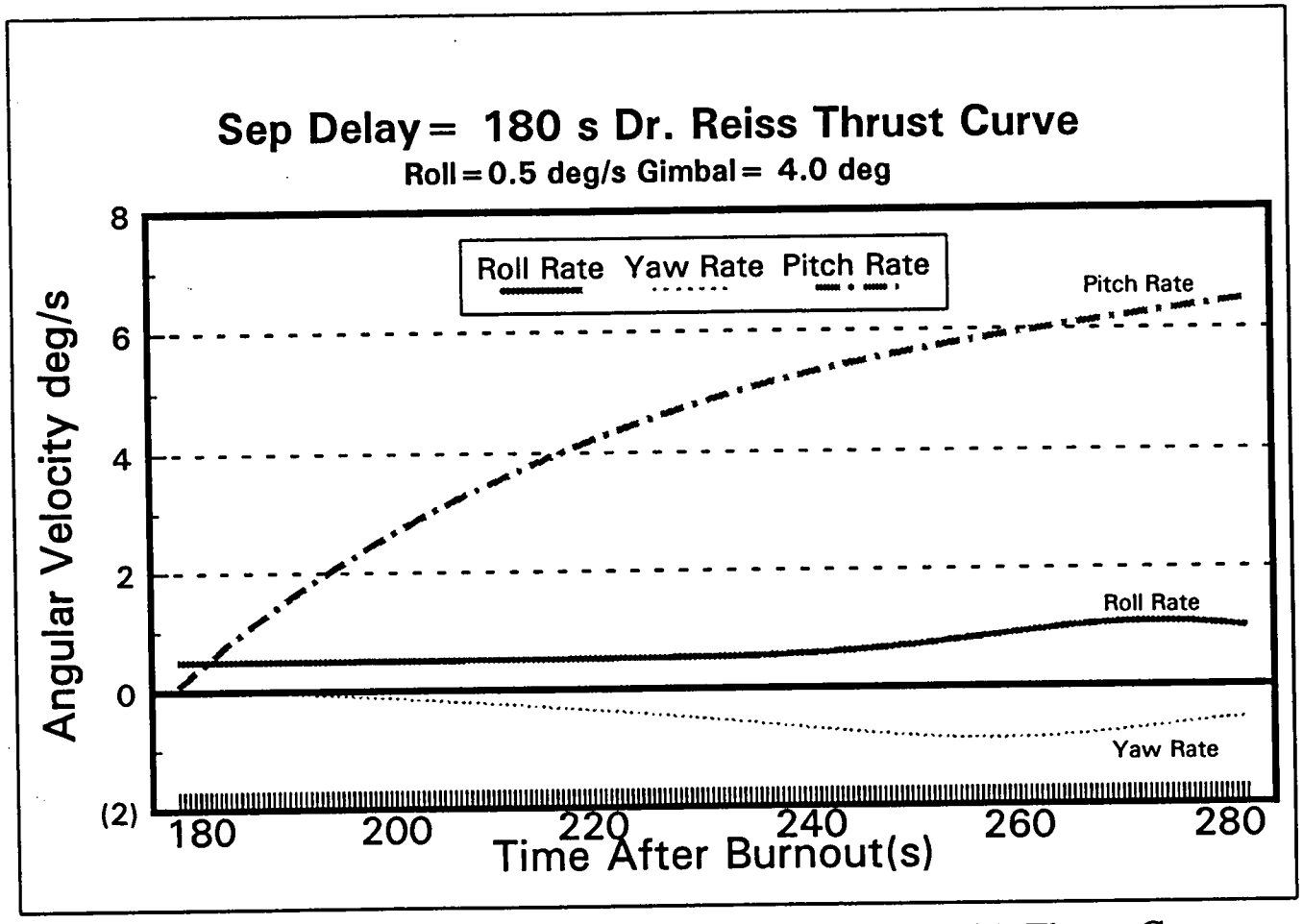


Figure 3.3 STAR-48V Inertial Angular Velocity With Thrust Curve Developed by Dr. Reiss in Reference #15

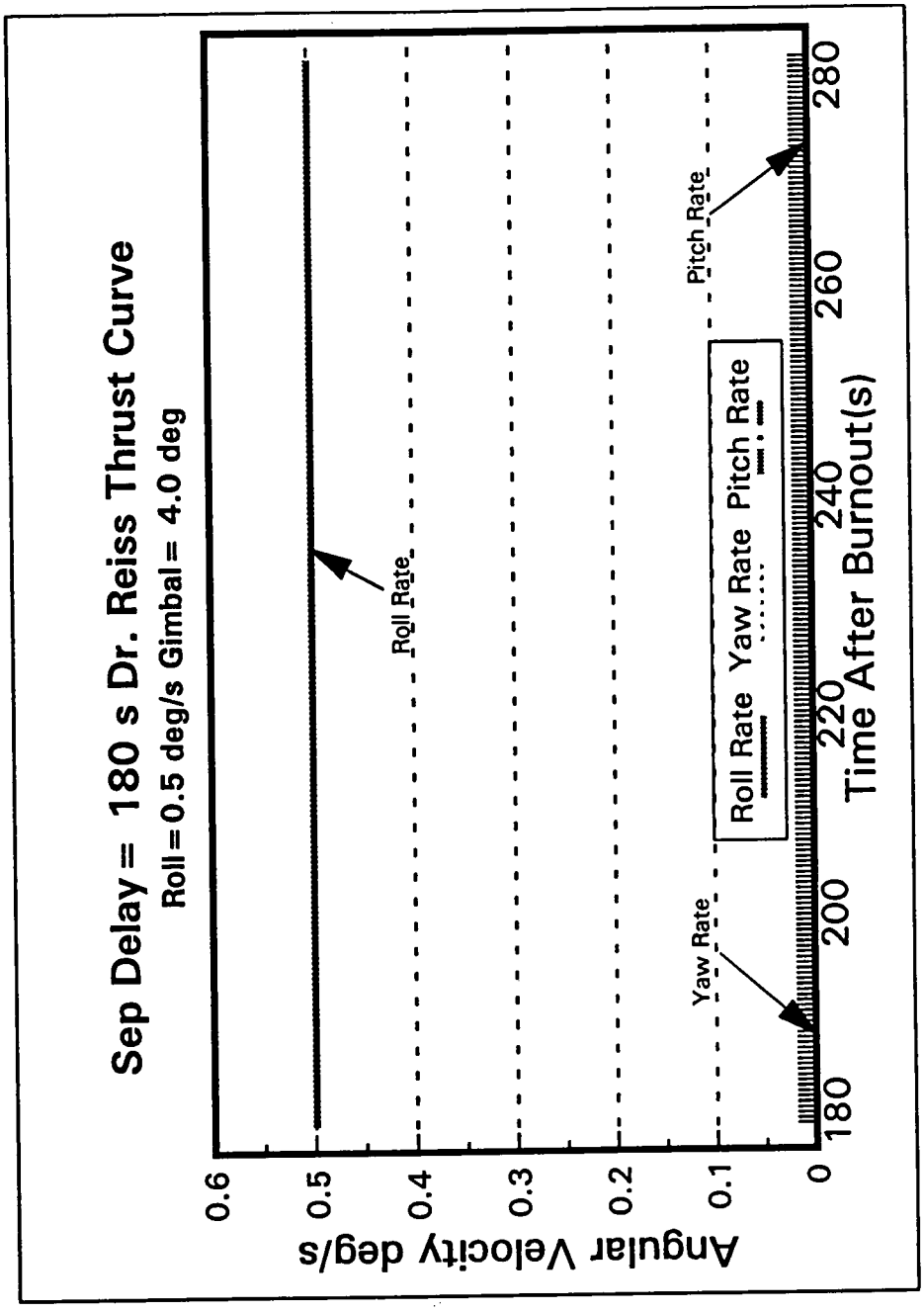


Figure 3.4 FreeFlyer Inertial Angular Velocity With Thrust Curve Developed by Dr. Reiss in Reference #15

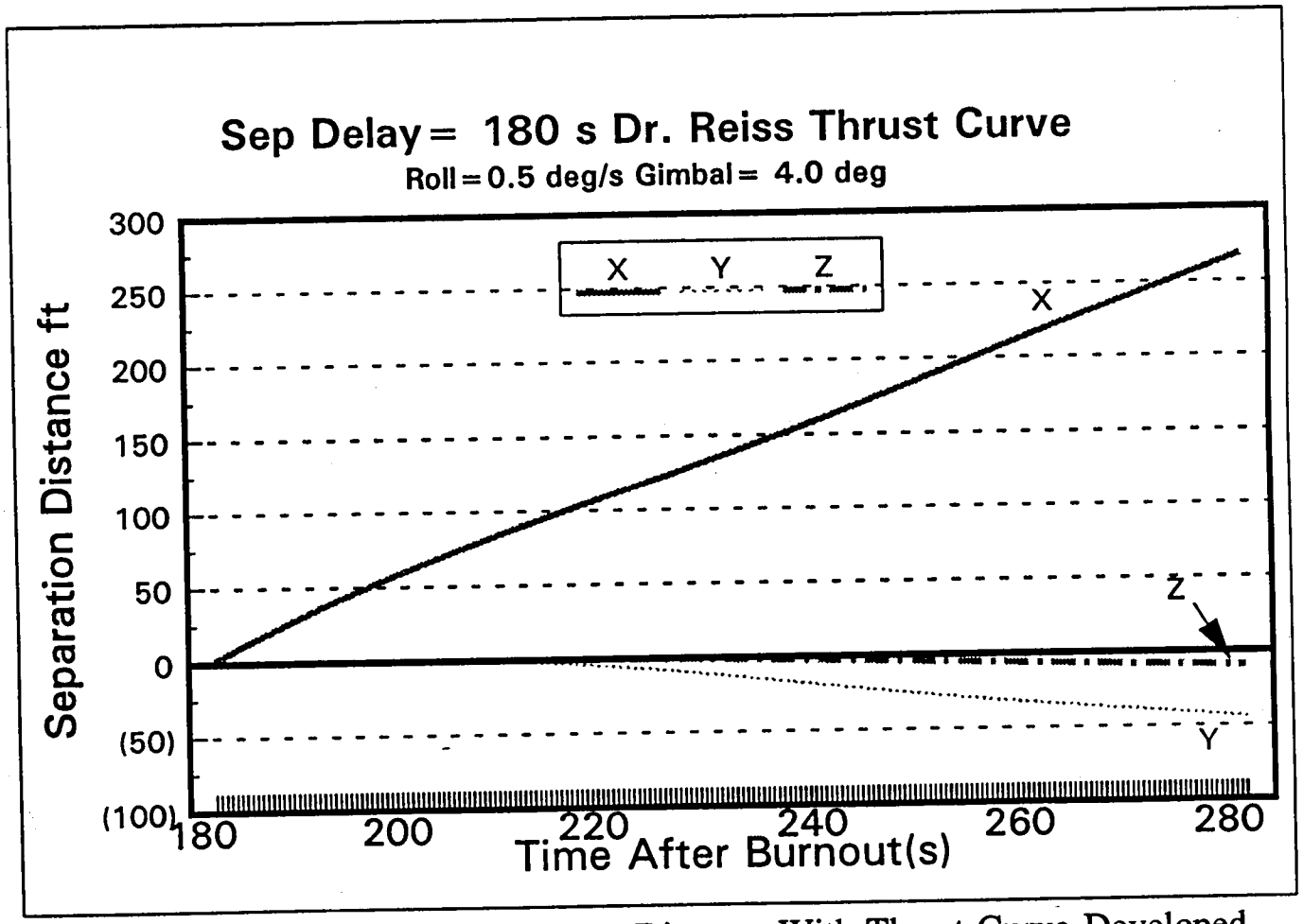


Figure 3.5 Inertial Separation Distance With Thrust Curve Developed by Dr. Reiss in Reference #15

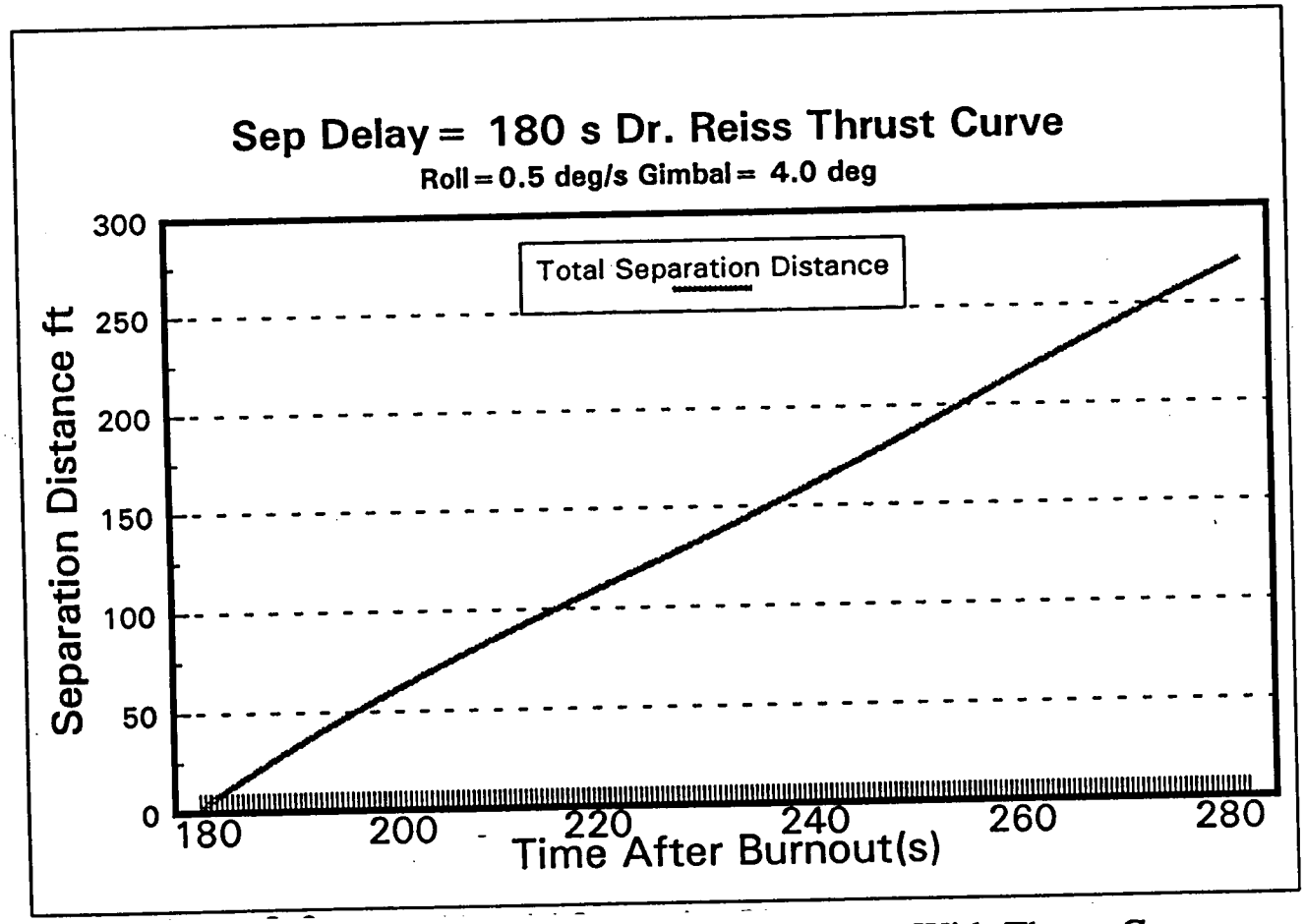


Figure 3.6 Total Inertial Separation distance With Thrust Curve Developed by Dr. Reiss in Reference #15

By subtracting the inertial separation velocity of the STAR-48V from the inertial separation velocity of the FreeFlyer, a velocity for the separation between these two bodies can be determined. By integrating this separation velocity, the distance between the center of mass of the STAR-48V and the center of mass of the FreeFlyer can be determined at all times along each of the axes of the inertial coordinate system. This can be seen in Figure 3.5. In this figure, a +Y displacement represents the STAR-48V being above the FreeFlyer and a +Z displacement represents the STAR-48V being left of the FreeFlyer when looking along the +X axis. In Figure 3.6, the total separation distance using the thrust curve developed by Dr. Reiss can be observed. This is obtained by taking the root mean square of the separation distances in Figure 3.5. It is this total separation distance that must be greater than 5 ft, as discussed in Section 2.1, in order for there to be a safe separation.

3.2 Separation Results Using the STAR-48 #1 Thrust Curve

Figure 3.7 shows the velocity of the center of mass of the STAR-48V as measured in the inertial coordinate system using the curve fitted data for the test of the STAR-48 #1 test motor. From this figure it can be seen that this thrust curve produces a much larger thrust force than the one developed by Dr. Reiss. This is apparent by comparing the velocity in the X direction in Figure 3.7 to the velocity in the X direction of the center of mass of the STAR-48V using the thrust curve developed by Dr. Reiss, as was seen in Figure 3.1. In Figure 3.1, the X axis velocity is always negative, implying that the center of mass is always traveling away from the original

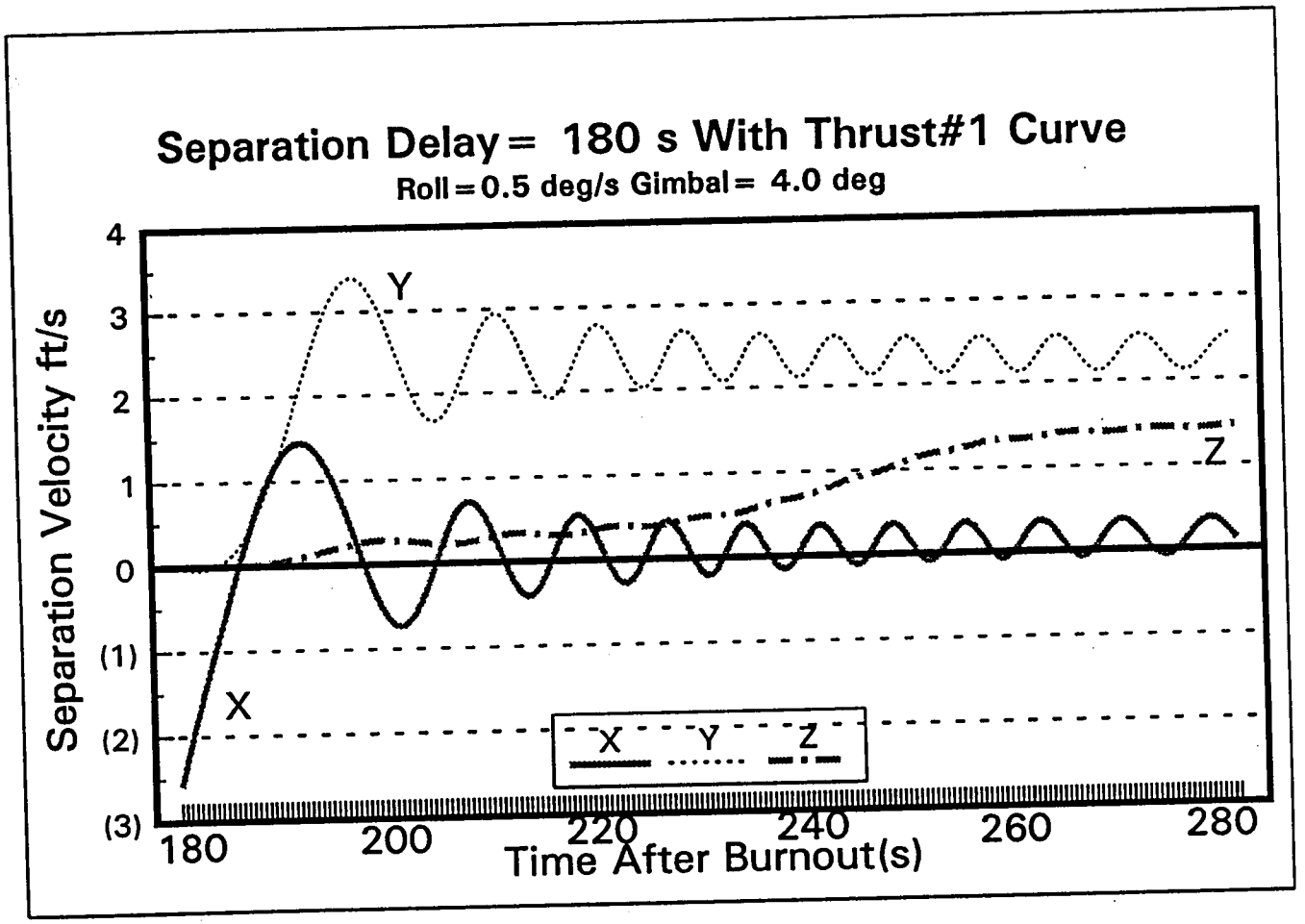


Figure 3.7 STAR-48V Inertial Velocity With Thrust #1 Curve

separation point. But in Figure 3.7, the X velocity acts in the +X direction at the peaks of this oscillation. This causes the STAR-48V to move in the +X direction and creates a situation where there is a possibility for the STAR-48V to collide with the FreeFlyer.

Figure 3.8 also shows this increase in thrust as compared to the curve developed by Dr. Reiss. It can be observed that the pitch rate using the STAR-48 #1 thrust curve is much higher than the pitch rate as seen in Figure 3.8 using the thrust curve developed by Dr. Reiss as seen in Figure 3.2. Figure 3.9 shows the separation distances along the three axes of the inertial coordinate system and Figure 3.10 shows the root mean square of the separation distances in the inertial coordinate system. From Figure 3.10, it can be seen that the separation is successful using this thrust curve, but by comparing this figure with Figure 3.6, it can be observed that this thrust curve produces a much smaller separation distance during the first 20 seconds of the separation. It is this first 20 seconds, when the STAR-48V is traveling generally aligned with the X axis, that is critical in order for there to be a safe separation. Because this separation distance is smaller in Figure 3.10 than in Figure 3.6, it can be concluded that the thrust curve developed from the STAR-48 #1 test data produces a worse case scenario than does the thrust curve developed by Dr. Reiss.

3.3 Separation Results Using the STAR-48 #2 Thrust Curve

The results from the Runge-Kutta program using the thrust curve developed for the STAR-48 #2 test motor can be observed in Figure 3.11 and Figure 3.12. These

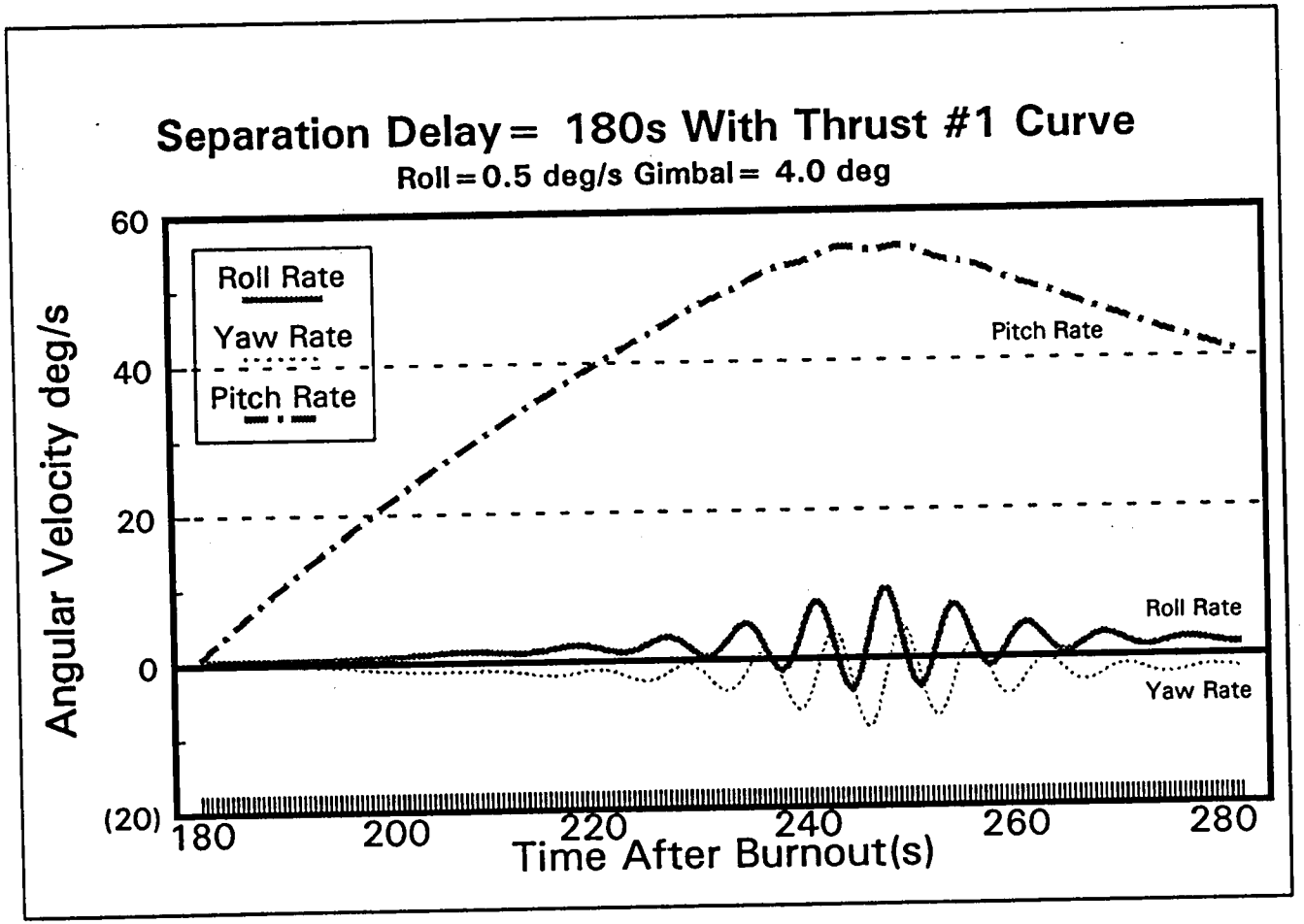


Figure 3.8 STAR-48V Inertial Angular Velocity With Thrust #1 Curve

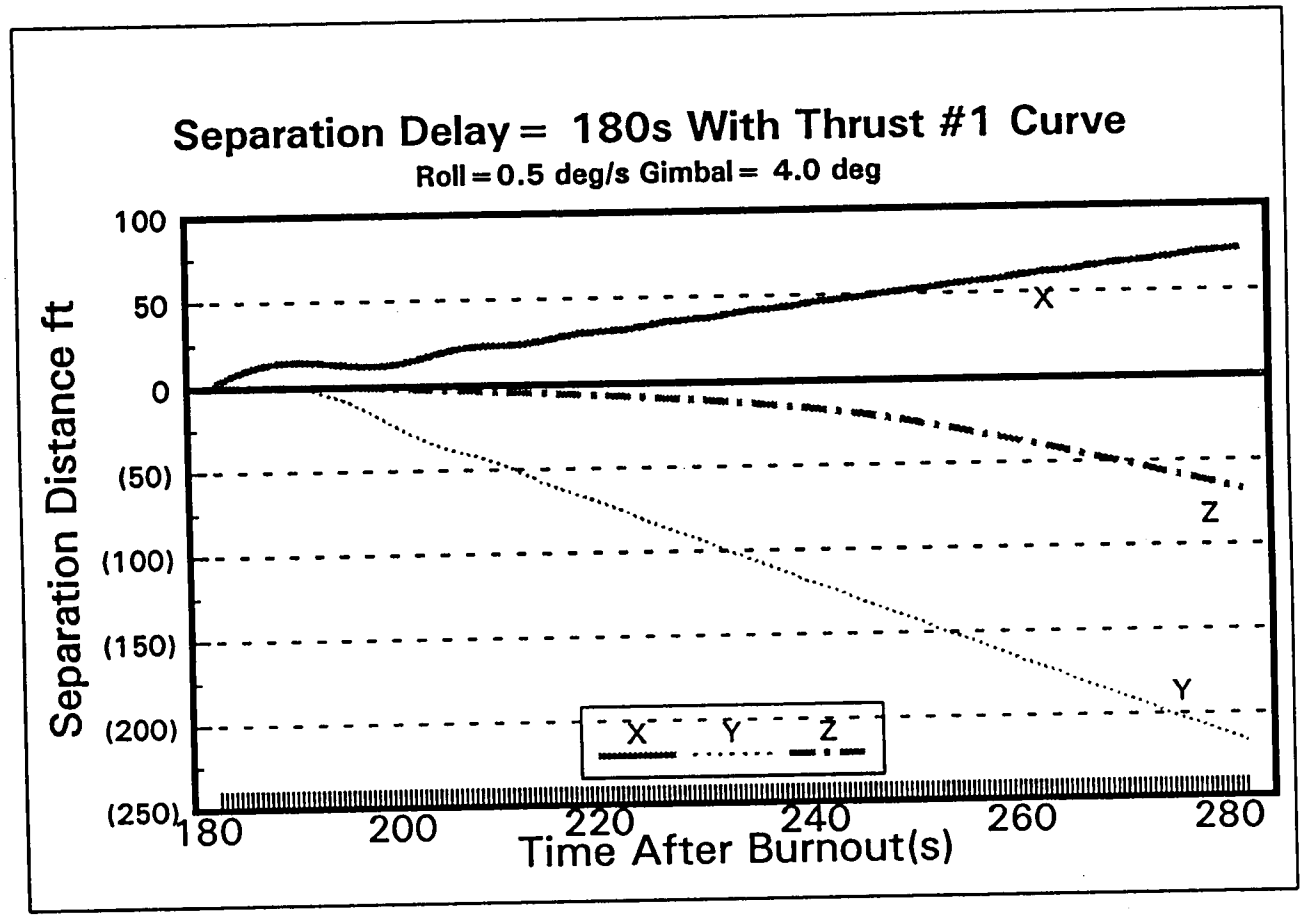


Figure 3.9 Inertial Separation Distance With Thrust #1 Curve

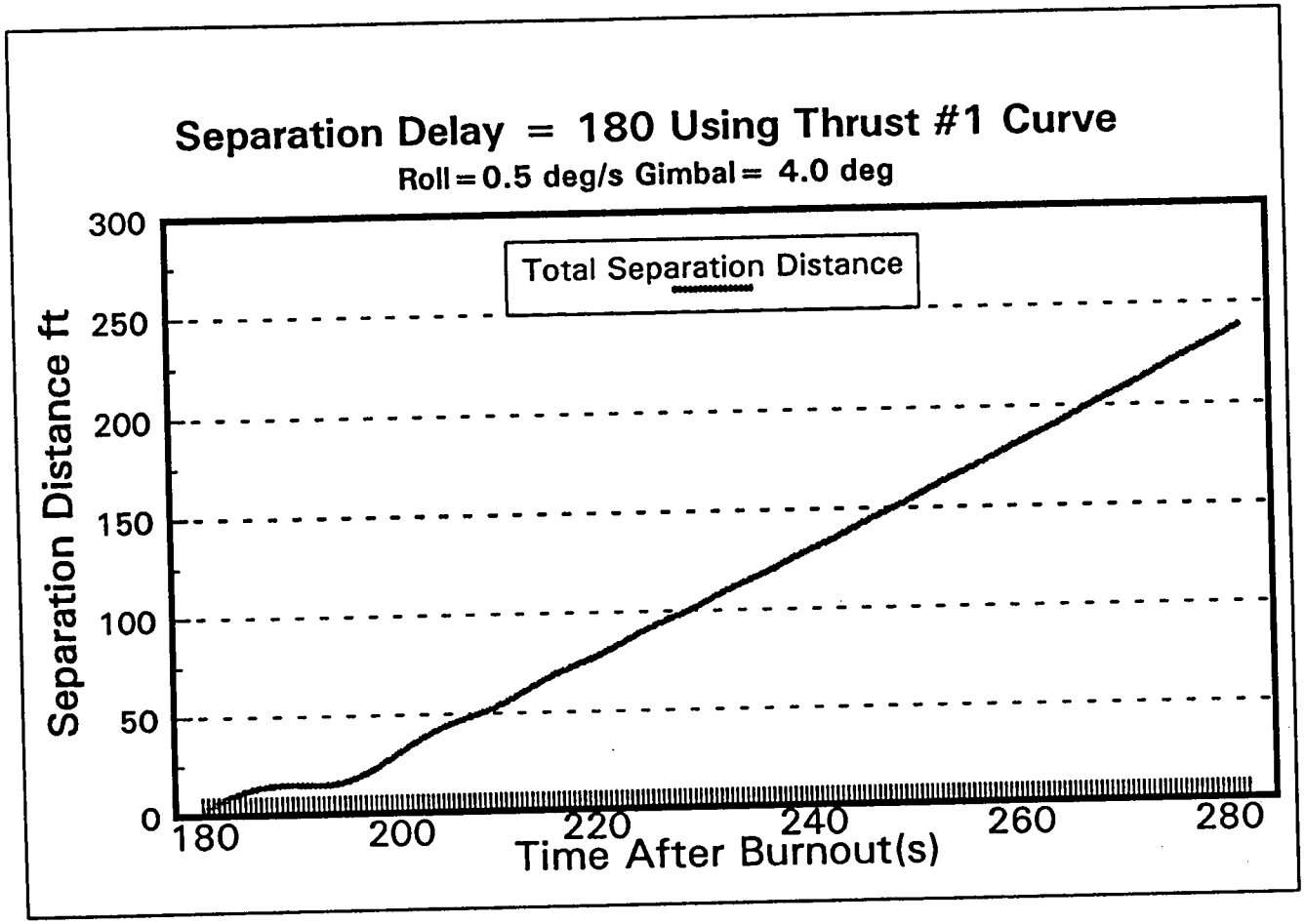


Figure 3.10 Total Inertial Separation Distance With Thrust #1 Curve

figures show the separation distance along each axis and the resultant separation distance for the Thrust #2 curve, respectively. By comparing Figure 3.12 with Figure 3.10, it can be observed that the separation distance during the critical first 20 seconds of separation is less for thrust #2 curve than for thrust #1 curve. Thus it can be concluded that, between these two curves, the thrust #2 curve is the curve to be used when defining a worse case separation analysis. Also, plots of the STAR-48V angular velocity are not given because they are very similar to the angular velocity developed for the thrust #1 curve as seen in Figure 3.8.

3.4 Separation Results Using the STAR-48 #3 Thrust Curve

Similarly, the results using the STAR-48 #3 test motor can be observed in Figure 3.13 and Figure 3.14. By comparing the total separation distance for the first 20 seconds in Figure 3.14 with the total separation distance using thrust #2 curve, as seen in Figure 3.12, it can be observed that the separation distance for the #3 motor is larger than the separation distance for the #2 motor. Thus it can be concluded that the thrust data for the #2 motor will produce the worst case separation out of all of the thrust curves developed in this thesis for the tail-off characteristics of the STAR-48 solid rocket motors. By simulating the known worst case thrust curve in the remainder of this thesis, the chances that the actual thrust curve for the STAR-48V will be higher than this are smaller than the chances for any of the other thrust curves. From this deduction, then, the thrust curve developed from the STAR-48 #2 test motor data will be used in the Runge-Kutta program to simulate baseline tail-off thrust force of the

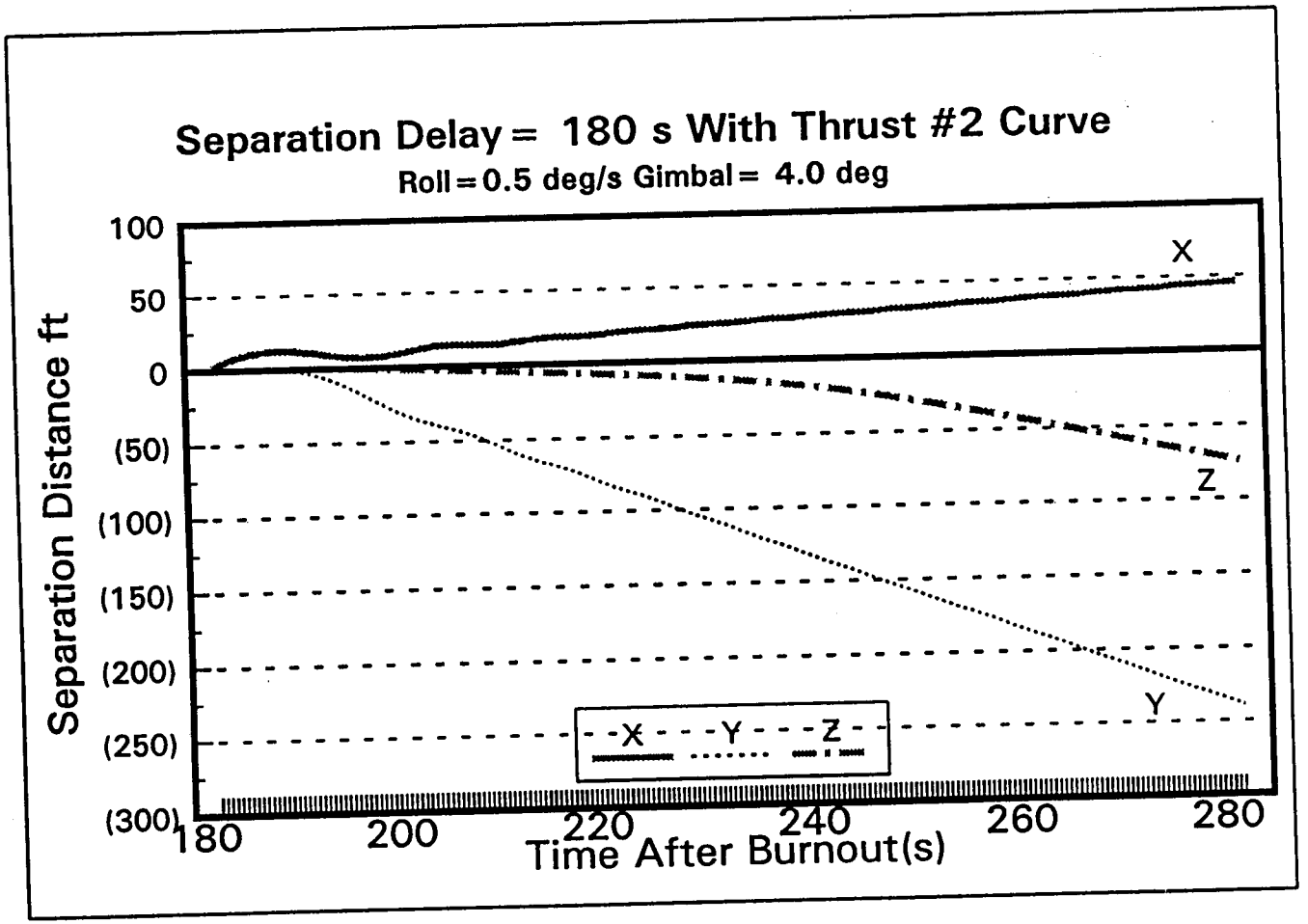


Figure 3.11 Inertial Separation Distance With Thrust #2 Curve

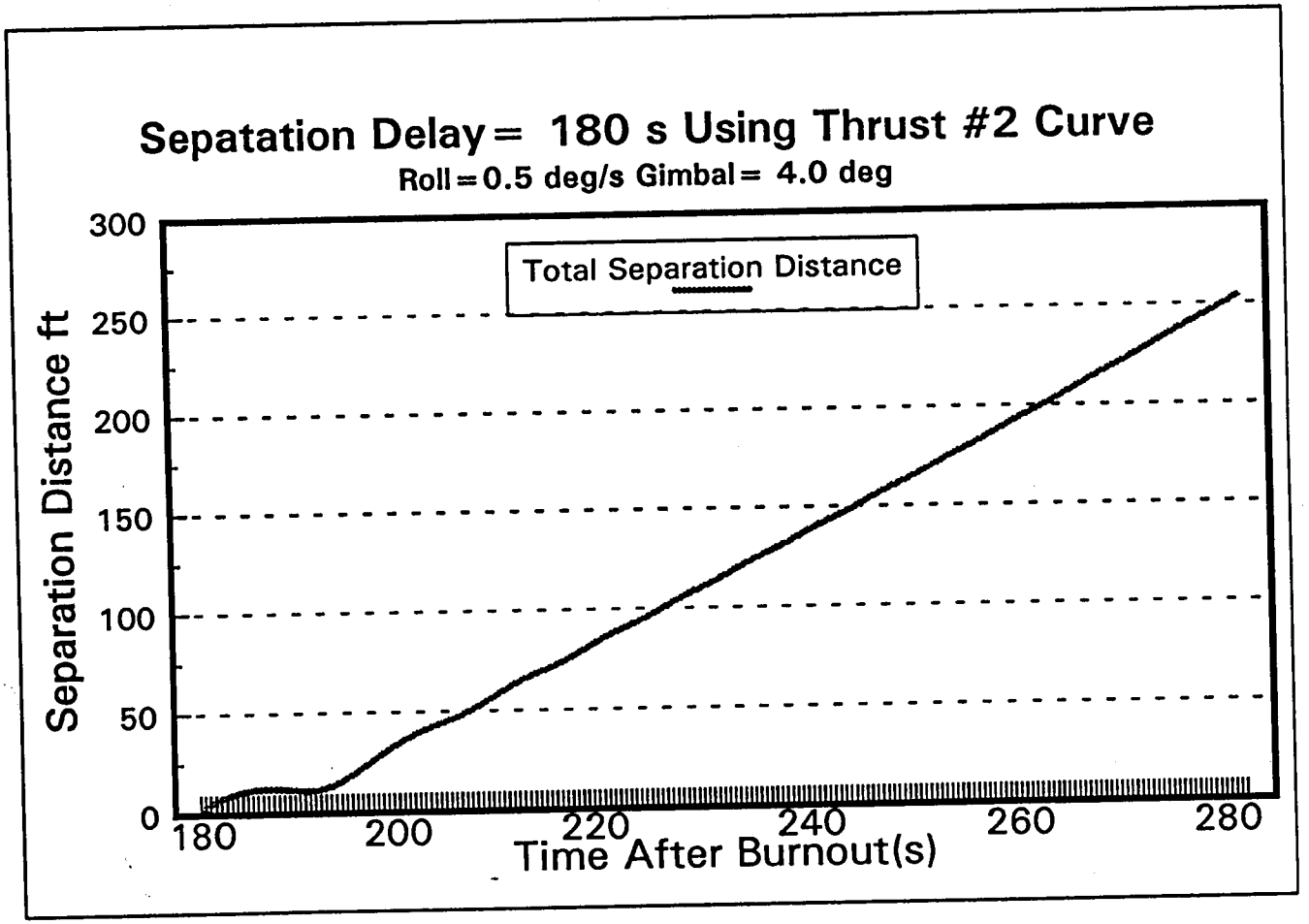


Figure 3.12 Total Inertial Separation Distance With Thrust #2 Curve

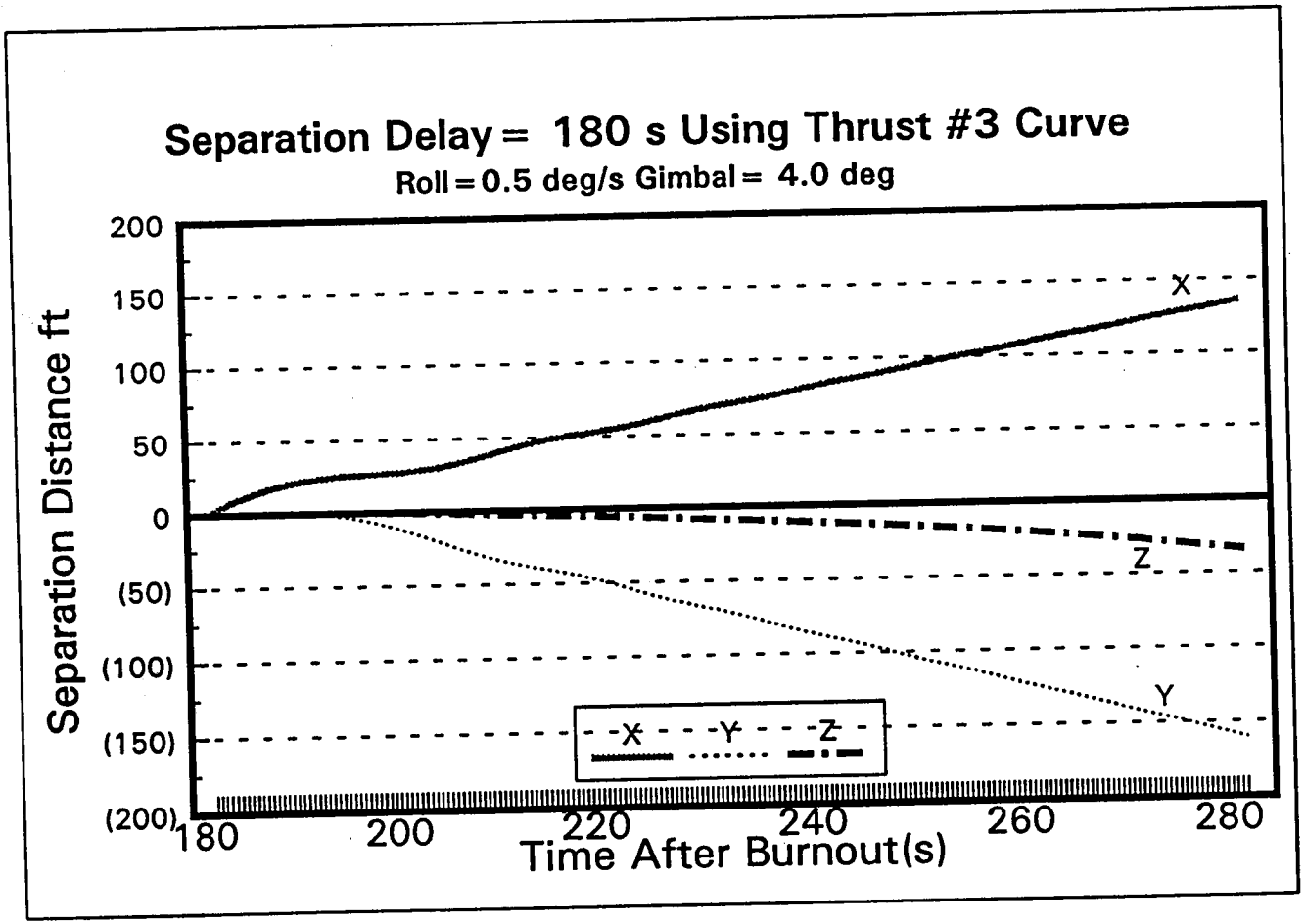


Figure 3.13 Inertial Separation Distance With Thrust #3 Curve

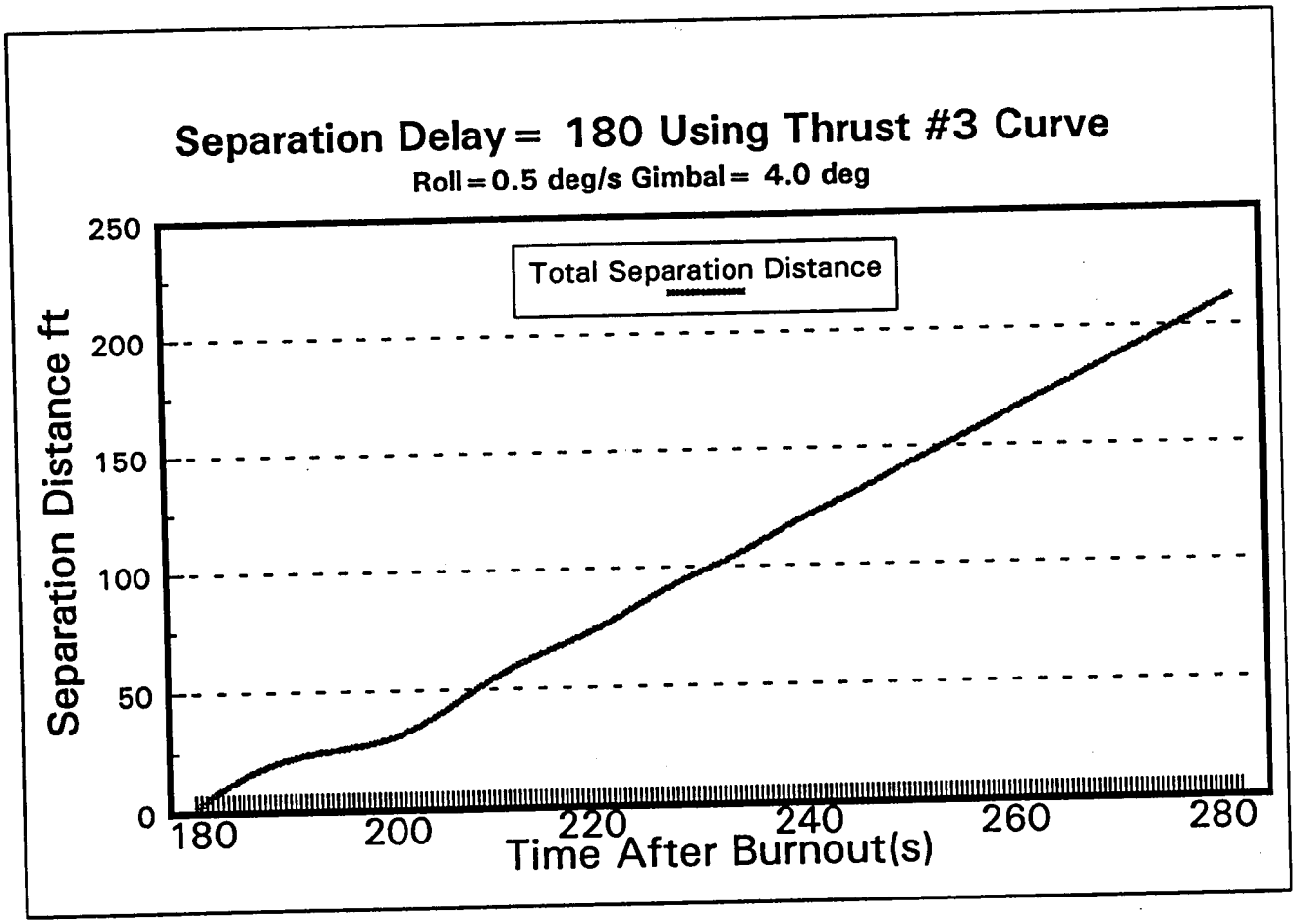


Figure 3.14 Total Inertial Separation Distance With Thrust #3 Curve

STAR-48V in the chapters to follow.

Chapter 4: Effect on the Separation of Altering Certain Configuration Variables

4.1 Effect of Separation Delay Time

In Chapter 4 it was shown that the separation between the STAR-48V and the COMET FreeFlyer is successful using the tail-off thrust characteristics of the STAR-48 #2 test motor and a separation delay of 180 s after the nominal burnout of the STAR-48V motor. But a question arises as to how the length of this separation delay time will affect the success of the separation. If this separation delay time could be shortened without resulting in a collision, then the requirements on the COMET FreeFlyer power system could be reduced. This in turn could result in a reduction in the weight of the on-board batteries of the COMET FreeFlyer power system. This reduction in weight results in a 1 to 1 increase in the weight of the allowable payload of the COMET FreeFlyer. Thus it is highly desirable to design the separation delay time to be as small as possible. By reducing the separation delay time and by comparing the minimum separation distances of each separation delay, a minimum separation delay time can be determined for the separation between the STAR-48V and the COMET FreeFlyer.

Figure 4.1 shows the separation distances between the center of mass of the STAR-48V and the center of mass of the FreeFlyer using the baseline configuration and a separation delay time of 180 seconds. Figure 4.2 shows the resultant total separation distance between these two bodies at this same separation delay time. Note that the

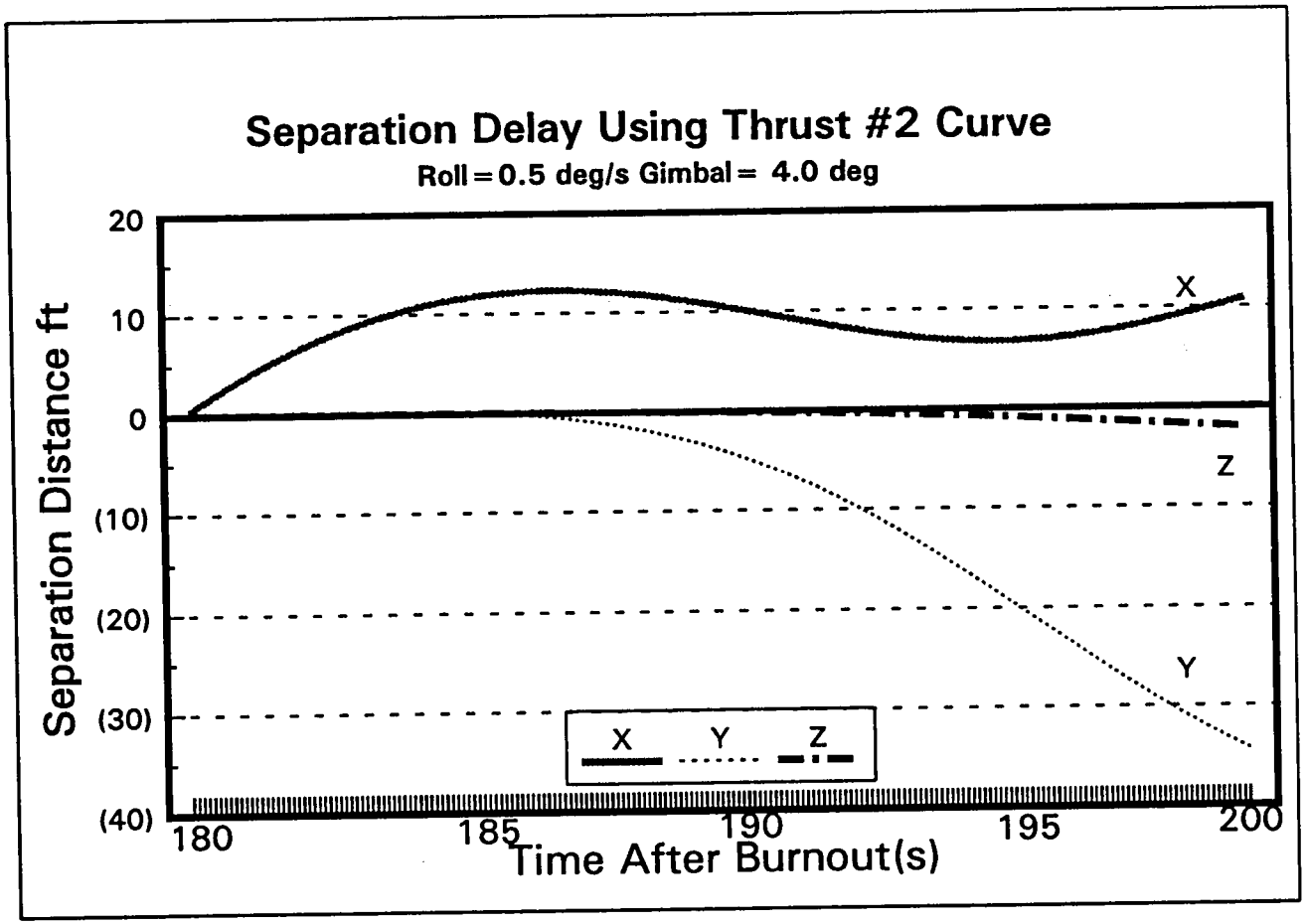


Figure 4.1 Inertial Separation Distance for 180 s Separation Delay

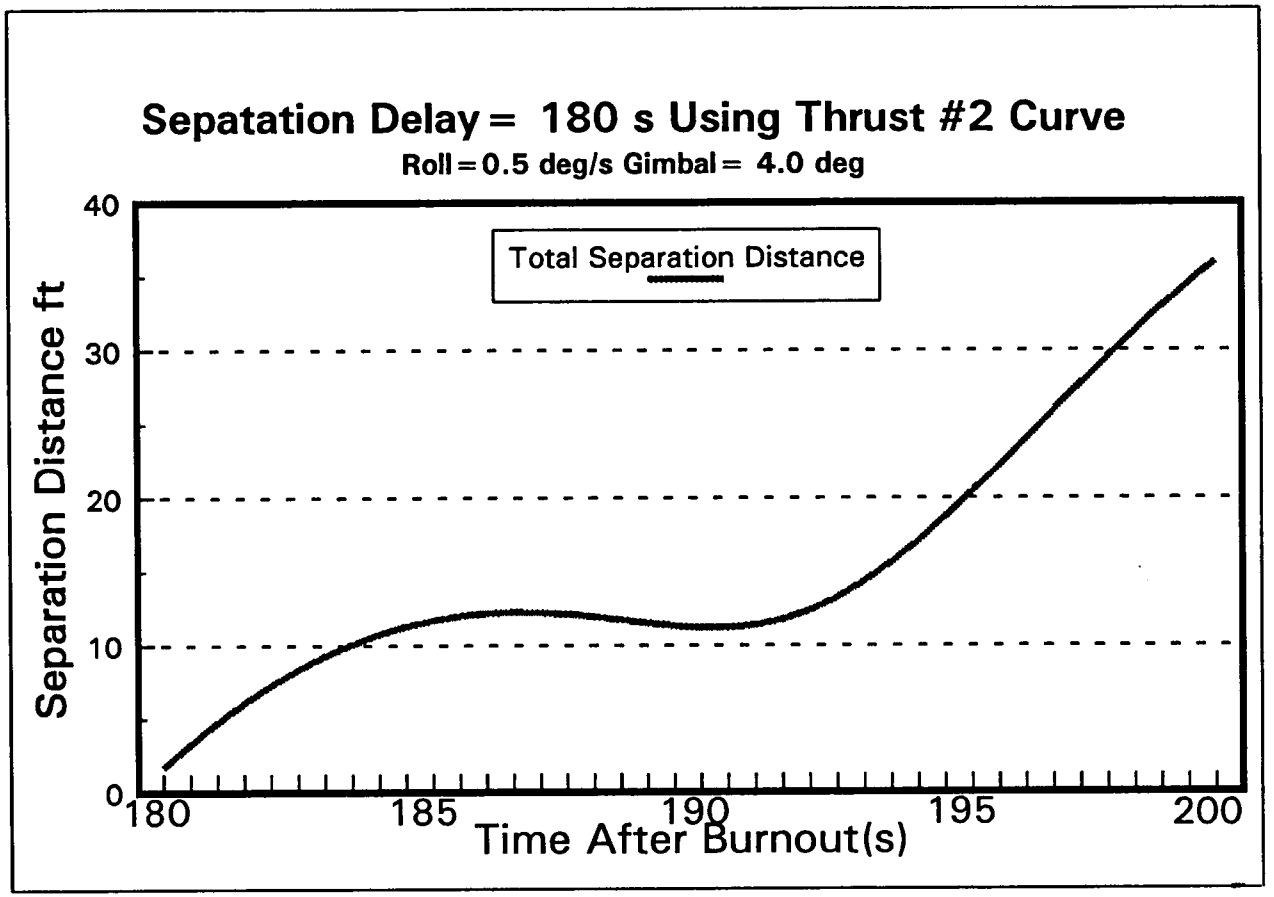


Figure 4.2 Total Inertial Separation Distance for 180 s Separation Delay

time length of these figures has been reduced from 100 seconds, as was seen in Chapter 4, to only 20 seconds. This switch in time length is performed in order to more carefully observe the critical separation time frame of 20 seconds as was noted in Chapter 4. After 20 seconds, there is no longer a possibility for a collision between the STAR-48V and the COMET FreeFlyer, no matter what the value of the separation delay time is. Since the gimballing of the STAR-48V nozzle drives the STAR-48V into either the X or the Y direction, depending upon the initial conditions, the STAR-48V has either moved a safe distance in the Y direction or in the Z direction once the critical collision time has been reached. After this time, the STAR-48V has traveled too far in either the Y direction or the Z direction in order for a collision to result. In Figure 4.3 and Figure 4.4, the separation distances for a separation delay time of 140 seconds can be seen. It can also be seen in Figure 4.3 that at approximately 148 seconds, the STAR-48V has returned to its original X position, but that it is about 6 ft above the FreeFlyer as it passes by. Since the minimum safe distance is only 5 ft, it can be concluded that this separation delay time results in a safe separation, although just barely. This is also brought out in Figure 4.4 where the minimum total separation distance can be observed to be about 6.5 feet.

This safe separation, however, is not the case for separation delay times significantly smaller than 140 seconds. Figure 4.5 and Figure 4.6 show the separation distances of the STAR-48V and the FreeFlyer with a separation delay time of 100 seconds. From either one of these two figures it can be observed that the separation distance between the center of mass of the STAR-48V and the FreeFlyer is less than

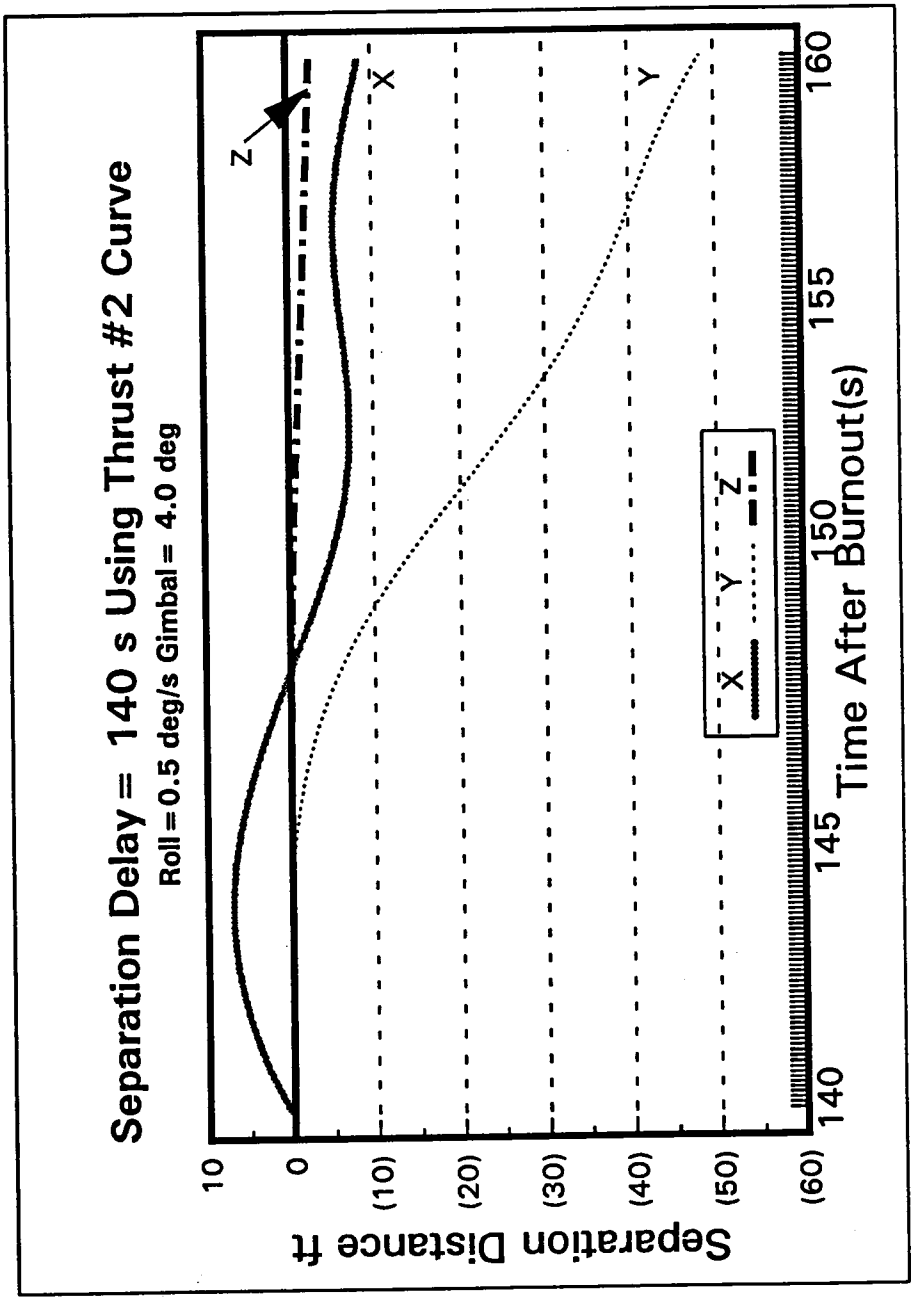


Figure 4.3 Inertial Separation Distance for 140 s Separation Delay

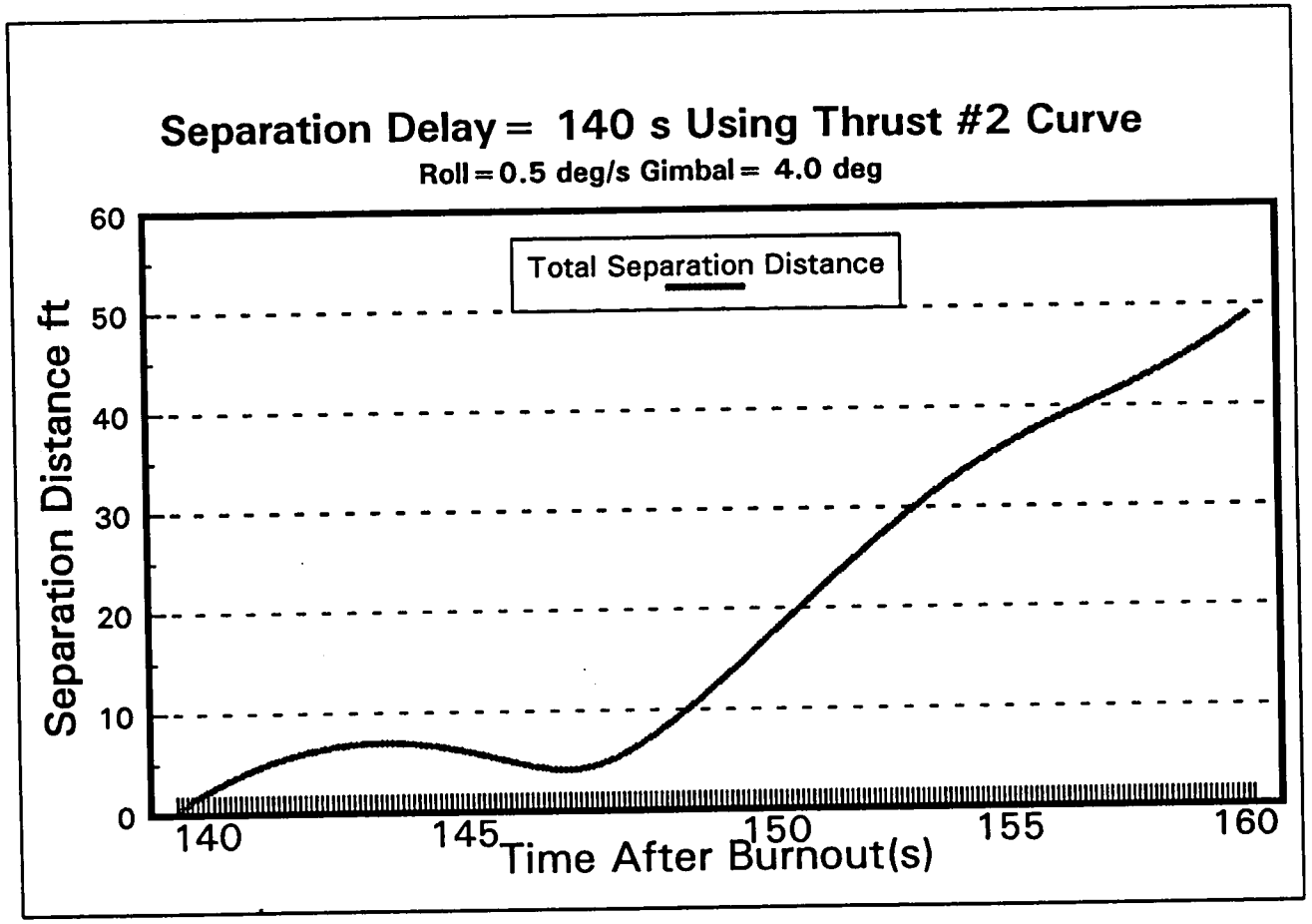


Figure 4.4 Total Inertial Separation Distance for 140 s Separation Delay

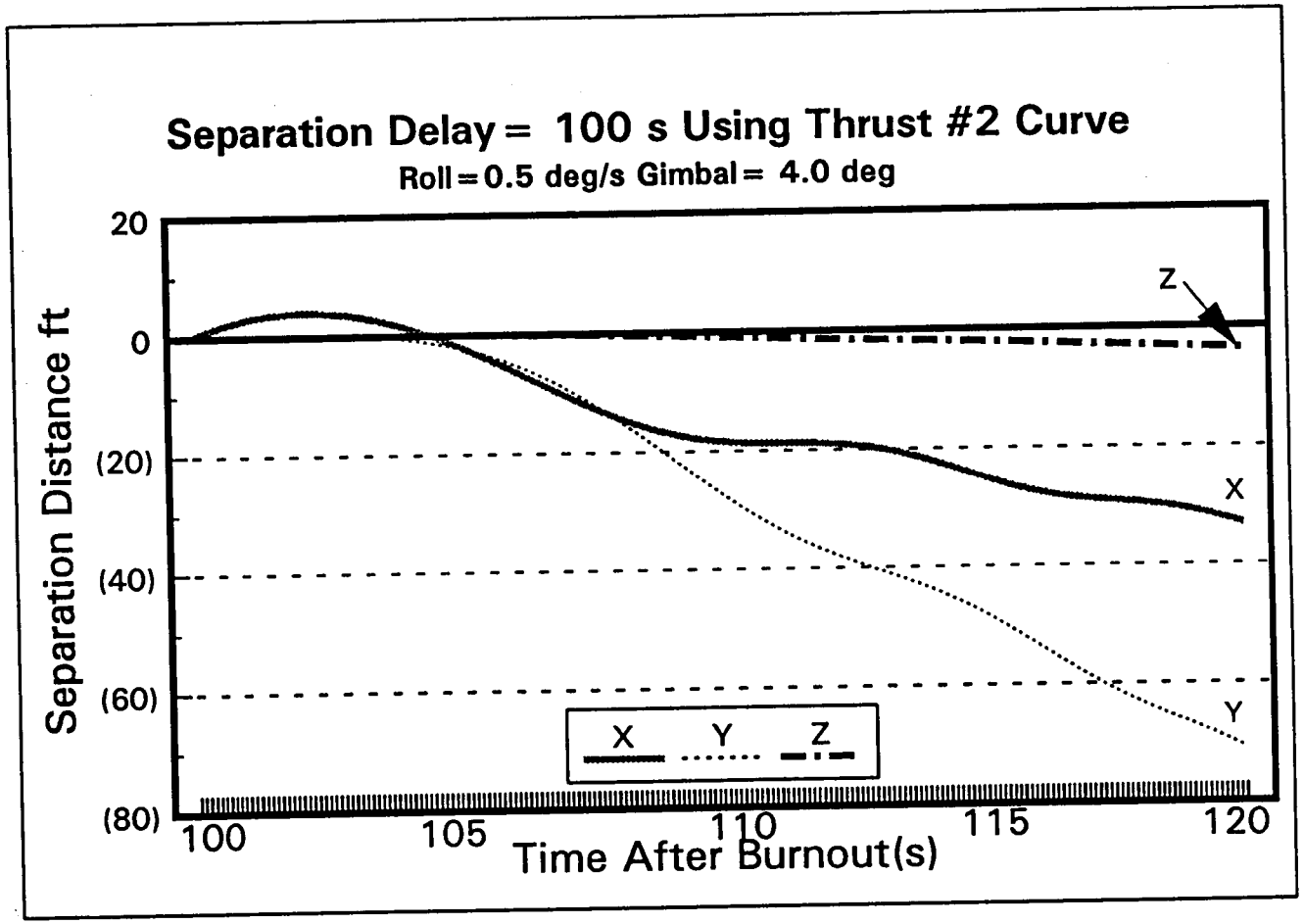


Figure 4.5 Inertial Separation Distance for 100 s Separation Delay

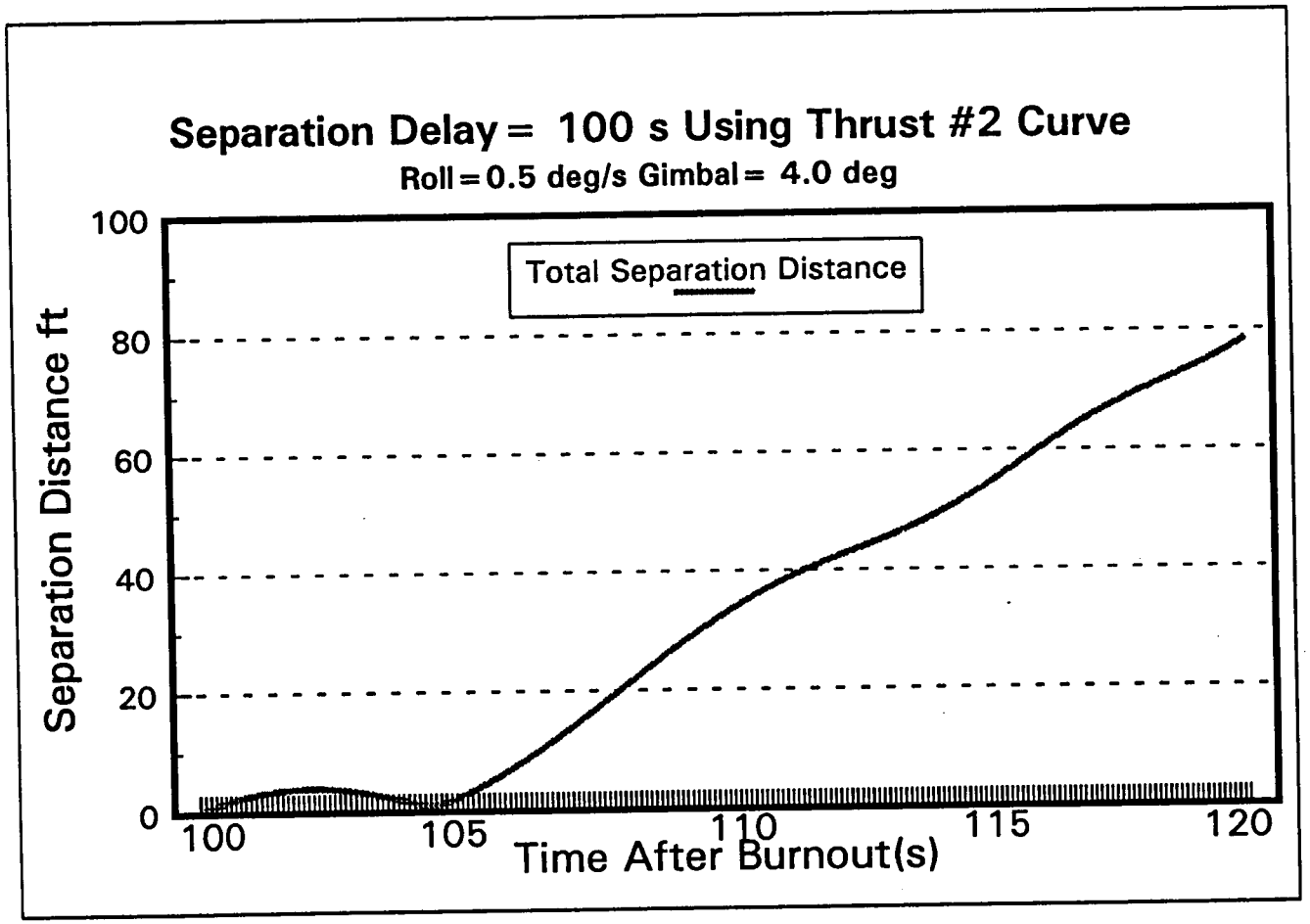


Figure 4.6 Total Inertial Separation Distance for 100 s Separation Delay

the safe separation distance of 5 feet. Thus it can be concluded that this separation delay time results in a collision and, therefore, a separation delay of 100 seconds is not allowable for this mission. Since the thrust force increases as the separation delay time decreases, it can also be concluded that any separation delay time less than about 140 seconds will result in the collision between the STAR-48V and the FreeFlyer. Because of this, the minimum separation delay time for this mission is determined to be about 140 seconds and the use of a smaller separation delay time will result in a collision between the FreeFlyer and the STAR-48V.

4.2 Effect of Nozzle Gimbal Angle

In Figure 4.7, the effects of the gimbal angle of the STAR-48V on the total separation distance can be observed. Using a baseline separation delay time of 180 seconds and a baseline roll rate of 0.5 deg/s, gimbal angles of 0, 1, 3, and 6 degrees were used in the Runge-Kutta program and the results were determined. From Figure 4.7 it can be observed that a collision will result at approximately 194 seconds after nominal burnout if there is no nozzle gimballing. The benefits of gimballing the nozzle on the STAR-48V by only 1° can be clearly seen in this figure. It shows that there is a safe (although guarded) separation for a nozzle gimbal angle of only 1° and that there is also a reasonably safe separation for a nozzle gimbal of 3° and 6°. Figure 4.7 shows that the ability to gimbal the STAR-48V nozzle, once the separation process has been initiated, is critical for a safe separation between the STAR-48V and the FreeFlyer. If this nozzle does not gimbal during separation process, then the STAR-

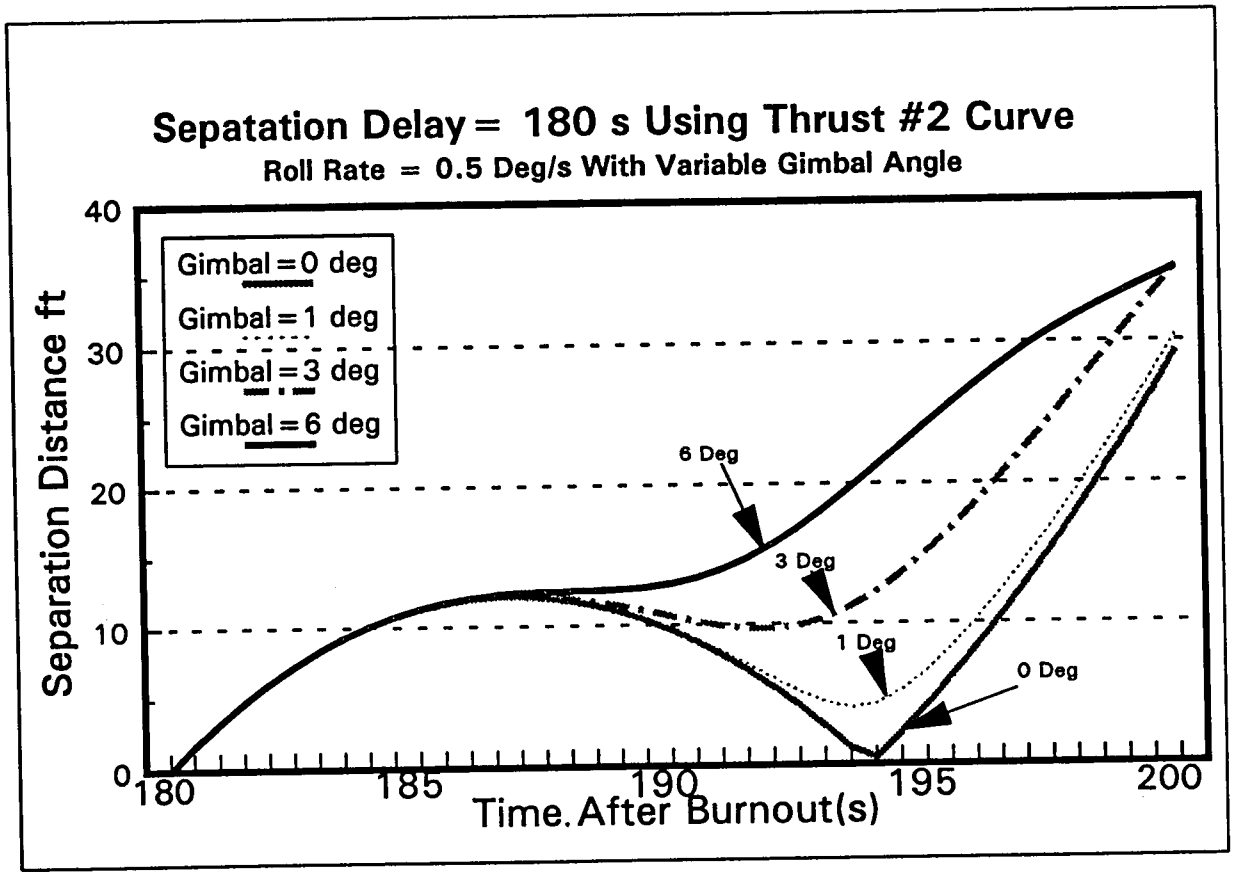


Figure 4.7 Total Inertial Separation Distance With Variable Gimbal Angle

48V is certain to collide with the FreeFlyer.

4.3 Effect of Roll Rate

As stated in Section 3.2, the initial roll rate of the STAR-48V and the COMET FreeFlyer is not expected to be over 0.5°/s since the STAR-48V does not require spin stabilization during its burn. But if this value is inaccurate, then it is advisable to determine the effects that the initial roll rate will have upon the success of the separation. In order to accomplish this, different values for the initial roll rate were selected in the Runge-Kutta program and Figure 4.8 shows the results of this. It can be seen from this figure that there is almost no difference in the total separation distance between an initial roll rate of 0°/s and an initial roll rate of 5°/s. In fact, the total separation distance is relatively unaffected by the initial roll rate from 0°/s on up to about 5°/s for the mission as currently designed. But as the initial roll rate is increased, the spin stabilization effects of the STAR-48V become apparent and the result is a collision. This can be seen in Figure 4.8 for a roll rate of 50°/s. Thus at very high initial roll rates, the effect of gimballing the STAR-48V nozzle in order to reduce the possibility of collision is offset by the spin stabilization of this very high roll rate.

This spin stabilization, though, should not be a problem for the current mission as designed since the spin stabilization roll rate of about 50°/s is two orders of magnitude higher than the maximum expected initial roll rate of 0.5°/s. It is because of this that it is concluded that the initial roll rate of the COMET FreeFlyer does not

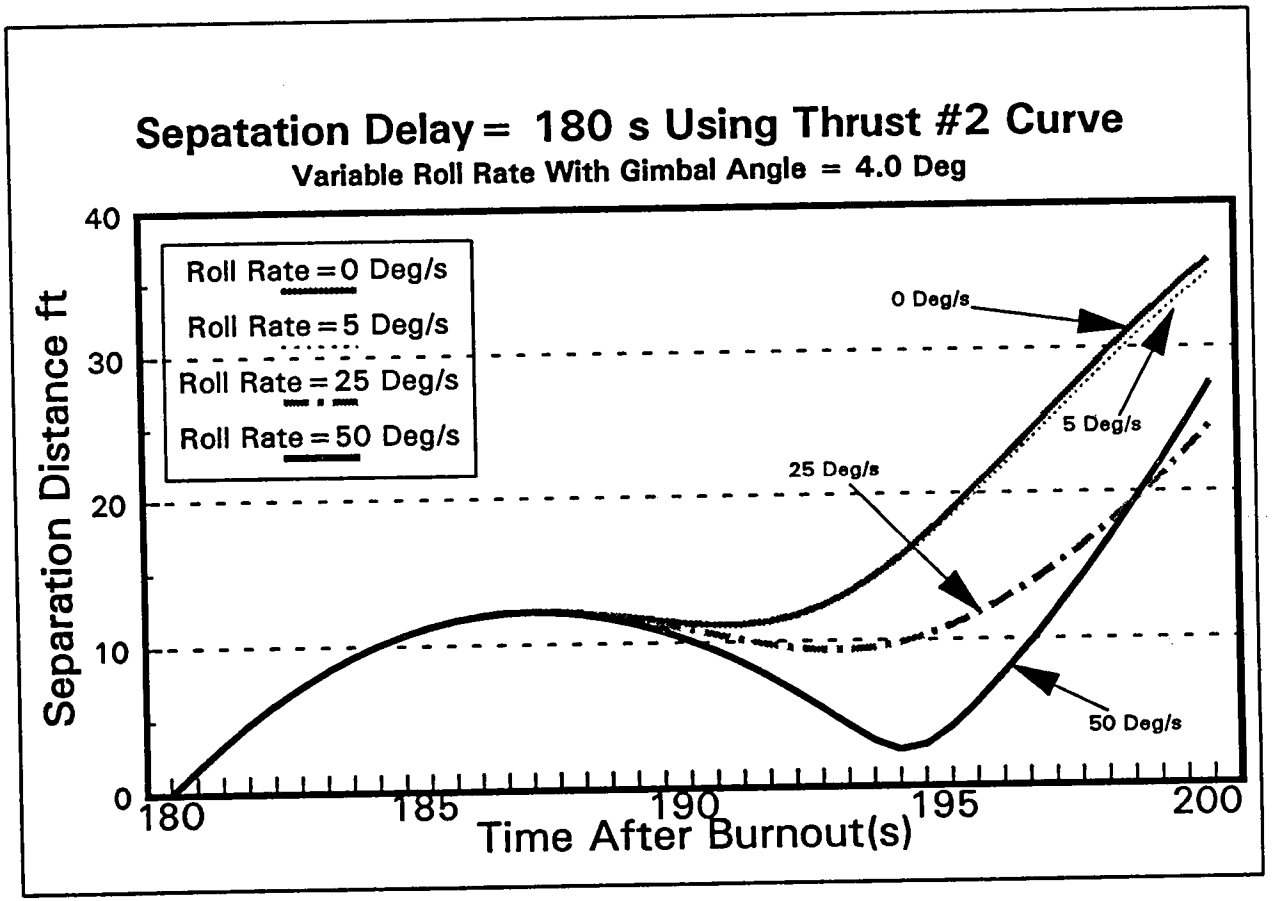


Figure 4.8 Total Inertial Separation Distance With Variable Initial Roll Rate

pose a large threat to the success of the separation between the STAR-48V and the COMET FreeFlyer.

4.4 Effect of Initial Wobble Rates

Another problem that could arise is that an initial wobble rate about the Y axis and/or the Z axis could be placed upon both the STAR-48V and the FreeFlyer due to an asymmetric firing of the pyrotechnic separation bolts during the initial separation phase. This could cause the separation springs to uncoil at slightly different times, resulting in an asymmetric application of the spring force. This in turn could cause initial wobble rates to be placed upon both the STAR-48V and the FreeFlyer which could create two problems for the mission. The first problem is that these wobble rates might be significant enough to cause problems with the separation between the STAR-48V and the COMET FreeFlyer. This is the problem that will be investigated in the following analysis. The other problem that may arise is that these wobble rates could become significant enough to cause stability problems for the remainder of the 120 day mission. This problem will not be investigated in this thesis since the focus of this thesis is on the separation dynamics between the STAR-48V and the FreeFlyer. Much care, though, has been taken to insure that this separation spring system will not cause any significant adverse wobble rates when it fires and many tests have been performed in the laboratory. While none of these tests have been conclusive, it is believed that the initial wobble rates, due to the asymmetric application of the spring force, will be small. Since the maximum initial wobble rates are unknown, values for the initial

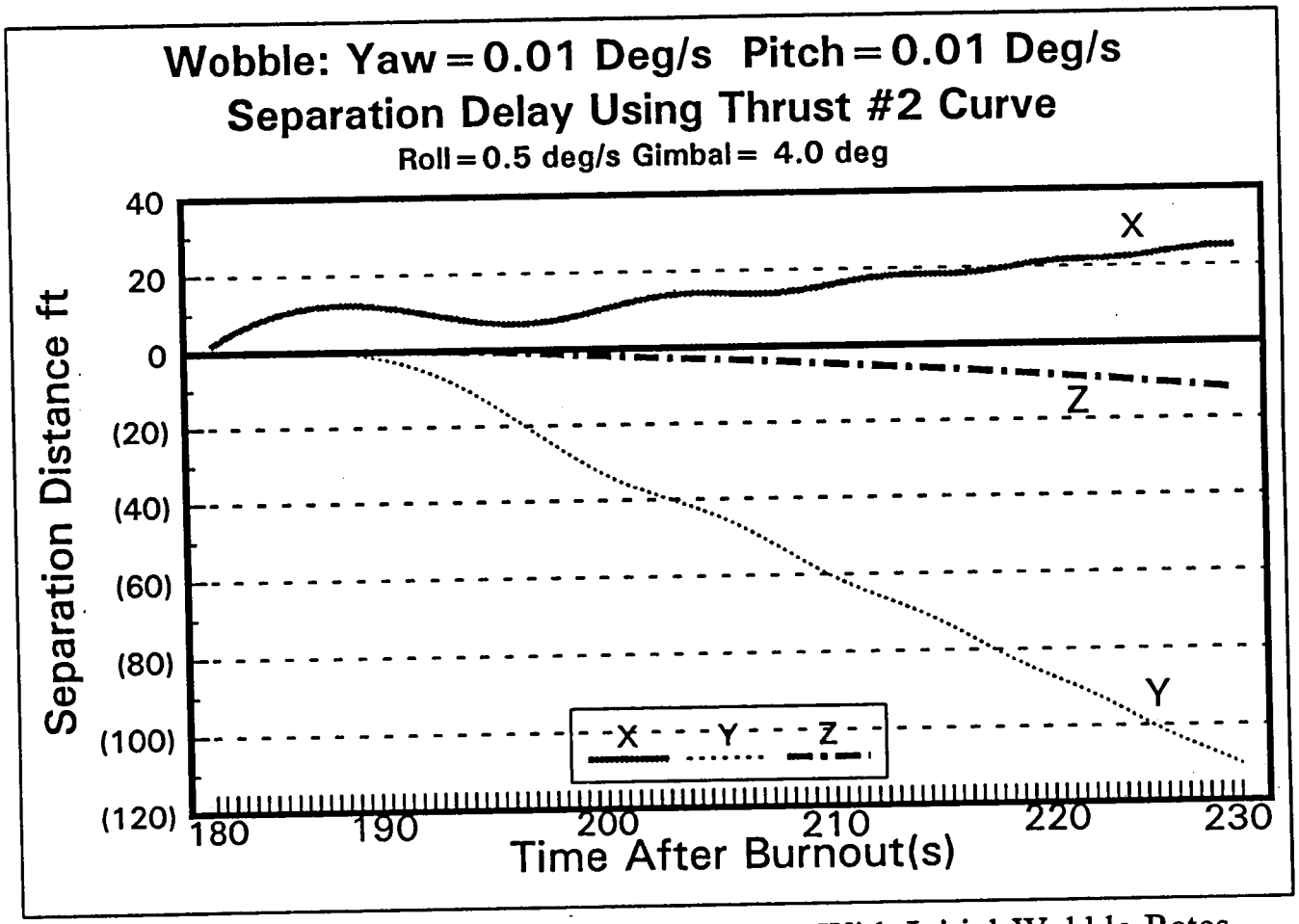


Figure 4.9 Inertial Separation Distance With Initial Wobble Rates of 0.01°/s and 0.01°/s

wobble rates with different orders of magnitude will be investigated in order to see their effects upon the separation between the STAR-48V and the COMET FreeFlyer.

Figure 4.9 shows the inertial separation distance between the center of mass of the STAR-48V and the center of mass of the FreeFlyer if a wobble rate of 0.01°/s is initially placed upon the yaw axis and a wobble rate of 0.01°/s is initially placed upon the pitch axis of both the STAR-48V and the FreeFlyer. Note that the separation time frame of the remaining figures in this chapter has been adjusted to 50 seconds and that the separation configuration is a baseline configuration with only the initial wobble rates added. In Figure 4.10 and 4.11, the angular velocities about each of the inertial coordinate axes for both the STAR-48V and the FreeFlyer, respectively, can be observed. These two figures point out the tumbling nature of the STAR-48V and the stable nature of the FreeFlyer. By comparing the total separation distance of the configuration with the initial wobble rates as seen in Figure 4.12 with the separation distance of the configuration without the initial wobble rates as seen in Figure 4.2 and noting the change in time scale, it can be concluded that the separation is not affected by initial wobble rates on the order of 0.01°/s. It can be observed that the minimum separation distance after the separation process has been initiated is about 12 ft in both Figure 4.12 and Figure 4.2. This minimum separation distance results in a successful separation, even with the initial wobble rates of 0.01°/s about the Y axis and 0.01°/s about the Z axis.

In Figure 4.13, the separation distance between the center of mass of the STAR-48V and the center of mass of the FreeFlyer is determined using the same baseline

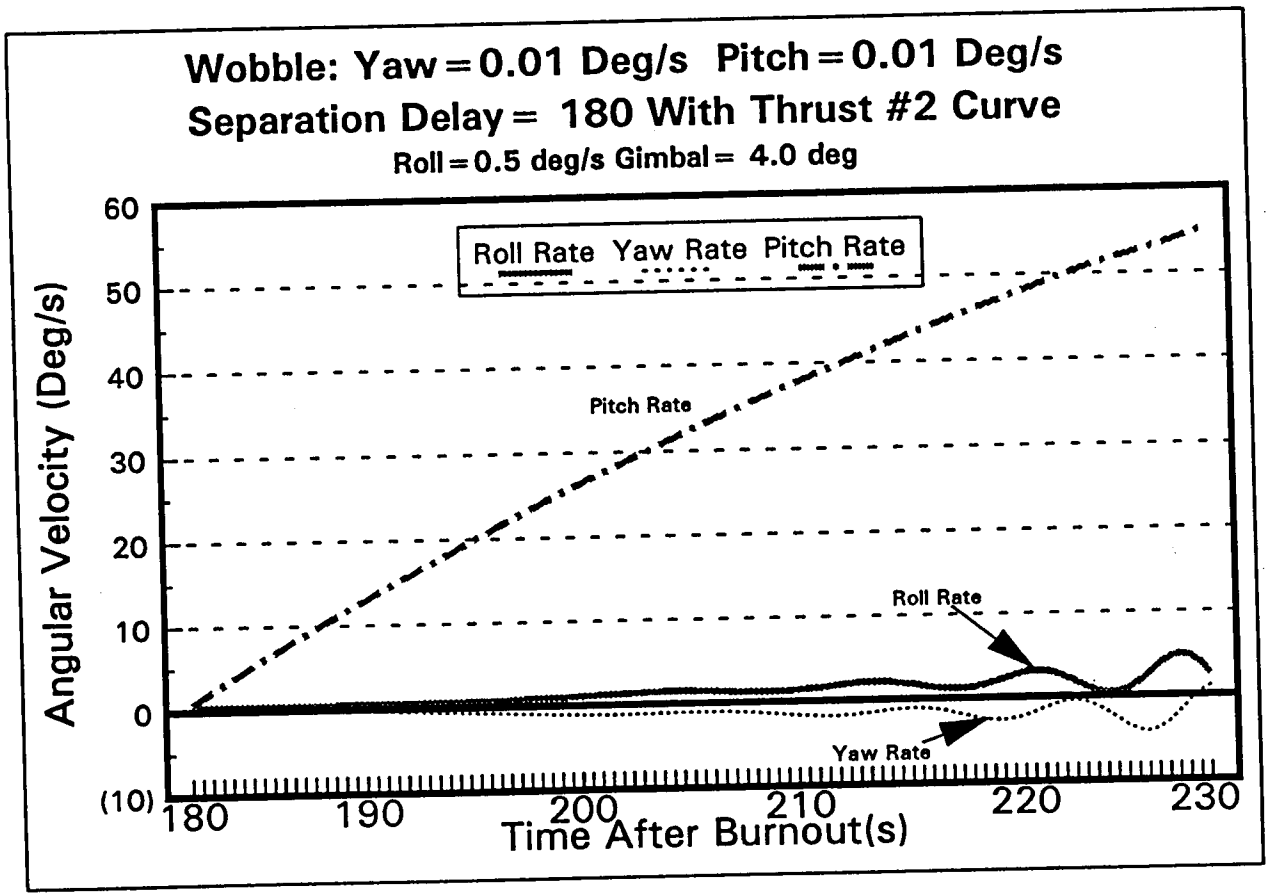


Figure 4.10 Inertial Angular Velocity of STAR-48V With Initial Wobble Rates of 0.01°/s and 0.01°/s

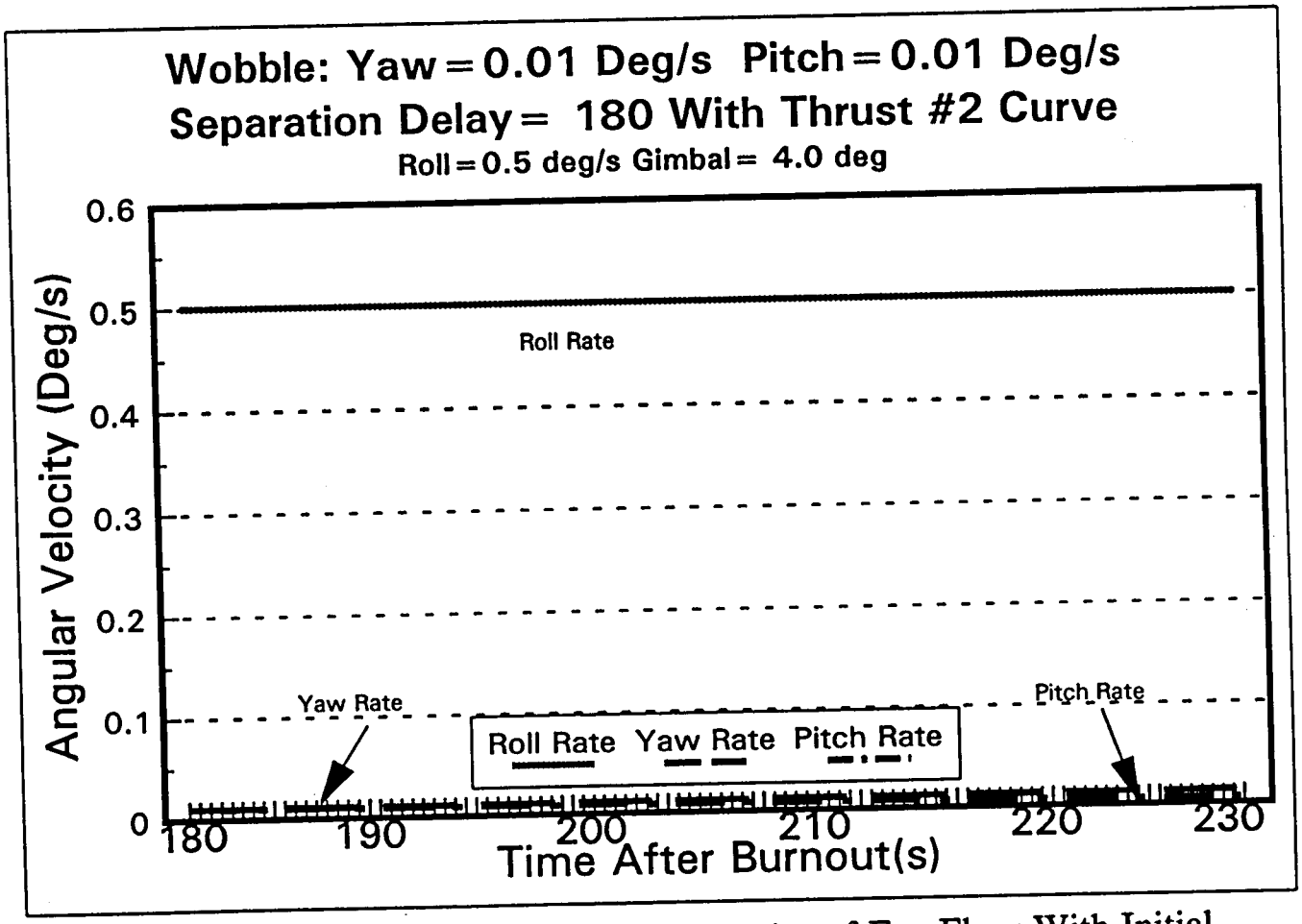


Figure 4.11 Inertial Angular Velocity of FreeFlyer With Initial Wobble Rates of 0.01°/s and 0.01°/s

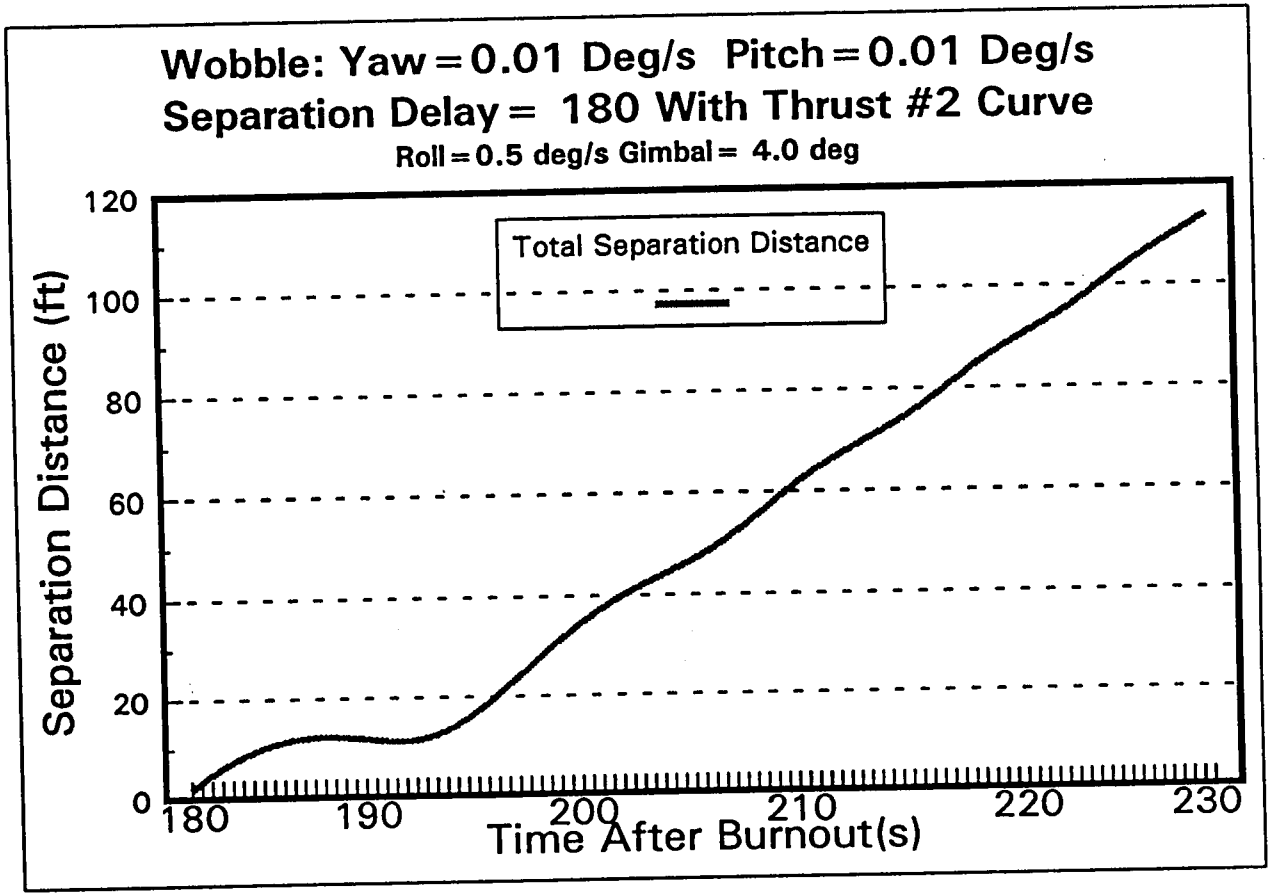


Figure 4.12 Total Inertial Separation Distance With Initial Wobble Rates of 0.01°/s and 0.01°/s

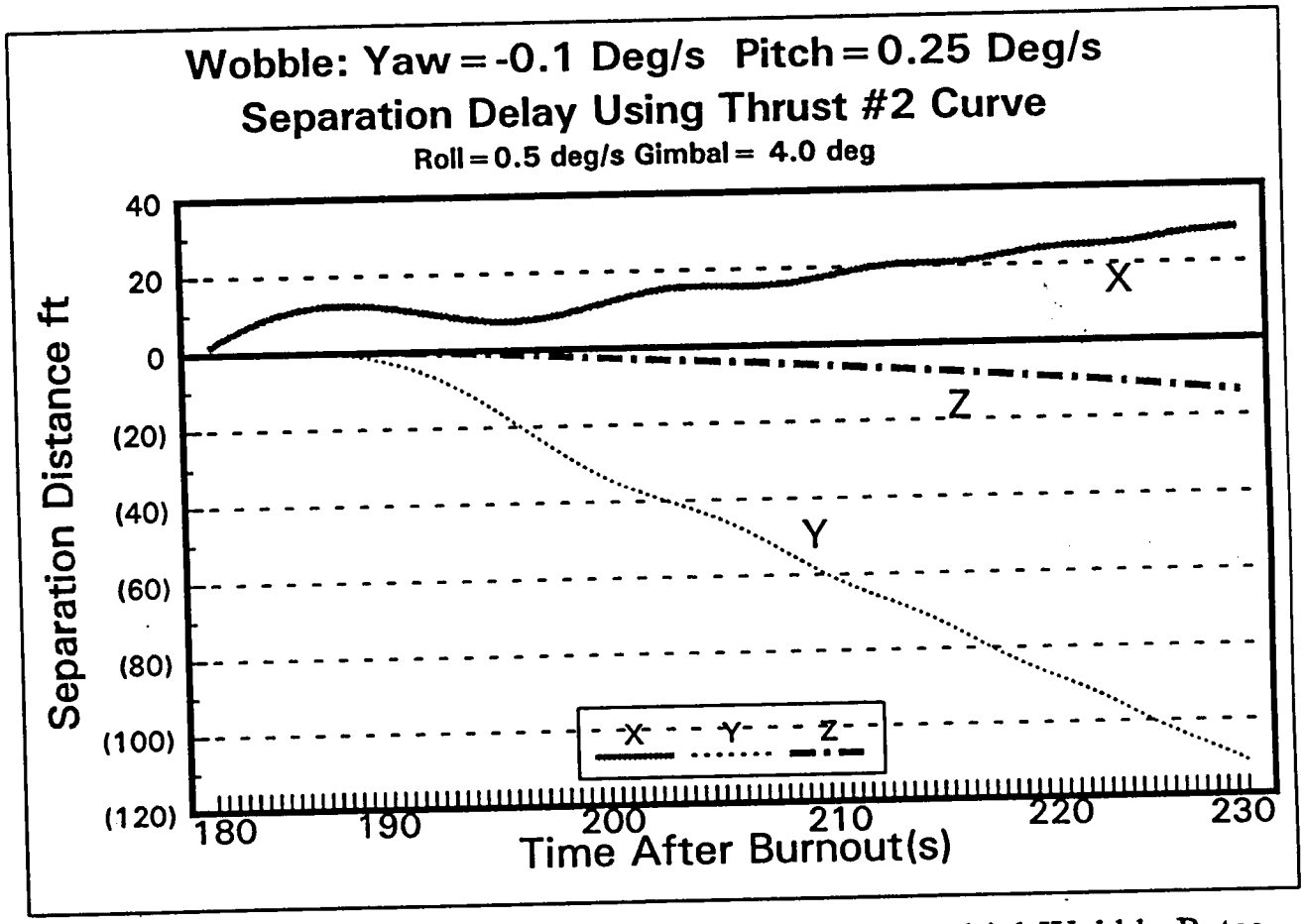


Figure 4.13 Inertial Separation Distance With Initial Wobble Rates of 0.1°/s and 0.25°/s

configuration, but with an increase in the order of magnitude of the yaw wobble rate and the pitch wobble rate to -0.1°/s and 0.25°/s respectively. The negative yaw wobble rate is also investigated since it is just as likely for a negative wobble rate to be applied to each body as a positive wobble rate. It will be seen, though, that the sign of the wobble rates does not play a significant roll in the success of the separation. By comparing Figure 4.13 to Figure 4.9 it can be seen that the increase in the magnitude of the wobble rates has very little effect upon the separation distance between the center of mass of the STAR-48V and the center of mass of the FreeFlyer. The angular velocity of the STAR-48V for an initial wobble rate of -0.1°/s and 0.25°/s can be seen in Figure 4.14 and the angular velocity of the FreeFlyer can be seen in Figure 4.15. It can be seen that both of these angular velocities are larger than the angular velocities as seen in Figure 4.10 and Figure 4.11, but these larger angular velocities are simply due to the larger initial wobble rates and it can be seen in Figure 4.16 that there is no effect upon the total separation distance as compared with the lesser wobble rates.

Figures 4.17 through 4.20 show the same results for a larger wobble rate of 1.0°/s in the yaw direction and 0.9°/s in the pitch direction. Again, from Figure 4.20, it can be seen that this increase in the order of magnitude of the wobble rates has had little effect upon the total separation distance between the center of mass of the STAR-48V and the center of mass of the FreeFlyer. There is, however, a slight change in the separation distances along all three inertial axes for these larger wobble rates as compared to the earlier wobble rates. This can be observed in Figure 4.17 and it can be compared with either Figure 4.13 or Figure 4.9. Even though the separation

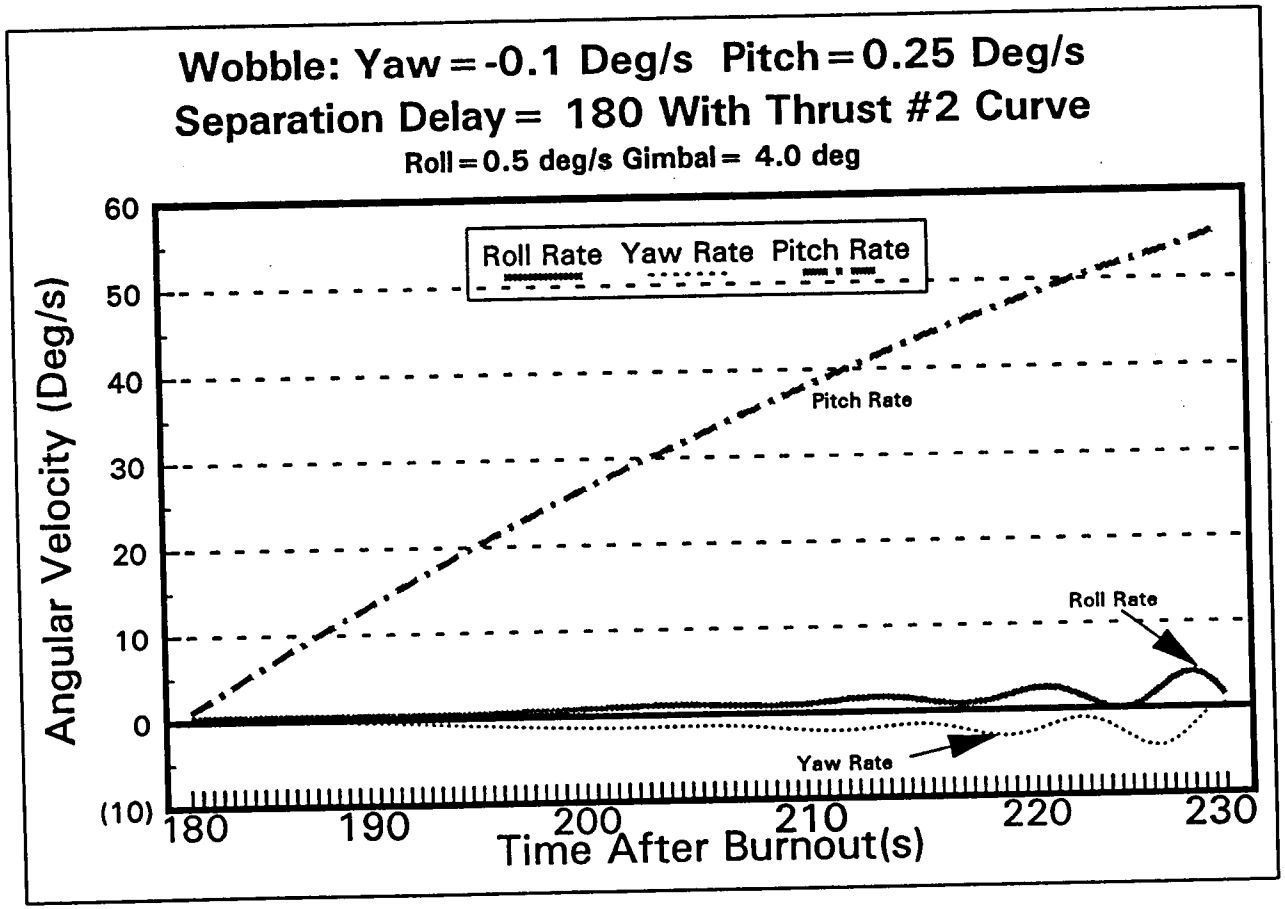


Figure 4.14 Inertial Angular Velocity of STAR-48V With Initial Wobble Rates of 0.1°/s and 0.25°/s

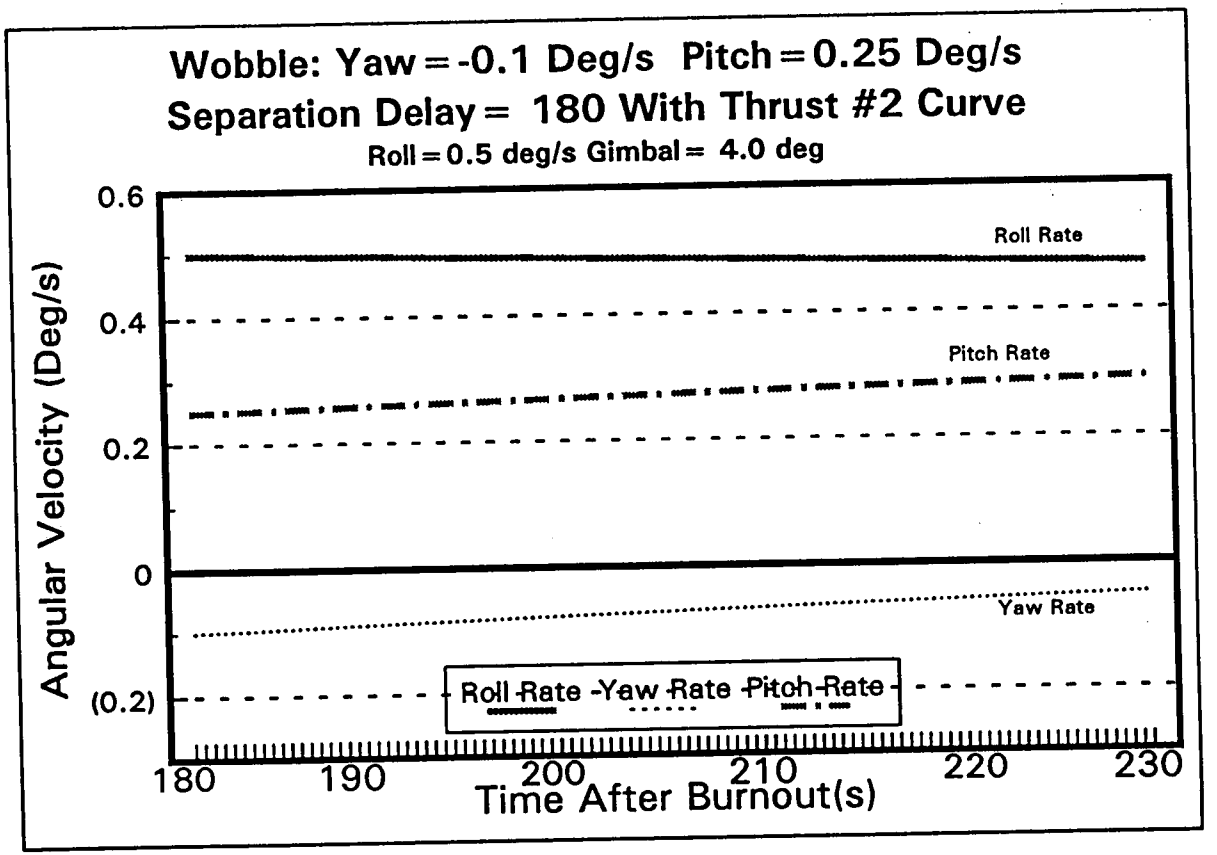


Figure 4.15 Inertial Angular Velocity of FreeFlyer With Initial Wobble Rates of 0.1°/s and 0.25°/s

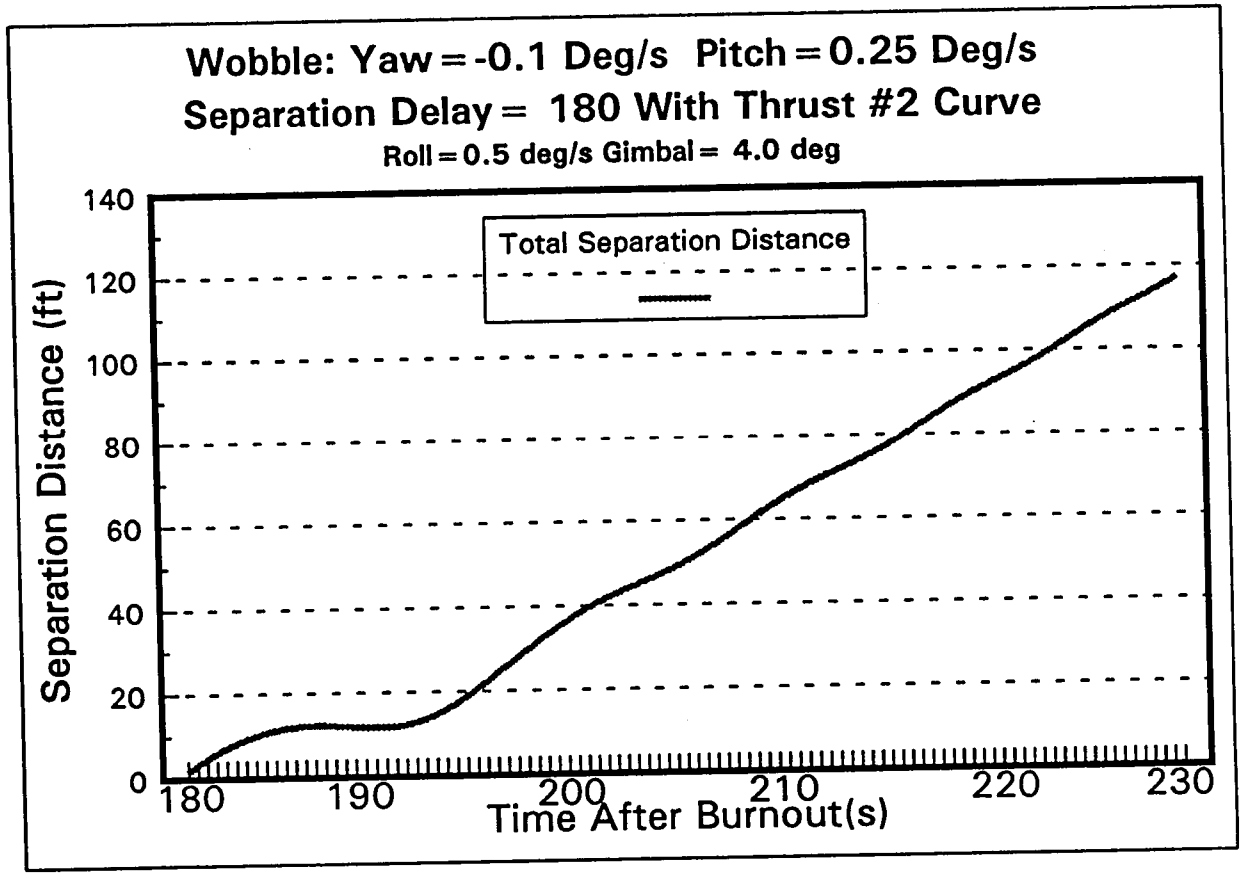


Figure 4.16 Total Inertial Separation Distance With Initial Wobble Rates of 0.1°/s and 0.25°/s

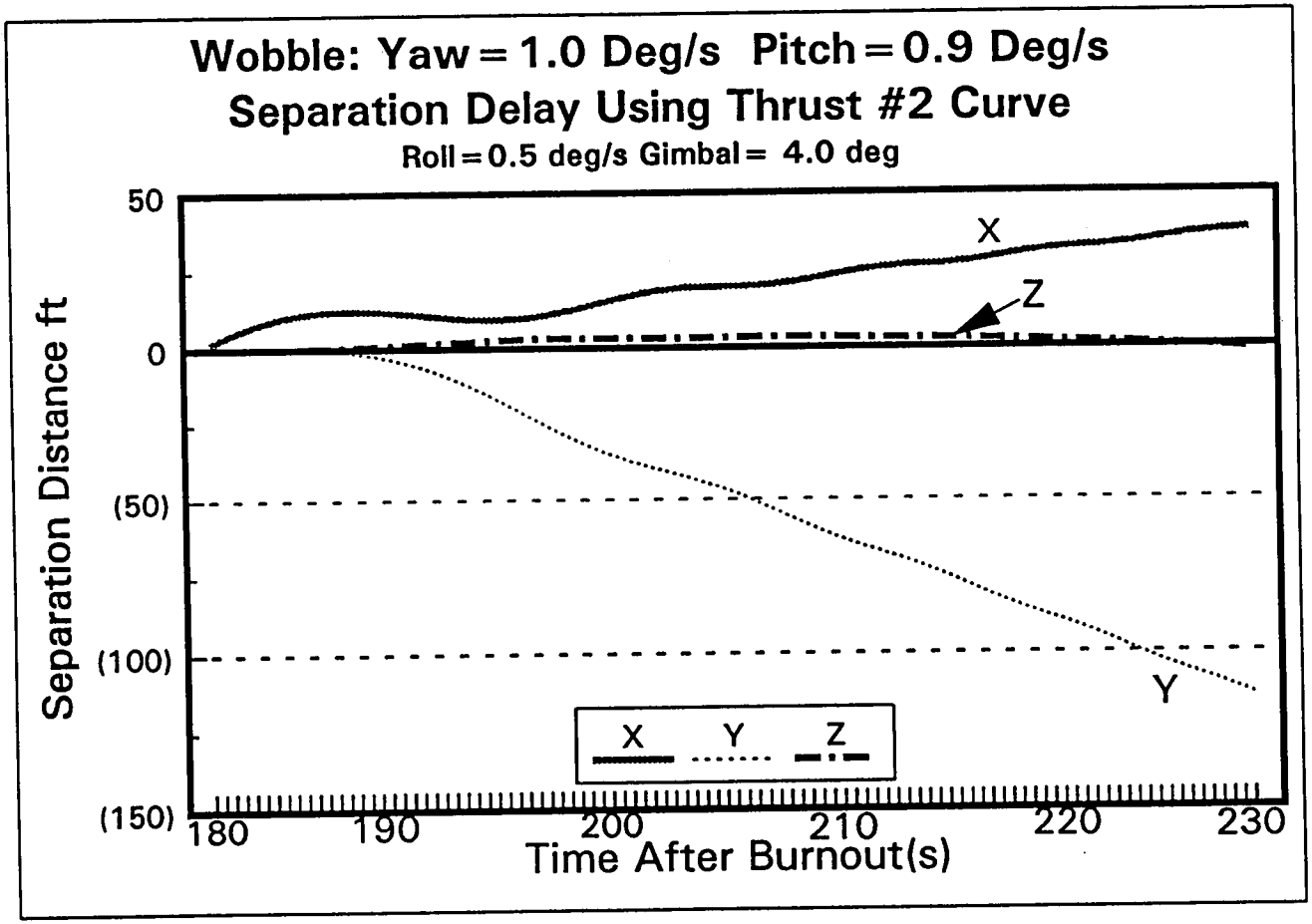


Figure 4.17 Inertial Separation Distance With Initial Wobble Rates of 1.0°/s and 0.9°/s

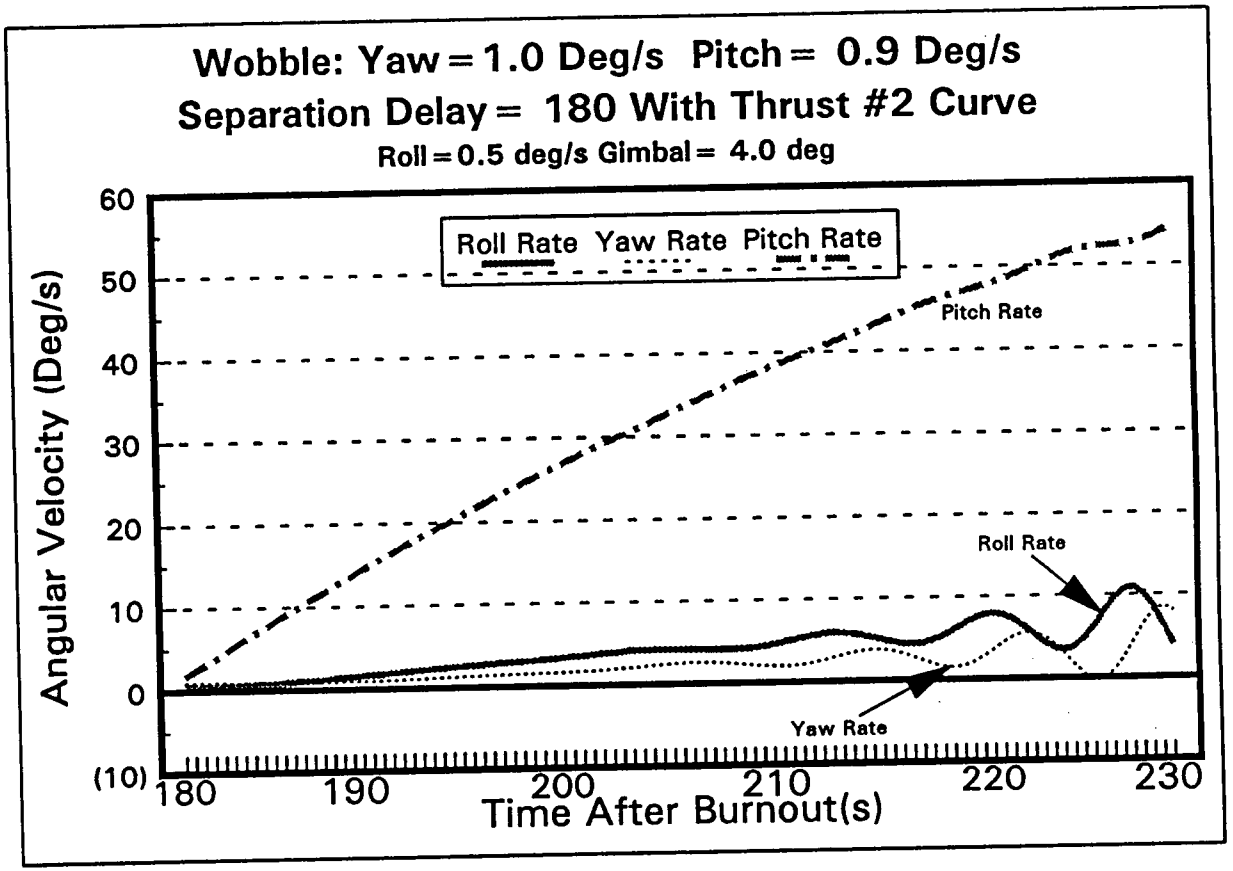


Figure 4.18 Inertial Angular Velocity of STAR-48V With Initial Wobble Rates of 1.0°/s and 0.9°/s

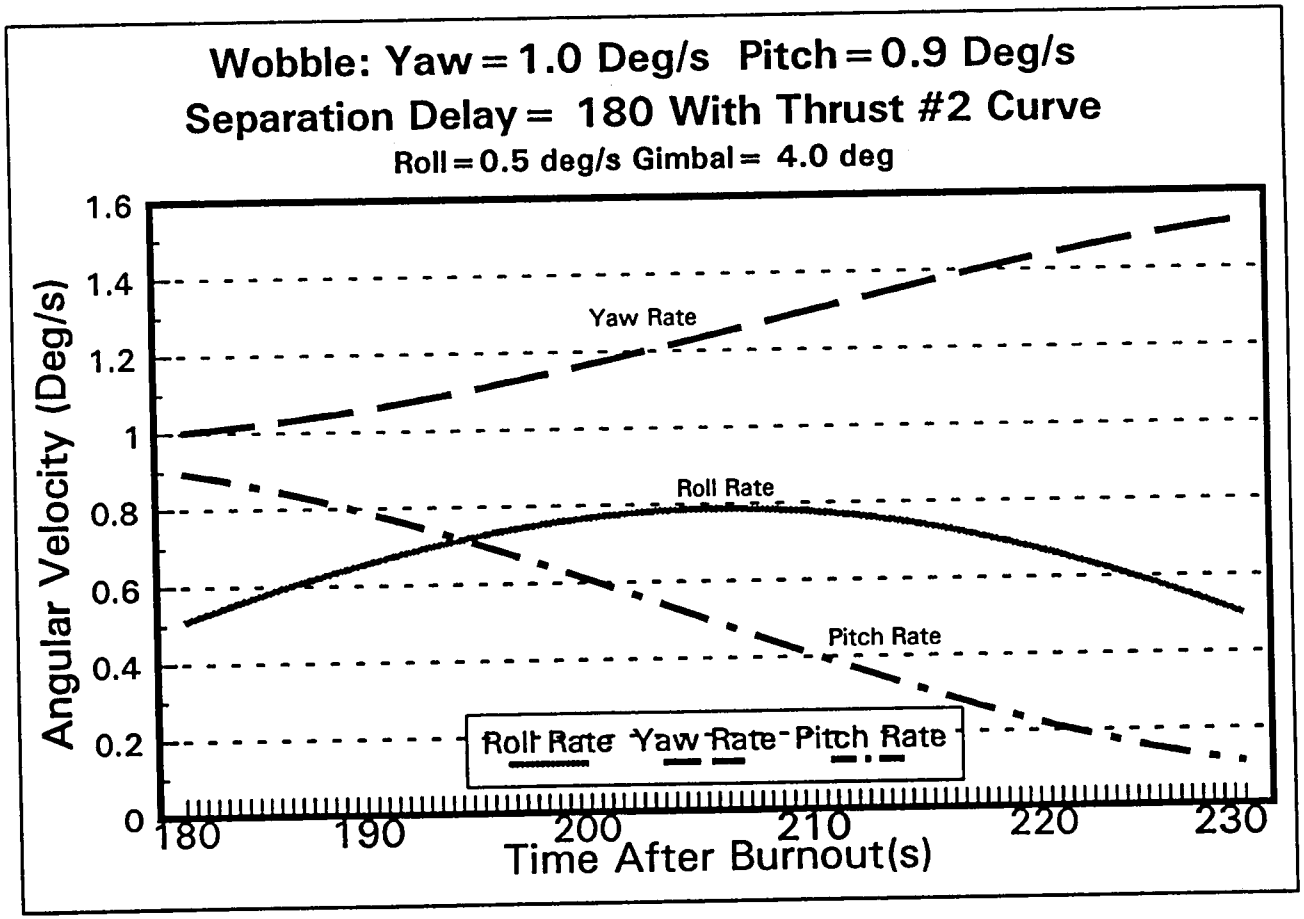


Figure 4.19 Inertial Angular Velocity of FreeFlyer With Initial Wobble Rates of 1.0°/s and 0.9°/s

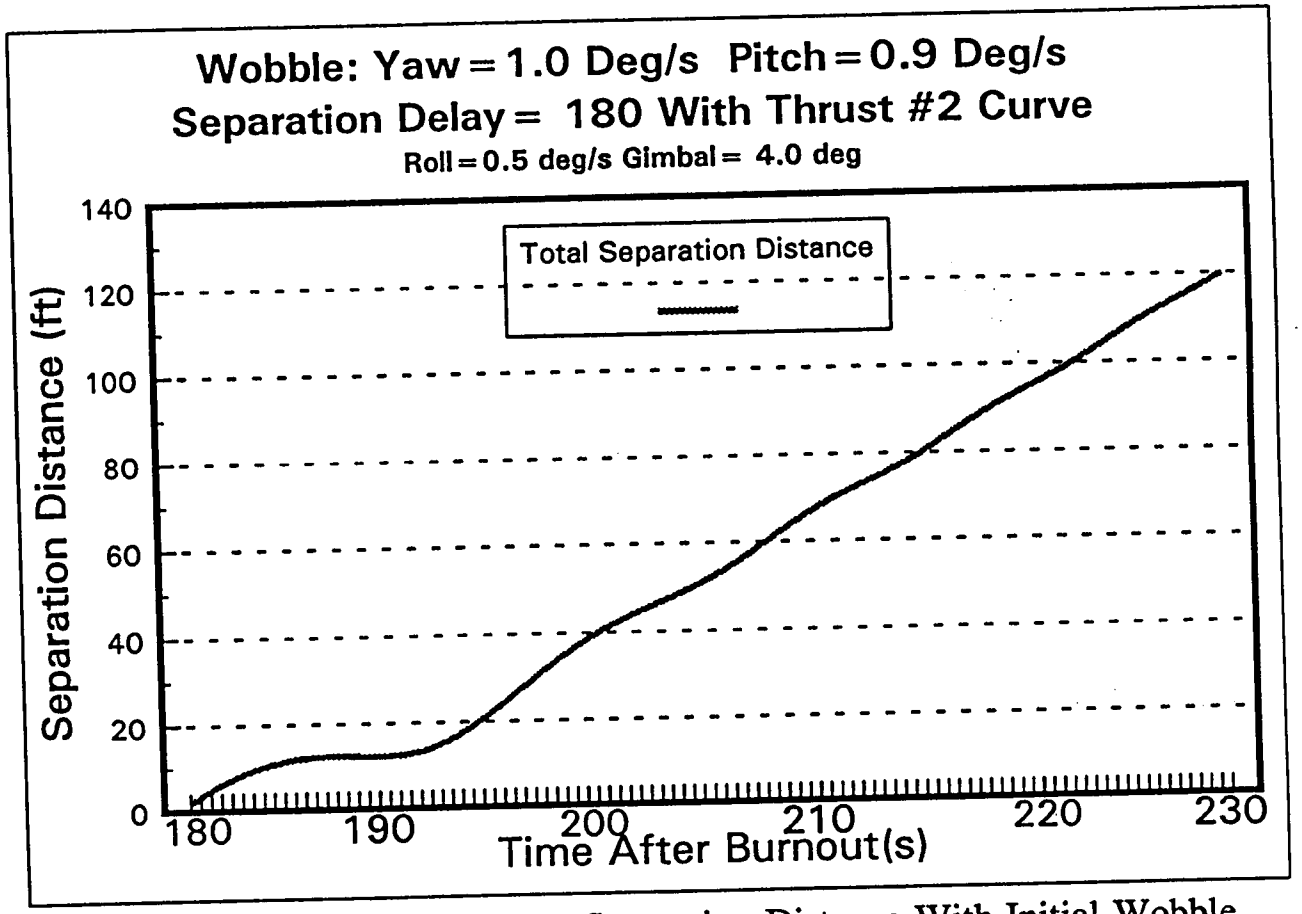


Figure 4.20 Total Inertial Separation Distance With Initial Wobble Rates of 1.0°/s and 0.5°/s

distances along each axis are somewhat altered in Figure 4.17 as compared to the lesser wobble rates in Figure 4.13 or Figure 4.9, the resultant total separation distance remains relatively unchanged for all three cases discussed up to this point.

It can also be seen in Figures 4.18 and 4.19 that the larger initial wobble rates have a more significant effect upon the angular velocity of both the STAR-48V and the FreeFlyer. This can especially be seen in Figure 4.19 for the FreeFlyer since the angular velocity vector of the FreeFlyer is not dominated by the relatively large pitch rate the way in which the STAR-48V is. Although these initial wobble rates do not have much effect upon the success of the separation, they do cause significant angular velocity oscillations on the FreeFlyer, as is evident in Figure 4.19, and these oscillations will have a negative effect upon the remainder of the COMET mission.

The results for very large initial wobble rates of -10.0°/s around the Y axis and 5.0°/s around the Z axis can be seen in Figures 4.20 through 4.24. In Figure 4.24 it can be seen that this high initial wobble rate does affect the total separation distance, but it acts to increase, not decrease, the minimum separation distance as compared with the other initial wobble rates as seen earlier. The separation distance along each inertial axis can be observed in Figure 4.21 for these very large wobble rates and it can be seen that the magnitude in both the X direction and in the Z direction are substantially larger than in Figure 4.9 for the smaller wobble case. It can also be seen that the separation distance in the Y direction is only slightly smaller for the very large wobble rate case as compared to the smaller wobble rate case. This shows that the separation between the STAR-48V and the FreeFlyer is successful even at these high

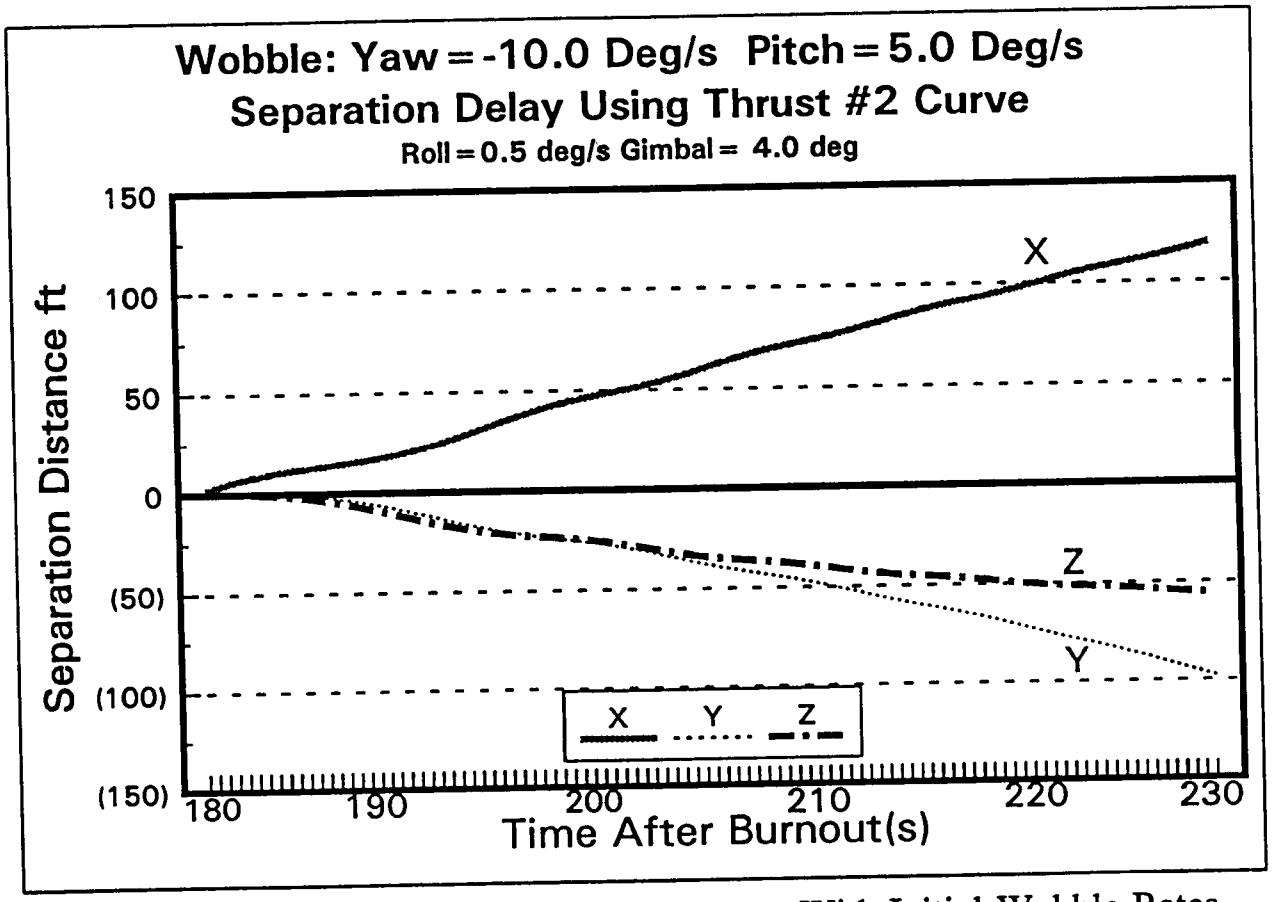


Figure 4.21 Inertial Separation Distance With Initial Wobble Rates of -10.0°/s and 5.0°/s

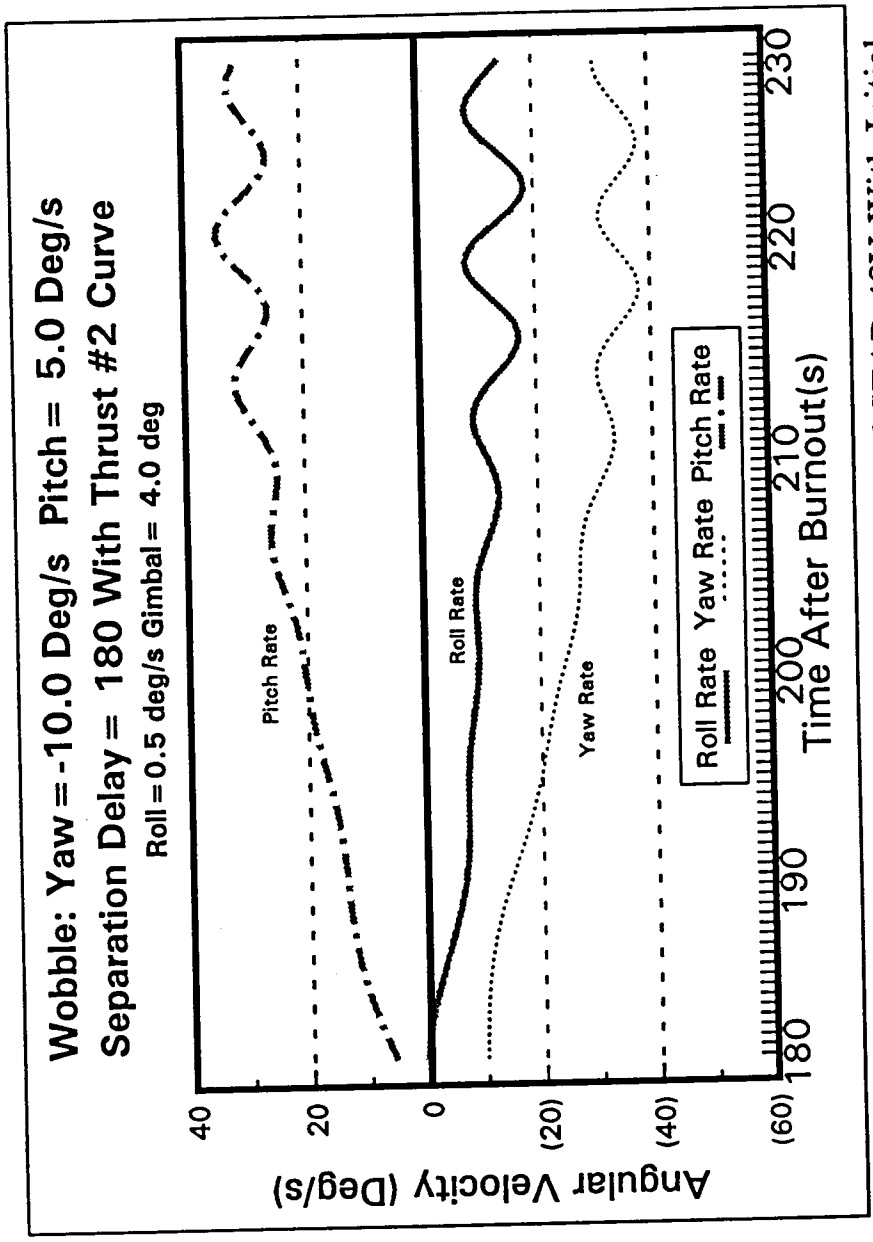


Figure 4.22 Inertial Angular Velocity of STAR-48V With Initial Wobble Rates of -10.0°/s and 5.0°/s

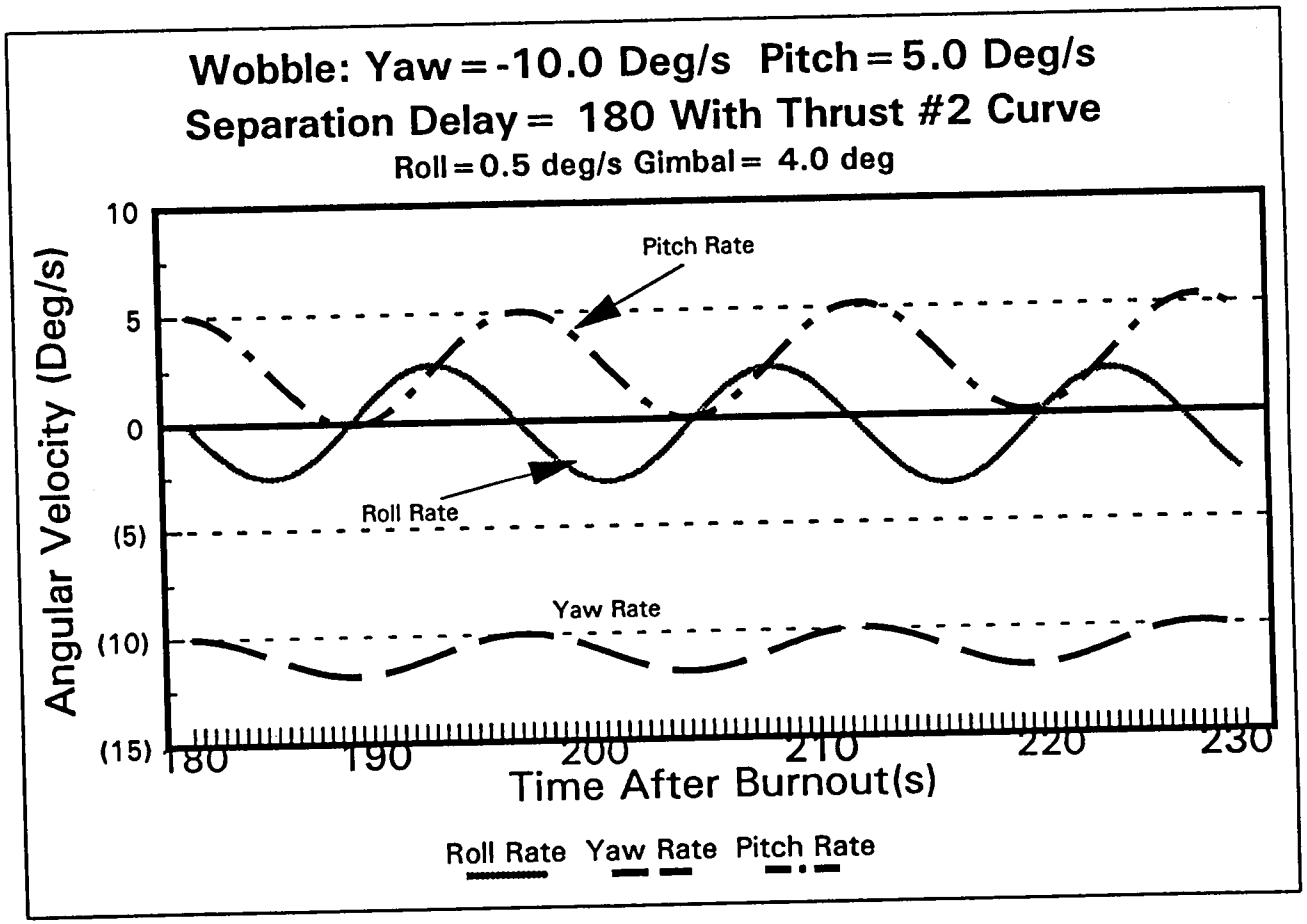


Figure 4.23 Inertial Angular Velocity of FreeFlyer With Initial Wobble Rates of -10.0°/s and 5.0°/s

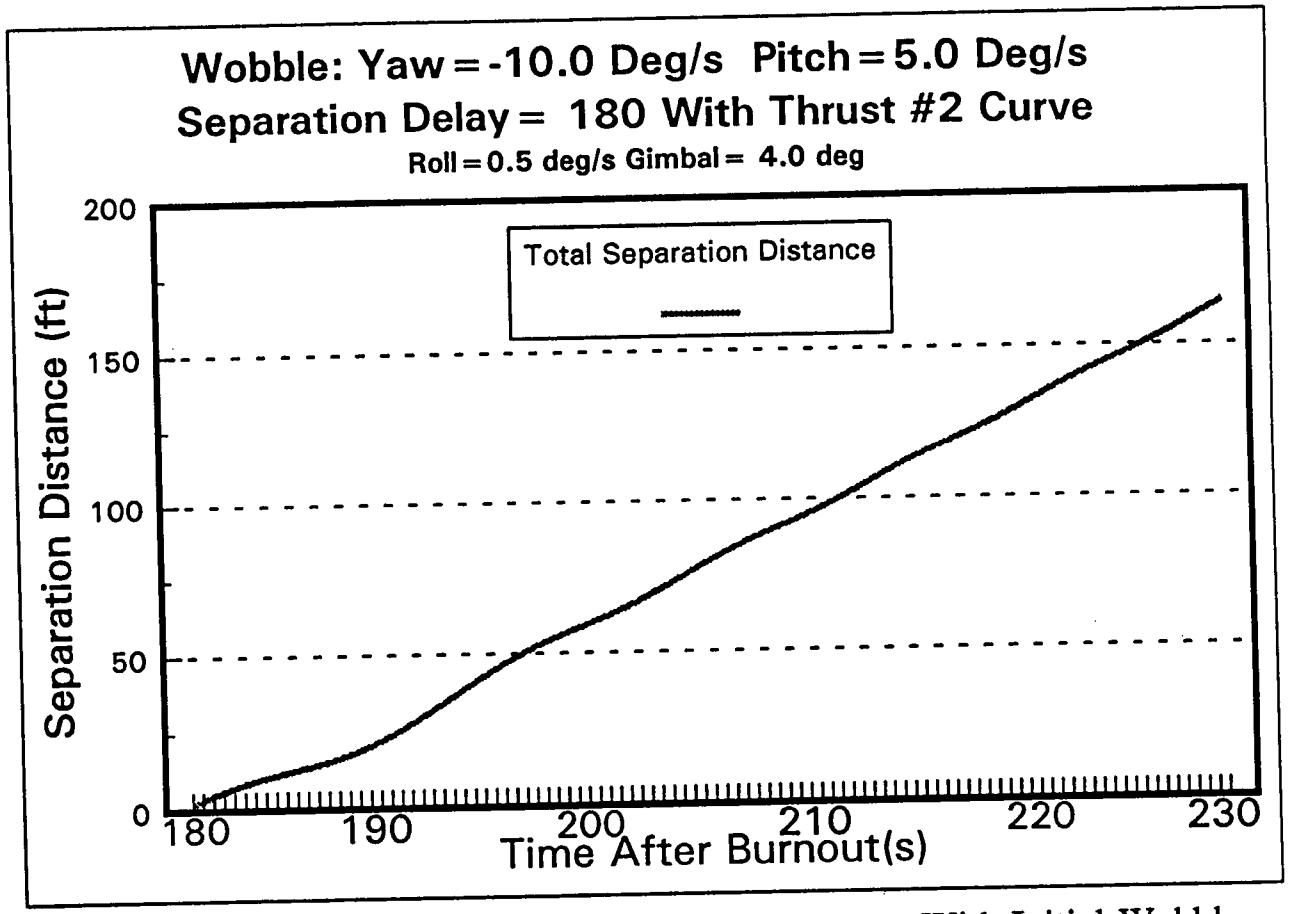


Figure 4.24 Total Inertial Separation Distance With Initial Wobble Rates of -10.0°/s and 5.0°/s

wobble rates. It is apparent, though, in Figure 4.22 and Figure 4.23, that these wobble rates cause very large oscillations in the angular velocity of both the STAR-48V and the FreeFlyer. These spin rates are acceptable for the STAR-48V since it is designed to tumble back through the atmosphere and burn up in the COMET mission anyway, but the FreeFlyer is designed to be as stable as possible after its separation from the STAR-48V. It can be seen in Figure 4.23 that the angular velocity of the FreeFlyer under these conditions is in no way conducive for the COMET mission. It is because of this reason that the initial wobble rates caused by the separation process, or any other process for that matter, need to be minimized. It can be seen in Figure 4.24 that the success of the separation is even achieved at the very high initial wobble rates of -10.0°/s and 5.0°/s.

There is a problem, though, if the initial wobble rates are much higher than 10.0°/s. These even higher rates will cause the STAR-48V and the FreeFlyer to wobble so fast that they wobble into each other before the spring system can initially separate these two bodies. But the chance of the magnitude of the wobble rate being of this order is very remote. As discussed earlier, much analysis has been performed upon the spring separation system and it is believed that the initial wobble rates will be on the order of 0.1°/s and could even be on the order of 0.01°/s. Since it has been shown here that wobble rates on the order of 1.0°/s pose little problem for the separation (although it may have adverse effects upon the remainder of the mission) it can be concluded that the chances that the initial wobble rates will cause a collision between the STAR-48V and the FreeFlyer will be very remote.

Chapter 5: Conclusions

From the preceding discussion in Chapter 3, it can be concluded that the separation between the STAR-48V and the COMET FreeFlyer will be successful under the expected conditions if the separation delay time between the nominal burnout of the STAR-48V and the initiation of the separation process is 180 seconds. It can also be concluded that the separation between these two bodies will be successful for all four thrust curves that were used to model the tail-off thrust characteristics of the STAR-48V rocket motor. Also in Chapter 3, it was determined that the thrust curve for the STAR-48 #2 test motor thrust data gives the highest probability for collision as compared to the other three thrust curves. It was concluded that by using this thrust curve to simulate the tail-off thrust that a worse case scenario for the collision would be produced and, thus, if the separation were successful using this curve, then the separation would be successful for the other three thrust curves as well.

In Section 4.1 it was concluded that the separation delay time could be reduced even a little further in order to reduce the weight of the power system. But since the separation delay time of 180 seconds has already been successfully designed into the mission, it was determined that it would be best to use the separation delay time of 180 seconds instead of the shorter delay time of 140 seconds. This is because the tail-off thrust of the STAR-48V with a separation delay time of 180 seconds would have a longer period of time in which to burn the remaining unwanted fuel on-board the STAR-48V. This extra burning period, with the separation delay time of 180 seconds, results in a reduction in the possibility of collision between the STAR-48V and the

FreeFlyer than if the separation were to be initiated at the minimum separation delay time of 140 seconds.

Also in Chapter 4, it was seen that the separation will be successful even if some of the configuration variables are altered at the separation delay time of 180 seconds. In Section 4.2 it was concluded that the gimballing ability of the STAR-48V Motor nozzle is critical in order for there to be a safe separation. Without the gimballing of this nozzle immediately after separation has been initiated, the STAR-48V will collide with the FreeFlyer. But it was also concluded that a nozzle gimbal angle of only 1° is necessary in order for there to be successful separation. Since the gimbal angle is designed to be 4°, there is a fairly large tolerance in the size of the expected gimbal angle and the size of the minimum gimbal angle required to ensure a safe separation. Therefore, it is concluded that the chances that the STAR-48V nozzle will be gimbaled by at least 1° is fairly large. Of all of the configuration variables studied in this thesis, though, it is the gimbal angle that poses the largest threat to the success of the separation between the FreeFlyer and the STAR-48V.

In Section 4.3, it was concluded that the initial roll rate of the STAR-48V and the FreeFlyer has little effect upon the success of the separation as long as the initial roll rate is below about 25°/s. Again, there is a large tolerance between the anticipated initial roll rate of 0.5°/s and the initial roll rate of 25°/s where the effects of spin stabilization become apparent. In Section 4.4, it was seen that the STAR-48V and the FreeFlyer could even be subjected to some fairly high initial wobble rates without much effect upon the success of the separation. Therefore it was determined that the initial

wobble rates applied to both the STAR-48V and the FreeFlyer will not effect the success of the separation as long as these rates are not significantly larger than about 10°/s. These initial wobble rates, though, do affect the stability of the FreeFlyer for the remainder of the mission. They are allowable for the separation process but, because of this stability problem, it has been concluded that it is best to design the separation spring system such that these initial wobble rates will be minimized. It is the stability problem, not the separation problem, that drives this conclusion.

Considering all of the analysis performed on the separation dynamics between the STAR-48V and the COMET FreeFlyer in this thesis, it is believed that the separation delay time of 180 seconds is sufficient in order to avoid re-contact with the COMET FreeFlyer.

Bibliography

Bibliography

1). Beletskii, V.V. *Motion of an Artificial Satellite About its Center of Mass.* Jerusalem, Isreal: Isreal Program for Scientific Translations, 1966.

2). Carmen, J.B. and D.W. Hill and J.P. Christopher. *Store Separation Testing Techniques at the Arnold Engineering Development Center.* Volume II. Tullahoma, Tennessee: ARO, Inc., AEDC Division, 1980.

3). Center for Space Transportation and Applied Research (CSTAR). *Customer's Operational Guide.* Tullahoma, Tennessee: CSTAR, 1992.

4). Chety, P.R.K. *Satellite Technology and its Applications.* Blue Ridge Summit, Pennsylvania: Tab Books, Inc., 1988.

5). Chobotov, Vladimir A. *Spacecraft Attitude Dynamics and Control.* Malabar, Florida: Krieger Publishing Company, 1991.

6). Daniels, Mark. Telephone Conversation, March 1993.

7). Fortescue, Peter W. and John P. Stark. *Spacecraft Systems Engineering.* Chinchester, England: John Wiley & Sons, LTD, 1991.

8). Fowles, Grant R. *Analytical Mechanics.* Fourth Edition. New York: Saunders College Publishing, 1986.

9). Greenwood, Donald T. *Principles of Dynamics.* Englewood Cliffs, New Jersey: Prentice-Hall, Inc., 1988.

10). Goldstein, Herbert. *Classical Mechanics.* Reading, Massachusets: Addison-Wesely Publishing Company, 1980.

11). Isakewitz, Steven J. *International Reference Guide to Space Launch Systems.* Washington D.C.: American Institute of Aeronautics and Astronautics, 1991.

12). Kaplan, Marshall H. *Modern Spacecraft Dynamics and Control.* New York: John Wiley & Sons, 1976.

13). Meirovitch, Leonard. *Method of Analytical Dynamics.* New York: McGraw-Hill Book Company, 1970.

14). Pilpott, William. "AEDC STAR-48 Thrust Test Data". Tullahoma: AEDC, 1994.

15). Reiss, Keith W. *"COMET Study and Options for STAR-48/FreeFlyer Separation"*. Vienna, Virginia: EER Corporation, October 19,1992.

16). Thiokol Corporation. *Thiokol Corporation Space Motor Catalog*. Elkton, Maryland: Thiokol Corporation, 1992.

17). Thompson, William Tyrrell. *Introduction to Space Dynamics*. New York: Dover Publications, Inc., 1986.

18). Webster, Arthur Gordon. *The Dynamics of Particles and of Rigid, Elastic, and Fluid Bodies*. New York: G.E. Stechert and Company, 1922.

19). Wells, Dare A. *Theory and Problems of Lagrangian Dynamics*. Schaum's Outline Series. New York: McGraw-Hill Book Company, 1967.

20). Wertz, James R. *Spacecraft Attitude Determination and Control*. Dordrecht, The Netherlands: Kluwer Academic Publishers, 1978.

21). Wiesel, William E. *Spaceflight Dynamics*. New York: McGraw-Hill Book Company, 1989.

22). Woodhouse, N.M.J. *Introduction to Analytical Dynamics*. Oxford, England: Oxford University Press, 1987.

Appendices

Appendix 1: The Equations of Motion for a Rigid Body

Let B in Figure A1.1 be an arbitrary rigid body with center of mass, c. The coordinate system OXYZ is inertial while the coordinate system cxyz is body-fixed. Further more, ω is the angular velocity vector of the body.

When c is chosen as the origin of the body-fixed coordinate system, the translational motion and the rotational motion of the body decouple and the equations of motion become

$$\mathbf{F} = m\, d^2(\mathbf{R}_c)/dt^2 \tag{A1.1}$$

$$\mathbf{N}_c = \mathbf{I}\, d(\omega)/dt + \omega \times \mathbf{I}\omega \tag{A1.2}$$

where m is the total mass of the body, $\mathbf{R}_c$ is the inertial position vector of c, and $\mathbf{F}$ is the resultant vector of all of the external forces that act on the body. Furthermore, $\mathbf{N}_c$ is the moment vector about c and

$$\mathbf{I} = \begin{bmatrix} I_{xx} & 0 & 0 \\ 0 & I_{yy} & 0 \\ 0 & 0 & I_{zz} \end{bmatrix} \tag{A1.3}$$

where I_{xx}, I_{yy}, and I_{zz} are the principal moments of inertia about the principal axes x, y, and z, respectively. Also, $d(\omega)/dt$ is the time rate of change of ω as seen by a relative observer attached to cxyz. It turns out, however, that $d(\omega)/dt$ is the same as the time rate of change as seen by an absolute observer attached to OXYZ.

The attitude or orientation of the rigid body relative to OXYZ can be determined by a set of Euler angles, ϕ, θ, and ψ. Choosing a 3-1-3 set of Euler angles yields

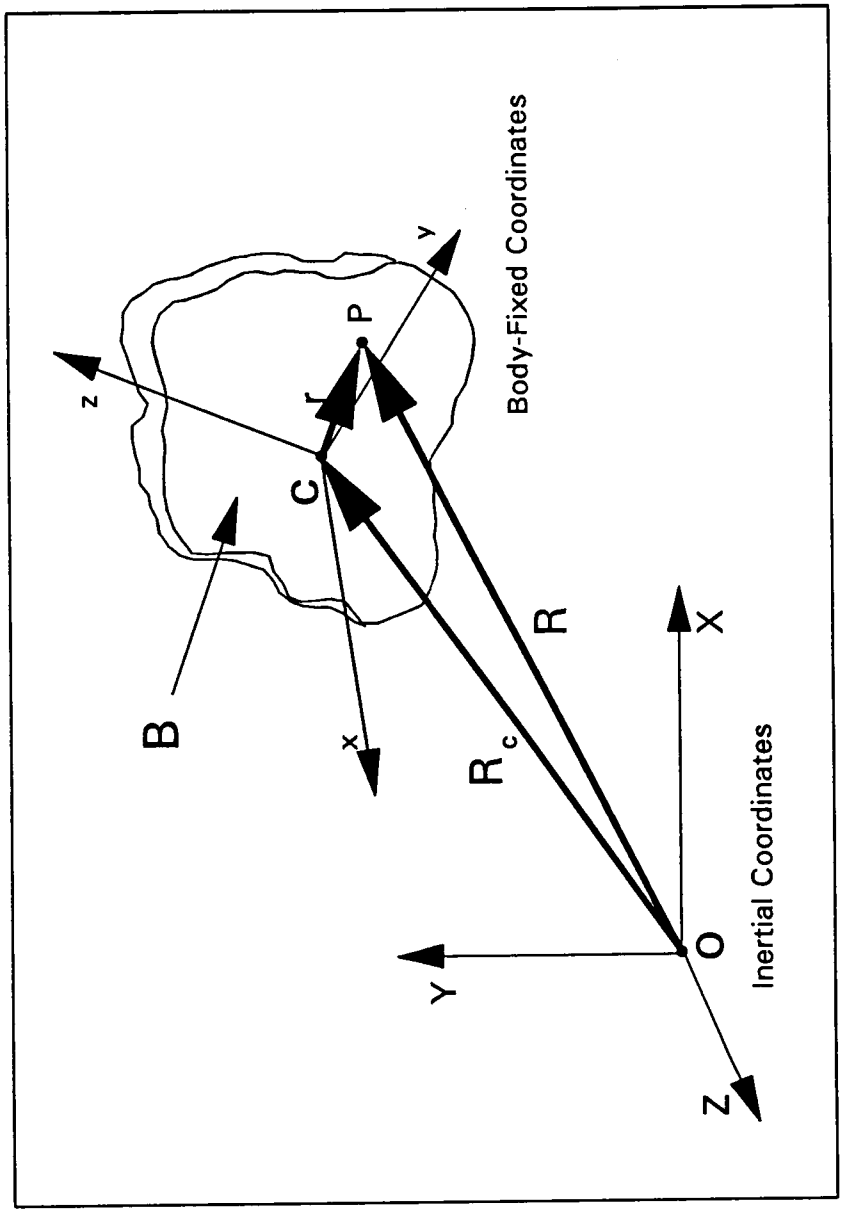


Figure A1.1 Arbitrary Rigid Body in Space

$$\begin{bmatrix} u_x \\ u_y \\ u_z \end{bmatrix} = R(\phi, \theta, \psi) \begin{bmatrix} u_X \\ u_Y \\ u_Z \end{bmatrix} \qquad \text{(A1.4)}$$

where

$$\mathbf{u} = u_X \mathbf{I} + u_Y \mathbf{J} + u_Z \mathbf{K} = u_x \mathbf{i} + u_y \mathbf{j} + u_z \mathbf{k} \qquad \text{(A1.5)}$$

is an arbitrary vector expressed in the OXYZ and cxyz coordinate systems, respectively, and

$$R(\phi, \theta, \psi) = \begin{bmatrix} C\psi C\phi - C\theta S\psi S\phi & C\psi S\phi + C\theta S\psi C\phi & S\theta S\psi \\ -S\psi C\phi - C\theta C\psi S\phi & -S\psi S\phi + C\theta C\psi C\phi & S\theta C\psi \\ S\theta S\phi & -S\theta C\phi & C\theta \end{bmatrix} \qquad \text{(A1.6)}$$

is an orthogonal transformation matrix with C = Cos and S = Sin. Therefore,

$$\begin{bmatrix} u_X \\ u_Y \\ u_Z \end{bmatrix} = R^T(\phi, \theta, \psi) \begin{bmatrix} u_x \\ u_y \\ u_z \end{bmatrix} \qquad \text{(A1.7)}$$

Equation (A1.4) and equation (A1.7) yield the relationship between the components of a vector in the OXYZ coordinate system and the components of this same vector as described in the cxyz coordinate system.

Finally, the components of ω relative to the cxyz coordinate system can be related to the time derivatives of the Euler angles as

$$\begin{bmatrix} \omega_x \\ \omega_y \\ \omega_z \end{bmatrix} = \begin{bmatrix} Sin\ \theta Sin\ \psi & Cos\ \psi & 0 \\ Sin\ \theta Cos\ \psi & -Sin\ \psi & 0 \\ Cos\ \theta & 0 & 1 \end{bmatrix} \begin{bmatrix} d(\phi)/dt \\ d(\theta)/dt \\ d(\psi)/dt \end{bmatrix} \tag{A1.8}$$

or in inverse form

$$\begin{bmatrix} d(\phi)/dt \\ d(\theta)/dt \\ d(\psi)/dt \end{bmatrix} = \begin{bmatrix} Sin\ \psi / Sin\ \theta & Cos\ \psi / Sin\ \theta & 0 \\ Cos\ \psi & -Sin\ \psi & 0 \\ -Sin\ \psi Cot\ \theta & -Cos\ \psi Cot\ \theta & 1 \end{bmatrix} \begin{vmatrix} \omega_x \\ \omega_y \\ \omega_z \end{vmatrix} \tag{A1.9}$$

Appendix 2: STAR-48 Tail-off Thrust Test Data

Table A2.1 shows the AEDC Test Data as compiled by Mr. Billy Philpott of AEDC for the STAR-48 #1 test motor. The second column in this table is the time after the nominal burnout of the motor, the third column is the chamber pressure of the STAR-48, and the fourth column is the tail-off thrust force being produced by a comparable STAR-48V motor. Also, the fifth column labeled MFR is the mass flow rate of a comparable STAR-48V and the next column to the right is the time step between data points. From this data, the amount of propellant that is burned during each time step is determined and this data is given in the seventh column labeled Flow Mass. The final column to the right is a running sum of the burned propellant and from the last entry in this column, it can be seen that the amount of propellant burned during the first 30 seconds after nominal burnout of the STAR-48 is 3.18 lbs. Since the mass flow curve is an exponentially decaying curve, it can be concluded that the amount of propellant burned during the entire time frame under consideration is only about 5 lbs. This can be also concluded for the other STAR-48 test motors, as can be seen in Table A2.2 and Table A2.3. Also, Figure A2.1 shows the thrust as a function of time for the STAR-48 #1 test motor and the curve fit associated with it.

Table A2.2 shows the same columns as above for the STAR-48 #2 test motor and Figure A2.2 shows the thrust for this same motor as a function of time, along with the curve fit. Table A2.3 and Figure A2.3 shows similar data for the STAR-48 #3 test motor. In Figure A2.4, the thrust curve as determined by the equation developed by

Dr. Reiss can be observed and, finally, the data associated with this curve can be observed in Table A2.4.

Table A2.1 STAR-48 #1 Test Data

	Time(s)	Pres(PSIA)	THRUST(lbf)	MFR(lbm/s)	dt(s)	Flow Mass lbm	FM Sum lbm
1	0.000	4.480	133.862	0.458	0.200	0.092	0.092
2	0.200	3.780	112.946	0.387	0.200	0.077	0.169
3	0.400	3.340	99.799	0.342	0.200	0.068	0.237
4	0.600	3.010	89.939	0.308	0.200	0.062	0.299
5	0.800	2.860	85.457	0.293	0.200	0.059	0.357
6	1.000	2.740	81.871	0.280	0.200	0.056	0.413
7	1.200	2.690	80.377	0.275	0.200	0.055	0.469
8	1.400	2.640	78.883	0.270	0.200	0.054	0.523
9	1.600	2.520	75.298	0.258	0.200	0.052	0.574
10	1.800	2.330	69.620	0.238	0.200	0.048	0.622
11	2.000	2.200	65.736	0.225	0.200	0.045	0.667
12	2.200	2.110	63.047	0.216	0.200	0.043	0.710
13	2.400	1.970	58.864	0.202	0.200	0.040	0.750
14	2.600	1.850	55.278	0.189	0.200	0.038	0.788
15	2.800	1.790	53.485	0.183	0.200	0.037	0.825
16	3.000	1.730	51.692	0.177	0.200	0.035	0.860
17	3.200	1.650	49.302	0.169	0.200	0.034	0.894
18	3.400	1.560	46.613	0.160	0.200	0.032	0.926
19	3.600	1.510	45.119	0.154	0.200	0.031	0.957
20	3.800	1.460	43.625	0.149	0.200	0.030	0.987
21	4.000	1.420	42.430	0.145	0.200	0.029	1.016
22	4.200	1.380	41.234	0.141	0.200	0.028	1.044
23	4.400	1.350	40.338	0.138	0.200	0.028	1.071
24	4.600	1.323	39.531	0.135	0.200	0.027	1.098
25	4.800	1.290	38.545	0.132	0.200	0.026	1.125
26	5.000	1.260	37.649	0.129	0.200	0.026	1.151
27	5.200	1.230	36.752	0.126	0.200	0.025	1.176
28	5.400	1.220	36.454	0.125	0.200	0.025	1.201
29	5.600	1.190	35.557	0.122	0.200	0.024	1.225
30	5.800	1.180	35.258	0.121	0.200	0.024	1.249
31	6.000	1.160	34.661	0.119	0.200	0.024	1.273
32	6.200	1.140	34.063	0.117	0.200	0.023	1.296
33	6.400	1.130	33.764	0.116	0.200	0.023	1.319
34	6.600	1.120	33.466	0.115	0.200	0.023	1.342
35	6.800	1.110	33.167	0.114	0.200	0.023	1.365
36	7.000	1.090	32.569	0.112	0.200	0.022	1.387
37	7.200	1.090	32.569	0.112	0.200	0.022	1.410
38	7.400	1.070	31.972	0.109	0.200	0.022	1.432
39	7.600	1.060	31.673	0.108	0.200	0.022	1.453
40	7.800	1.050	31.374	0.107	0.200	0.021	1.475
41	8.000	1.040	31.075	0.106	0.200	0.021	1.496
42	8.200	1.040	31.075	0.106	0.200	0.021	1.517
43	8.400	1.030	30.776	0.105	0.200	0.021	1.538
44	8.600	1.020	30.478	0.104	0.200	0.021	1.559
45	8.800	1.000	29.880	0.102	0.200	0.020	1.580
46	9.000	1.010	30.179	0.103	0.200	0.021	1.600
47	9.200	0.974	29.103	0.100	0.200	0.020	1.620
48	9.400	0.959	28.655	0.098	0.200	0.020	1.640
49	9.600	0.945	28.237	0.097	0.200	0.019	1.659
50	9.800	0.927	27.699	0.095	0.200	0.019	1.678
51	10.000	0.915	27.340	0.094	0.200	0.019	1.697
52	10.200	0.908	27.131	0.093	0.200	0.019	1.715
53	10.400	0.907	27.101	0.093	0.200	0.019	1.734
54	10.600	0.899	26.862	0.092	0.200	0.018	1.752
55	10.800	0.890	26.593	0.091	0.200	0.018	1.771
56	11.000	0.877	26.205	0.090	0.200	0.018	1.789

Table A2.1 STAR-48 #1 Test Data

	Time(s)	Pres(PSIA)	THRUST(lbf)	MFR(lbm/s)	dt(s)	Flow Mass lbm	FM Sum lbm
57	11.200	0.870	25.996	0.089	0.200	0.018	1.806
58	11.400	0.860	25.697	0.088	0.200	0.018	1.824
59	11.600	0.853	25.488	0.087	0.200	0.017	1.841
60	11.800	0.860	25.697	0.088	0.200	0.018	1.859
61	12.000	0.852	25.458	0.087	0.200	0.017	1.876
62	12.200	0.844	25.219	0.086	0.200	0.017	1.894
63	12.400	0.833	24.890	0.085	0.200	0.017	1.911
64	12.600	0.832	24.860	0.085	0.200	0.017	1.928
65	12.800	0.834	24.920	0.085	0.200	0.017	1.945
66	13.000	0.837	25.010	0.086	0.200	0.017	1.962
67	13.200	0.831	24.830	0.085	0.200	0.017	1.979
68	13.400	0.817	24.412	0.084	0.200	0.017	1.996
69	13.600	0.809	24.173	0.083	0.200	0.017	2.012
70	13.800	0.804	24.024	0.082	0.200	0.016	2.029
71	14.000	0.807	24.113	0.083	0.200	0.017	2.045
72	14.200	0.807	24.113	0.083	0.200	0.017	2.062
73	14.400	0.808	24.143	0.083	0.200	0.017	2.078
74	14.600	0.802	23.964	0.082	0.200	0.016	2.095
75	14.800	0.794	23.725	0.081	0.200	0.016	2.111
76	15.000	0.785	23.456	0.080	0.200	0.016	2.127
77	15.200	0.774	23.127	0.079	0.200	0.016	2.143
78	15.400	0.778	23.247	0.080	0.200	0.016	2.159
79	15.600	0.808	24.143	0.083	0.200	0.017	2.175
80	15.800	0.782	23.366	0.080	0.200	0.016	2.191
81	16.000	0.762	22.769	0.078	0.200	0.016	2.207
82	16.200	0.761	22.739	0.078	0.200	0.016	2.222
83	16.400	0.760	22.709	0.078	0.200	0.016	2.238
84	16.600	0.758	22.649	0.078	0.200	0.016	2.253
85	16.800	0.754	22.530	0.077	0.200	0.015	2.269
86	17.000	0.747	22.320	0.076	0.200	0.015	2.284
87	17.200	0.725	21.663	0.074	0.200	0.015	2.299
88	17.400	0.716	21.394	0.073	0.200	0.015	2.314
89	17.600	0.706	21.095	0.072	0.200	0.014	2.328
90	17.800	0.705	21.065	0.072	0.200	0.014	2.343
91	18.000	0.701	20.946	0.072	0.200	0.014	2.357
92	18.200	0.699	20.886	0.072	0.200	0.014	2.371
93	18.400	0.691	20.647	0.071	0.200	0.014	2.385
94	18.600	0.686	20.498	0.070	0.200	0.014	2.399
95	18.800	0.680	20.318	0.070	0.200	0.014	2.413
96	19.000	0.685	20.468	0.070	0.200	0.014	2.427
97	19.200	0.670	20.020	0.069	0.200	0.014	2.441
98	19.400	0.671	20.049	0.069	0.200	0.014	2.455
99	19.600	0.675	20.169	0.069	0.200	0.014	2.468
100	19.800	0.667	19.930	0.068	0.200	0.014	2.482
101	20.000	0.659	19.691	0.067	0.200	0.013	2.496
102	20.200	0.655	19.571	0.067	0.200	0.013	2.509
103	20.400	0.650	19.422	0.066	0.200	0.013	2.522
104	20.600	0.648	19.362	0.066	0.200	0.013	2.536
105	20.800	0.648	19.362	0.066	0.200	0.013	2.549
106	21.000	0.648	19.362	0.066	0.200	0.013	2.562
107	21.500	0.634	18.944	0.065	0.500	0.032	2.595
108	22.000	0.670	20.020	0.069	0.500	0.034	2.629
109	22.500	0.675	20.169	0.069	0.500	0.035	2.663
110	23.000	0.678	20.259	0.069	0.500	0.035	2.698
111	23.500	0.673	20.109	0.069	0.500	0.034	2.732
112	24.000	0.673	20.109	0.069	0.500	0.034	2.767

Table A2.1 STAR-48 #1 Test Data

	Time(s)	Pres(PSIA)	THRUST(lbf)	MFR(lbm/s)	dt(s)	Flow Mass lbm	FM Sum lbm
113	24.500	0.682	20.378	0.070	0.500	0.035	2.802
114	25.000	0.676	20.199	0.069	0.500	0.035	2.836
115	25.500	0.683	20.408	0.070	0.500	0.035	2.871
116	26.000	0.675	20.169	0.069	0.500	0.035	2.906
117	26.500	0.674	20.139	0.069	0.500	0.034	2.940
118	27.000	0.687	20.528	0.070	0.500	0.035	2.975
119	27.500	0.669	19.990	0.068	0.500	0.034	3.010
120	28.000	0.676	20.199	0.069	0.500	0.035	3.044
121	28.500	0.676	20.199	0.069	0.500	0.035	3.079
122	29.000	0.678	20.259	0.069	0.500	0.035	3.113
123	29.500	0.673	20.109	0.069	0.500	0.034	3.148
124	30.000	0.663	19.810	0.068	0.500	0.034	3.182

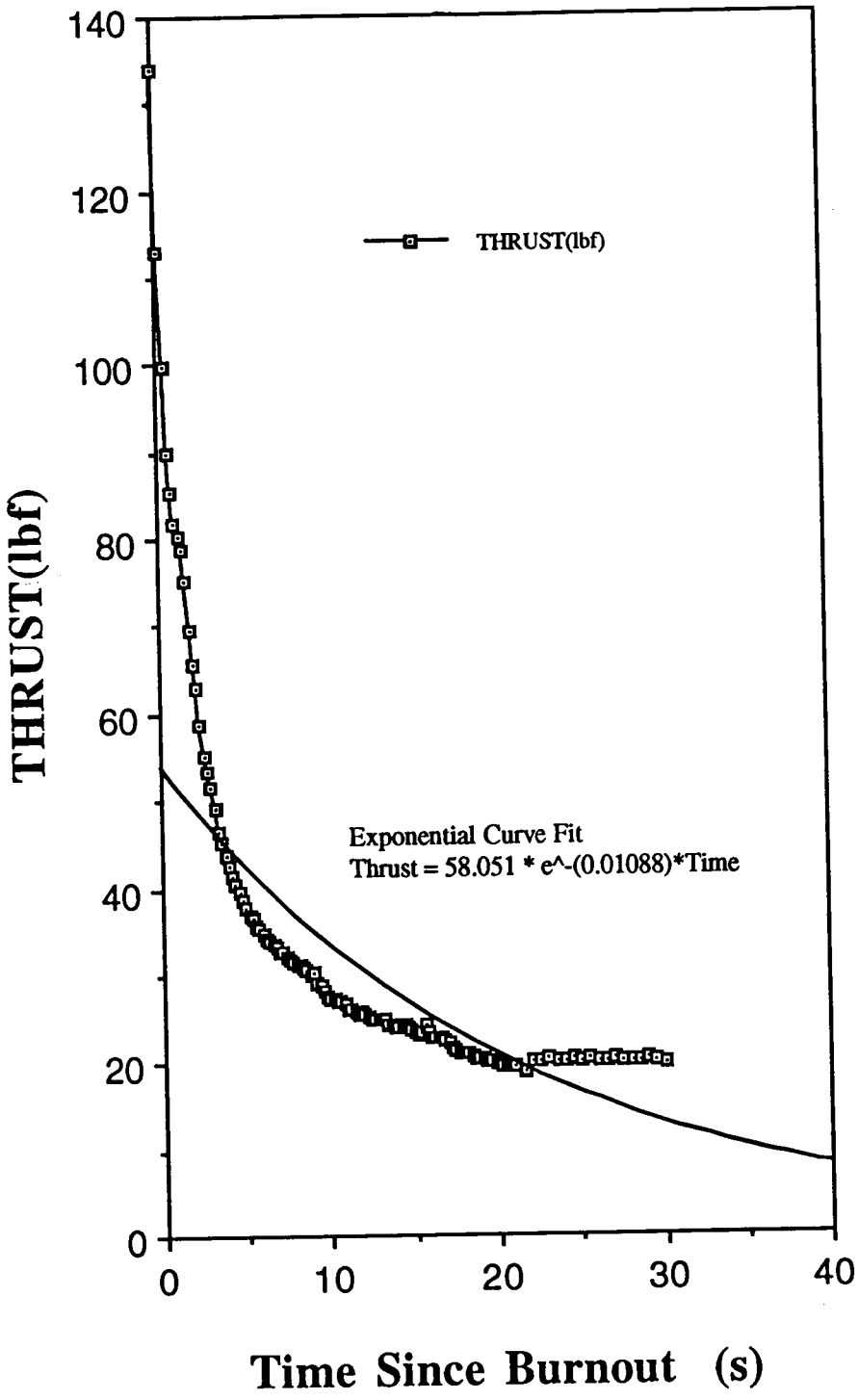


Figure A2.1 STAR-48 #1 Test Data

Table A2.2 STAR-48 #2 Test Data

	Time(s)	Pres(PSIA)	Thrust(lbf)	MFR(lbm/s)	dt(s)	Flow Mass lbm	FM Sum lbm
1	0.000	10.310	308.063	1.055	0.200	0.211	0.211
2	0.200	7.310	218.423	0.748	0.200	0.150	0.360
3	0.400	5.860	175.097	0.599	0.200	0.120	0.480
4	0.600	4.950	147.906	0.506	0.200	0.101	0.582
5	0.800	4.610	137.747	0.472	0.200	0.094	0.676
6	1.000	4.330	129.380	0.443	0.200	0.089	0.765
7	1.200	3.850	115.038	0.394	0.200	0.079	0.843
8	1.400	3.490	104.281	0.357	0.200	0.071	0.915
9	1.600	3.270	97.708	0.335	0.200	0.067	0.982
10	1.800	3.110	92.927	0.318	0.200	0.064	1.045
11	2.000	2.920	87.250	0.299	0.200	0.060	1.105
12	2.200	2.800	83.664	0.286	0.200	0.057	1.162
13	2.400	2.730	81.572	0.279	0.200	0.056	1.218
14	2.600	2.650	79.182	0.271	0.200	0.054	1.272
15	2.800	2.610	77.987	0.267	0.200	0.053	1.326
16	3.000	2.560	76.493	0.262	0.200	0.052	1.378
17	3.200	2.490	74.401	0.255	0.200	0.051	1.429
18	3.400	2.500	74.700	0.256	0.200	0.051	1.480
19	3.600	2.460	73.505	0.252	0.200	0.050	1.531
20	3.800	2.460	73.505	0.252	0.200	0.050	1.581
21	4.000	2.470	73.804	0.253	0.200	0.051	1.631
22	4.200	2.400	71.712	0.246	0.200	0.049	1.680
23	4.400	2.450	73.206	0.251	0.200	0.050	1.731
24	4.600	2.390	71.413	0.244	0.200	0.049	1.780
25	4.800	2.340	69.919	0.239	0.200	0.048	1.827
26	5.000	2.380	71.114	0.243	0.200	0.049	1.876
27	5.200	2.310	69.023	0.236	0.200	0.047	1.923
28	5.400	2.260	67.529	0.231	0.200	0.046	1.970
29	5.600	2.310	69.023	0.236	0.200	0.047	2.017
30	5.800	2.250	67.230	0.230	0.200	0.046	2.063
31	6.000	2.270	67.828	0.232	0.200	0.046	2.109
32	6.200	2.230	66.632	0.228	0.200	0.046	2.155
33	6.400	2.170	64.840	0.222	0.200	0.044	2.199
34	6.600	2.220	66.334	0.227	0.200	0.045	2.245
35	6.800	2.170	64.840	0.222	0.200	0.044	2.289
36	7.000	2.080	62.150	0.213	0.200	0.043	2.332
37	7.200	2.100	62.748	0.215	0.200	0.043	2.375
38	7.400	2.040	60.955	0.209	0.200	0.042	2.416
39	7.600	2.020	60.358	0.207	0.200	0.041	2.458
40	7.800	2.000	59.760	0.205	0.200	0.041	2.499
41	8.000	1.910	57.071	0.195	0.200	0.039	2.538
42	8.200	1.910	57.071	0.195	0.200	0.039	2.577
43	8.400	1.870	55.876	0.191	0.200	0.038	2.615
44	8.600	1.830	54.680	0.187	0.200	0.037	2.652
45	8.800	1.830	54.680	0.187	0.200	0.037	2.690
46	9.000	1.790	53.485	0.183	0.200	0.037	2.727
47	9.200	1.790	53.485	0.183	0.200	0.037	2.763
48	9.400	1.790	53.485	0.183	0.200	0.037	2.800
49	9.600	1.730	51.692	0.177	0.200	0.035	2.835
50	9.800	1.690	50.497	0.173	0.200	0.035	2.870
51	10.000	1.650	49.302	0.169	0.200	0.034	2.904
52	10.200	1.590	47.509	0.163	0.200	0.033	2.936
53	10.400	1.580	47.210	0.162	0.200	0.032	2.968
54	10.600	1.560	46.613	0.160	0.200	0.032	3.000
55	10.800	1.510	45.119	0.154	0.200	0.031	3.031
56	11.000	1.520	45.418	0.155	0.200	0.031	3.062

Table A2.2 STAR-48 #2 Test Data

	Time(s)	Pres(PSIA)	Thrust(lbf)	MFR(lbm/s)	dt(s)	Flow Mass lbm	FM Sum lbm
57	11.200	1.470	43.924	0.150	0.200	0.030	3.092
58	11.400	1.460	43.625	0.149	0.200	0.030	3.122
59	11.600	1.460	43.625	0.149	0.200	0.030	3.152
60	11.800	1.410	42.131	0.144	0.200	0.029	3.181
61	12.000	1.420	42.430	0.145	0.200	0.029	3.210
62	12.200	1.410	42.131	0.144	0.200	0.029	3.239
63	12.400	1.370	40.936	0.140	0.200	0.028	3.267
64	12.600	1.390	41.533	0.142	0.200	0.028	3.295
65	12.800	1.360	40.637	0.139	0.200	0.028	3.323
66	13.000	1.340	40.039	0.137	0.200	0.027	3.351
67	13.200	1.370	40.936	0.140	0.200	0.028	3.379
68	13.400	1.330	39.740	0.136	0.200	0.027	3.406
69	13.600	1.340	40.039	0.137	0.200	0.027	3.433
70	13.800	1.330	39.740	0.136	0.200	0.027	3.460
71	14.000	1.290	38.545	0.132	0.200	0.026	3.487
72	14.200	1.340	40.039	0.137	0.200	0.027	3.514
73	14.400	1.330	39.740	0.136	0.200	0.027	3.541
74	14.600	1.320	39.442	0.135	0.200	0.027	3.568
75	14.800	1.340	40.039	0.137	0.200	0.027	3.596
76	15.000	1.300	38.844	0.133	0.200	0.027	3.622
77	15.200	1.310	39.143	0.134	0.200	0.027	3.649
78	15.400	1.290	38.545	0.132	0.200	0.026	3.676
79	15.600	1.250	37.350	0.128	0.200	0.026	3.701
80	15.800	1.270	37.948	0.130	0.200	0.026	3.727
81	16.000	1.270	37.948	0.130	0.200	0.026	3.753
82	16.200	1.240	37.051	0.127	0.200	0.025	3.779
83	16.400	1.260	37.649	0.129	0.200	0.026	3.804
84	16.600	1.240	37.051	0.127	0.200	0.025	3.830
85	16.800	1.220	36.454	0.125	0.200	0.025	3.855
86	17.000	1.260	37.649	0.129	0.200	0.026	3.880
87	17.200	1.220	36.454	0.125	0.200	0.025	3.905
88	17.700	1.240	37.051	0.127	0.500	0.063	3.969
89	18.200	1.240	37.051	0.127	0.500	0.063	4.032
90	18.700	1.200	35.856	0.123	0.500	0.061	4.094
91	19.200	1.240	37.051	0.127	0.500	0.063	4.157
92	19.700	1.200	35.856	0.123	0.500	0.061	4.218
93	20.200	1.180	35.258	0.121	0.500	0.060	4.279
94	20.700	1.170	34.960	0.120	0.500	0.060	4.339
95	21.200	1.160	34.661	0.119	0.500	0.059	4.398
96	21.700	1.140	34.063	0.117	0.500	0.058	4.456
97	22.200	1.100	32.868	0.113	0.500	0.056	4.512
98	22.700	1.120	33.466	0.115	0.500	0.057	4.570
99	23.200	1.100	32.868	0.113	0.500	0.056	4.626
100	23.700	1.090	32.569	0.112	0.500	0.056	4.682
101	24.200	1.070	31.972	0.109	0.500	0.055	4.737
102	24.700	1.070	31.972	0.109	0.500	0.055	4.791
103	25.200	1.050	31.374	0.107	0.500	0.054	4.845
104	25.700	1.050	31.374	0.107	0.500	0.054	4.899
105	26.200	1.050	31.374	0.107	0.500	0.054	4.952

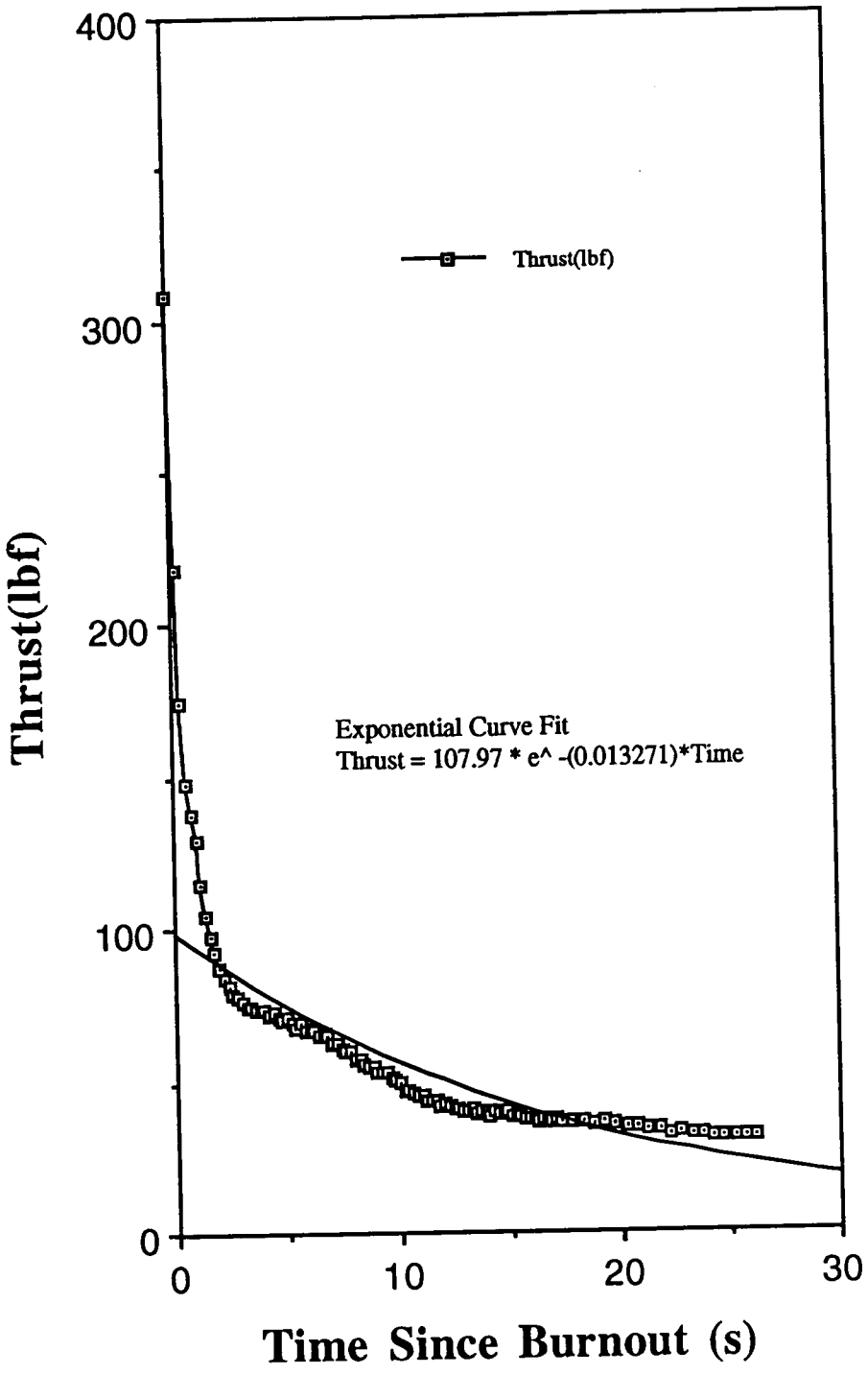


Figure A2.2 STAR-48 #2 Test Data

Table A2.3 STAR-48 #3 Test Data

	Time (s)	Pres(PSIA)	Thrust(lbf)	MFR (lbm/s)	dt(s)	Flow Mass lbm	FM Sum lbm
1	0.000	7.180	214.538	0.734	0.200	0.147	0.147
2	0.200	6.480	193.622	0.663	0.200	0.133	0.279
3	0.400	5.830	174.200	0.596	0.200	0.119	0.399
4	0.600	5.280	157.766	0.540	0.200	0.108	0.507
5	0.800	4.850	144.918	0.496	0.200	0.099	0.606
6	1.000	4.460	133.265	0.456	0.200	0.091	0.697
7	1.200	3.660	109.361	0.374	0.200	0.075	0.772
8	1.400	3.320	99.202	0.340	0.200	0.068	0.840
9	1.600	3.130	93.524	0.320	0.200	0.064	0.904
10	1.800	2.840	84.859	0.291	0.200	0.058	0.962
11	2.000	2.620	78.286	0.268	0.200	0.054	1.016
12	2.200	2.420	72.310	0.248	0.200	0.050	1.065
13	2.400	2.290	68.425	0.234	0.200	0.047	1.112
14	2.600	2.200	65.736	0.225	0.200	0.045	1.157
15	2.800	2.130	63.644	0.218	0.200	0.044	1.201
16	3.000	2.020	60.358	0.207	0.200	0.041	1.242
17	3.200	1.920	57.370	0.196	0.200	0.039	1.281
18	3.400	1.830	54.680	0.187	0.200	0.037	1.319
19	3.600	1.780	53.186	0.182	0.200	0.036	1.355
20	3.800	1.690	50.497	0.173	0.200	0.035	1.390
21	4.000	1.620	48.406	0.166	0.200	0.033	1.423
22	4.200	1.600	47.808	0.164	0.200	0.033	1.456
23	4.400	1.530	45.716	0.157	0.200	0.031	1.487
24	4.600	1.510	45.119	0.154	0.200	0.031	1.518
25	4.800	1.490	44.521	0.152	0.200	0.030	1.548
26	5.000	1.420	42.430	0.145	0.200	0.029	1.577
27	5.200	1.420	42.430	0.145	0.200	0.029	1.606
28	5.400	1.400	41.832	0.143	0.200	0.029	1.635
29	5.600	1.370	40.936	0.140	0.200	0.028	1.663
30	5.800	1.360	40.637	0.139	0.200	0.028	1.691
31	6.000	1.330	39.740	0.136	0.200	0.027	1.718
32	6.200	1.300	38.844	0.133	0.200	0.027	1.745
33	6.400	1.290	38.545	0.132	0.200	0.026	1.771
34	6.600	1.250	37.350	0.128	0.200	0.026	1.797
35	6.800	1.260	37.649	0.129	0.200	0.026	1.822
36	7.000	1.250	37.350	0.128	0.200	0.026	1.848
37	7.200	1.220	36.454	0.125	0.200	0.025	1.873
38	7.400	1.200	35.856	0.123	0.200	0.025	1.898
39	7.600	1.180	35.258	0.121	0.200	0.024	1.922
40	7.800	1.150	34.362	0.118	0.200	0.024	1.945
41	8.000	1.150	34.362	0.118	0.200	0.024	1.969
42	8.200	1.120	33.466	0.115	0.200	0.023	1.992
43	8.400	1.110	33.167	0.114	0.200	0.023	2.014
44	8.600	1.100	32.868	0.113	0.200	0.023	2.037
45	8.800	1.080	32.270	0.110	0.200	0.022	2.059
46	9.000	1.070	31.972	0.109	0.200	0.022	2.081
47	9.200	1.050	31.374	0.107	0.200	0.021	2.102
48	9.400	1.010	30.179	0.103	0.200	0.021	2.123
49	9.600	0.987	29.492	0.101	0.200	0.020	2.143
50	9.800	0.990	29.581	0.101	0.200	0.020	2.163
51	10.000	0.952	28.446	0.097	0.200	0.019	2.183
52	10.200	0.941	28.117	0.096	0.200	0.019	2.202
53	10.400	0.938	28.027	0.096	0.200	0.019	2.221
54	10.600	0.908	27.131	0.093	0.200	0.019	2.240
55	10.800	0.924	27.609	0.095	0.200	0.019	2.259
56	11.000	0.908	27.131	0.093	0.200	0.019	2.277

Table A2.3 STAR-48 #3 Test Data

	Time (s)	Pres(PSIA)	Thrust(lbf)	MFR (lbm/s)	dt(s)	Flow Mass lbm	FM Sum lbm
57	11.200	0.886	26.474	0.091	0.200	0.018	2.296
58	11.400	0.905	27.041	0.093	0.200	0.019	2.314
59	11.600	0.908	27.131	0.093	0.200	0.019	2.333
60	11.800	0.919	27.460	0.094	0.200	0.019	2.351
61	12.000	0.899	26.862	0.092	0.200	0.018	2.370
62	12.200	0.857	25.607	0.088	0.200	0.018	2.387
63	12.400	0.769	22.978	0.079	0.200	0.016	2.403
64	12.600	0.833	24.890	0.085	0.200	0.017	2.420
65	12.800	0.822	24.561	0.084	0.200	0.017	2.437
66	13.000	0.844	25.219	0.086	0.200	0.017	2.454
67	13.200	0.850	25.398	0.087	0.200	0.017	2.472
68	13.400	0.822	24.561	0.084	0.200	0.017	2.488
69	13.600	0.844	25.219	0.086	0.200	0.017	2.506
70	13.800	0.842	25.159	0.086	0.200	0.017	2.523
71	14.000	0.864	25.816	0.088	0.200	0.018	2.541
72	14.200	0.850	25.398	0.087	0.200	0.017	2.558
73	14.400	0.822	24.561	0.084	0.200	0.017	2.575
74	14.600	0.820	24.502	0.084	0.200	0.017	2.592
75	14.800	0.833	24.890	0.085	0.200	0.017	2.609
76	15.000	0.828	24.741	0.085	0.200	0.017	2.626
77	15.200	0.831	24.830	0.085	0.200	0.017	2.643
78	15.400	0.817	24.412	0.084	0.200	0.017	2.659
79	15.600	0.792	23.665	0.081	0.200	0.016	2.675
80	15.800	0.809	24.173	0.083	0.200	0.017	2.692
81	16.000	0.809	24.173	0.083	0.200	0.017	2.709
82	16.200	0.792	23.665	0.081	0.200	0.016	2.725
83	16.400	0.811	24.233	0.083	0.200	0.017	2.741
84	16.600	0.798	23.844	0.082	0.200	0.016	2.758
85	16.800	0.784	23.426	0.080	0.200	0.016	2.774
86	17.000	0.806	24.083	0.082	0.200	0.016	2.790
87	17.200	0.795	23.755	0.081	0.200	0.016	2.807
88	17.700	0.792	23.665	0.081	0.500	0.041	2.847
89	18.200	0.800	23.904	0.082	0.500	0.041	2.888
90	18.700	0.811	24.233	0.083	0.500	0.041	2.929
91	19.200	0.817	24.412	0.084	0.500	0.042	2.971
92	19.700	0.784	23.426	0.080	0.500	0.040	3.011
93	20.200	0.740	22.111	0.076	0.500	0.038	3.049
94	20.700	0.718	21.454	0.073	0.500	0.037	3.086
95	21.200	0.704	21.036	0.072	0.500	0.036	3.122
96	21.700	0.688	20.557	0.070	0.500	0.035	3.157
97	22.200	0.671	20.049	0.069	0.500	0.034	3.191
98	22.700	0.688	20.557	0.070	0.500	0.035	3.227
99	23.200	0.679	20.289	0.069	0.500	0.035	3.261
100	23.700	0.707	21.125	0.072	0.500	0.036	3.297
101	24.200	0.709	21.185	0.073	0.500	0.036	3.334
102	24.700	0.695	20.767	0.071	0.500	0.036	3.369
103	25.200	0.671	20.049	0.069	0.500	0.034	3.404
104	25.700	0.663	19.810	0.068	0.500	0.034	3.438
105	26.200	0.630	18.824	0.064	0.500	0.032	3.470
106	26.700	0.629	18.795	0.064	0.500	0.032	3.502
107	27.200	0.616	18.406	0.063	0.500	0.032	3.533
108	27.700	0.602	17.988	0.062	0.500	0.031	3.564
109	28.200	0.600	17.928	0.061	0.500	0.031	3.595
110	28.700	0.586	17.510	0.060	0.500	0.030	3.625
111	29.200	0.561	16.763	0.057	0.500	0.029	3.654
112	29.700	0.542	16.195	0.055	0.500	0.028	3.681

Table A2.3 STAR-48 #3 Test Data

	Time (s)	Pres(PSIA)	Thrust(lbf)	MFR (lbm/s)	dt(s)	Flow Mass lbm	FM Sum lbm
113	30.200	0.525	15.687	0.054	0.500	0.027	3.708
114	30.700	0.501	14.970	0.051	0.500	0.026	3.734
115	31.200	0.490	14.641	0.050	0.500	0.025	3.759
116	31.700	0.498	14.880	0.051	0.500	0.025	3.784
117	32.200	0.470	14.044	0.048	0.500	0.024	3.808
118	32.700	0.487	14.552	0.050	0.500	0.025	3.833
119	33.200	0.470	14.044	0.048	0.500	0.024	3.857
120	33.700	0.437	13.058	0.045	0.500	0.022	3.880
121	34.200	0.410	12.251	0.042	0.500	0.021	3.901
122	34.700	0.388	11.593	0.040	0.500	0.020	3.920
123	35.200	0.380	11.354	0.039	0.500	0.019	3.940
124	35.700	0.349	10.426	0.036	0.500	0.018	3.958

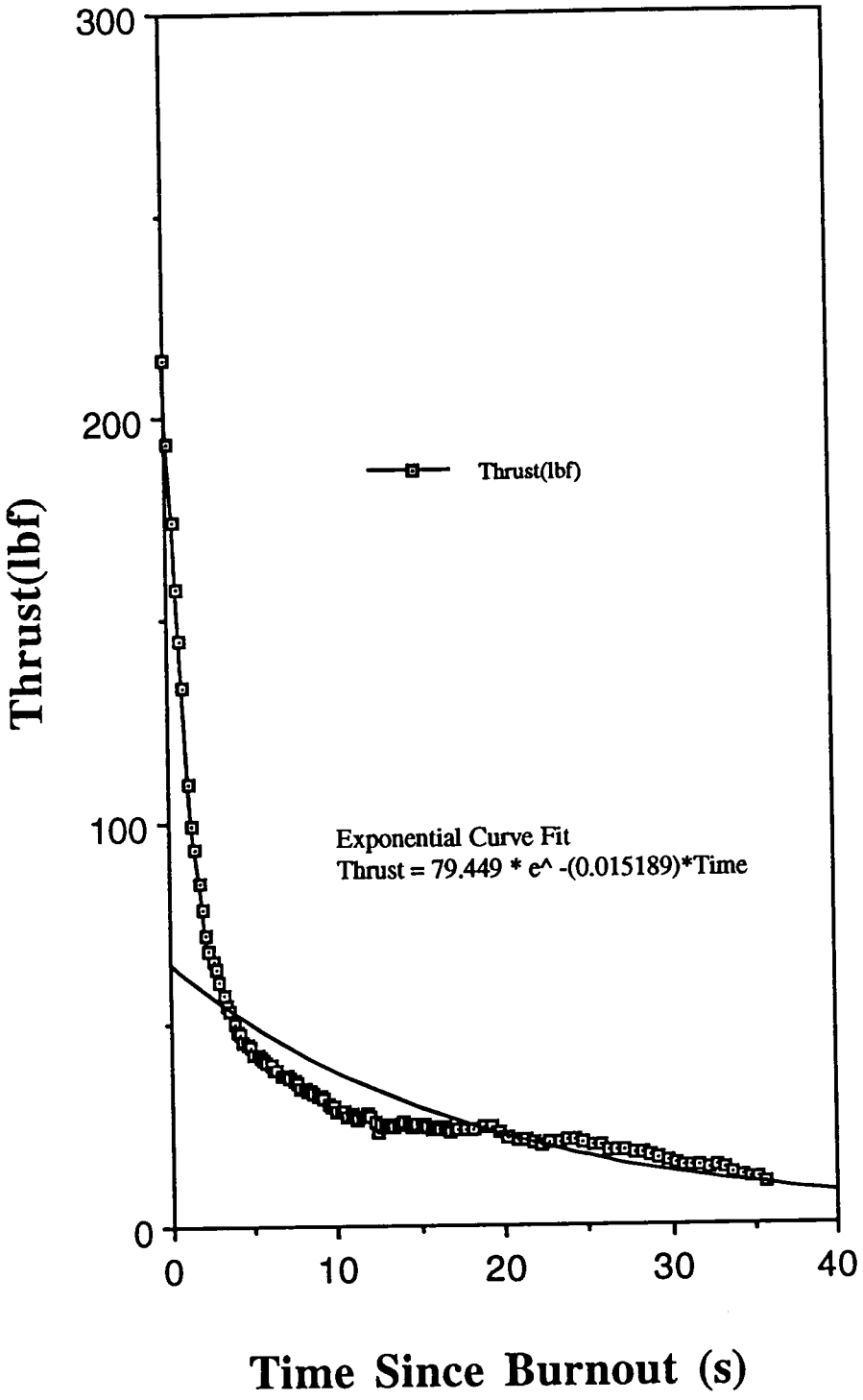


Figure A2.3 STAR-48 #3 Test Data

Table A2.4 Data Developed by Dr. Reiss in Reference #15

	Time (s)	Time*-0.0209	Exponential	Thrust(lbf)
1	0.000	0.000	1.000	44.275
2	0.200	-0.004	0.996	44.090
3	0.400	-0.008	0.992	43.906
4	0.600	-0.013	0.988	43.722
5	0.800	-0.017	0.983	43.540
6	1.000	-0.021	0.979	43.358
7	1.200	-0.025	0.975	43.177
8	1.400	-0.029	0.971	42.996
9	1.600	-0.033	0.967	42.817
10	1.800	-0.038	0.963	42.638
11	2.000	-0.042	0.959	42.460
12	2.200	-0.046	0.955	42.282
13	2.400	-0.050	0.951	42.106
14	2.600	-0.054	0.947	41.930
15	2.800	-0.059	0.943	41.755
16	3.000	-0.063	0.939	41.580
17	3.200	-0.067	0.935	41.406
18	3.400	-0.071	0.931	41.234
19	3.600	-0.075	0.927	41.061
20	3.800	-0.080	0.924	40.890
21	4.000	-0.084	0.920	40.719
22	4.200	-0.088	0.916	40.549
23	4.400	-0.092	0.912	40.379
24	4.600	-0.096	0.908	40.211
25	4.800	-0.100	0.904	40.043
26	5.000	-0.105	0.901	39.875
27	5.200	-0.109	0.897	39.709
28	5.400	-0.113	0.893	39.543
29	5.600	-0.117	0.889	39.378
30	5.800	-0.121	0.886	39.213
31	6.000	-0.126	0.882	39.049
32	6.200	-0.130	0.878	38.886
33	6.400	-0.134	0.875	38.724
34	6.600	-0.138	0.871	38.562
35	6.800	-0.142	0.867	38.401
36	7.000	-0.147	0.864	38.241
37	7.200	-0.151	0.860	38.081
38	7.400	-0.155	0.857	37.922
39	7.600	-0.159	0.853	37.763
40	7.800	-0.163	0.849	37.606
41	8.000	-0.167	0.846	37.448
42	8.200	-0.172	0.842	37.292
43	8.400	-0.176	0.839	37.136
44	8.600	-0.180	0.835	36.981
45	8.800	-0.184	0.832	36.827
46	9.000	-0.188	0.828	36.673
47	9.200	-0.193	0.825	36.519
48	9.400	-0.197	0.821	36.367
49	9.600	-0.201	0.818	36.215
50	9.800	-0.205	0.815	36.064
51	10.000	-0.209	0.811	35.913
52	10.200	-0.214	0.808	35.763
53	10.400	-0.218	0.804	35.614
54	10.600	-0.222	0.801	35.465
55	10.800	-0.226	0.798	35.317
56	11.000	-0.230	0.794	35.169

Table A2.4 Data Developed by Dr. Reiss in Reference #15

	Time (s)	Time*-0.0209	Exponential	Thrust(lbf)
57	11.200	-0.234	0.791	35.022
58	11.400	-0.239	0.788	34.876
59	11.600	-0.243	0.784	34.730
60	11.800	-0.247	0.781	34.585
61	12.000	-0.251	0.778	34.441
62	12.200	-0.255	0.775	34.297
63	12.400	-0.260	0.771	34.153
64	12.600	-0.264	0.768	34.011
65	12.800	-0.268	0.765	33.869
66	13.000	-0.272	0.762	33.727
67	13.200	-0.276	0.759	33.586
68	13.400	-0.280	0.755	33.446
69	13.600	-0.285	0.752	33.306
70	13.800	-0.289	0.749	33.167
71	14.000	-0.293	0.746	33.029
72	14.200	-0.297	0.743	32.891
73	14.400	-0.301	0.740	32.753
74	14.600	-0.306	0.737	32.616
75	14.800	-0.310	0.734	32.480
76	15.000	-0.314	0.731	32.344
77	15.200	-0.318	0.727	32.209
78	15.400	-0.322	0.724	32.075
79	15.600	-0.327	0.721	31.941
80	15.800	-0.331	0.718	31.807
81	16.000	-0.335	0.715	31.674
82	16.200	-0.339	0.712	31.542
83	16.400	-0.343	0.709	31.410
84	16.600	-0.347	0.706	31.279
85	16.800	-0.352	0.704	31.148
86	17.000	-0.356	0.701	31.018
87	17.200	-0.360	0.698	30.889
88	17.700	-0.370	0.690	30.567
89	18.200	-0.381	0.683	30.249
90	18.700	-0.391	0.676	29.934
91	19.200	-0.402	0.669	29.622
92	19.700	-0.412	0.662	29.314
93	20.200	-0.423	0.655	29.009
94	20.700	-0.433	0.648	28.707
95	21.200	-0.444	0.642	28.408
96	21.700	-0.454	0.635	28.112
97	22.200	-0.465	0.628	27.819
98	22.700	-0.475	0.622	27.530
99	23.200	-0.486	0.615	27.243
100	23.700	-0.496	0.609	26.959
101	24.200	-0.507	0.603	26.679
102	24.700	-0.517	0.596	26.401
103	25.200	-0.527	0.590	26.126
104	25.700	-0.538	0.584	25.854
105	26.200	-0.548	0.578	25.585

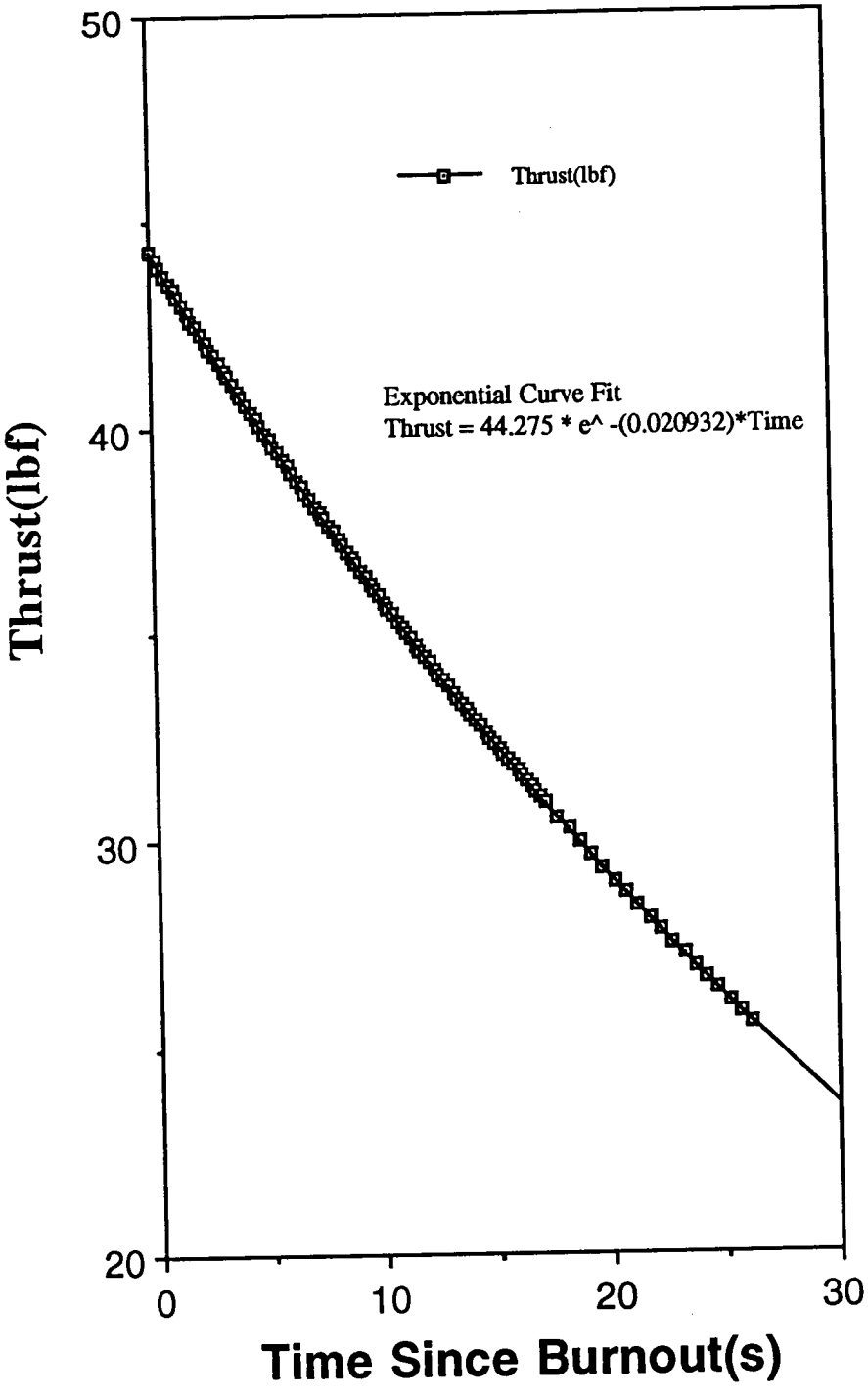


Figure A2.4 Thrust Curve as Designed by Dr. Reiss in Reference #15

Appendix 3: Runge-Kutta Program

The following pages in this appendix contain the Fortran code for the Runge-Kutta numerical integration scheme for the separation between the STAR-48V and the COMET FreeFlyer. In the first section of this program, the configuration of the STAR-48V and the FreeFlyer are selected along with the initial conditions needed to start the Runge-Kutta scheme. Next, data files are opened in order to store the results that are calculated during the Runge-Kutta process. Then, the main call line is made to subroutine RUNGE. Within this routine, the values for Euler's equations and the values for Newton's equations as determined in a body-fixed coordinate system for both the center of mass of the STAR-48V and the FreeFlyer are calculated in subroutine EULER and VELOC respectively. Once these equations of motion have been evaluated, the Euler angles that are needed for the transformation matrix used to transform a vector from body-fixed coordinates to inertial coordinates are calculated in subroutine ANGLE for both the STAR-48V and the FreeFlyer. Then the angular velocity vector and the translational velocity vector for both the STAR-48V and the FreeFlyer are transformed into the inertial coordinate system using the subroutines TRANS1 and TRANS2. These results are then integrated to obtain the position of both the center of mass of the STAR-48V and the FreeFlyer. It is these results that are finally output to the data files as discussed earlier. From this data, it can be determined if the separation between the center of mass of the STAR-48V and the COMET FreeFlyer will be successful or not.

```
*******************************************************************************
*
* THIS IS A 4TH ORDER RUNGE-KUTTA PROGRAM USED IN ORDER TO EVALUATE
* THE SEPARATION DYNAMICS BETWEEN THE COMET FREEFLYER AND A STAR-48V
* ROCKET MOTOR.  THIS PROGRAM WAS DEVELOPED BY KEVIN FULLER AT
* THE UNIVERSITY OF TENNESSEE SPACE INSTITUTE
*
*******************************************************************************

      REAL*8 W(1:100),DATA(1:100),IXX48,IYY48,IZZ48,IXXFF,IYYFF,IZZFF,
     C M48,MFF,GAMMA,TMULT,SMULT,D,KS,STROKE,FCON48,FCONFF,RAD,XSEP,
     C H,TTOTAL,T,HSPRING,TSPRING,STEP,VEL(1:100),CRASH,SEPDIS,
     C ANG(1:100),WIN(1:100),VELIN(1:100),DISTIN(1:100),ROT(1:100),
     C CONDIS,SEPDISX,SEPDISY,SEPDISZ,TIME,SEPTOT,SEPVELT,SEPVELX,
     C SEPVELY,SEPVELZ,ROTBOD(1:100)

      INTEGER NEQ,NSPRING,COUNT

C NUMBER OF DIFFERENTIAL EQUATIONS TO BE SOLVED
      NEQ = 6

C MOMENTS OF INERTIA OF THE STAR 48 IN SLUG * SQ FT
      IXX48 = 37.02
      IYY48 = 59.59
      IZZ48 = 57.51

      DATA(1) = IXX48
      DATA(2) = IYY48
      DATA(3) = IZZ48
C MOMENTS OF INERTIA OF THE FREEFLYER IN SLUG * SQ FT
      IXXFF = 142.84
      IYYFF = 550.76
      IZZFF = 550.17
      DATA(4) = IXXFF
      DATA(5) = IYYFF
      DATA(6) = IZZFF
C MASS OF THE STAR 48 IN SLUGS
      M48 = 17.86
      DATA(7) = M48
C MASS OF THE FREEFLYER IN SLUGS
      MFF = 59.82
      DATA(8) = MFF
C GIMBLE ANGLE OF THE STAR 48 IN DEGREES(PROGRAM CHANGES TO RADIANS
C LATER)
      GAMMA = 4.0
      DATA(9) = GAMMA
C MOMENT ARM FOR THE THRUST OF STAR 48 (CONVERT 26.5 INCHES TO FEET)
      D = 26.5/12.0
      DATA(10) = D
```

```
C THRUST MULTIPLIER OF THE STAR 48
      TMULT = 1.0
      DATA(11) = TMULT
C SPRING MULTIPLIER
      SMULT = 0.9
      DATA(12) = SMULT
C THE NUMBER OF SEPARATION SPRINGS
      NSPRING = 8
      DATA(13) = NSPRING
C SPRING CONSTANT FOR THE SPRINGS IN LB/FT (CONVERT TO FEET)
      KS = 180.0 *12.0
      DATA(14) = KS
C SPRING STROKE LENGTH IN INCHES (CONVERT TO FEET)
      STROKE = 1.3 / 12.0
      DATA(15) = STROKE
C MEASURED CONNECTOR FORCE ON THE STAR 48
      FCON48 = 20.0
      DATA(16) = FCON48
C MEASURED CONNECTOR FORCE ON THE FREEFLYEER
      FCONFF = -20
      DATA(17) = FCONFF
C MEASURED CONNECTOR DISTANCE
      CONDIS   = 0.2/12.0
      DATA(29) = CONDIS
C SET CRASH FLAG TO BE 0
      CRASH = 0.0
      DATA(28) = CRASH
C THE DEGREES TO RADIANS CONVERSION FACTOR
      RAD = 0.01745329252
      DATA(18) = RAD
C CONVERT THE GIMBLE ANGLE TO RADIANS
      DATA(9) = DATA(9)*RAD
C THE SEPARATION DISTANCE BETWEEN THE STAR48 AND THE FREEFLYER IN THE X
C DIRECTION
      XSEP = 0.0
      DATA(19) = XSEP
C THE TIME BETWEEN THE STAR 48 BURNOUT AND THE INITIAL SEPARATION
      TSEP = 180
      DATA(20) = TSEP
C THE TIME STEP
      H = 0.1
      DATA(21) = H
C THE TOTAL TIME OF THE SIMULATION
      TTOTAL = 50.0
      DATA(22) = TTOTAL
C THE CURRENT TIME OF THE SIMULATION
      T = 0.0
      DATA(23) = T
C THE TIME STEP DURING THE SPRING EXPANSION
      HSPRING = 0.001
      DATA(24) = HSPRING
```

```
C THE TIME LENGTH OF THE EXPANSION OF THE SEPARATION SPRINGS
      TSPRING = 0.1
      DATA(25) = TSPRING
************************ INITIAL CONDITIONS ************************************

C INITIAL ROLL RATE IN DEGREES/S OF THE STAR 48 IN BODY FIXED COORDINATES
      W(1) = 0.5*RAD
C INITIAL YAW RATE IN DEGREES/S OF THE STAR 48 IN BODY FIXED COORDINATES
      W(2) = 0.0*RAD
C INITIAL PITCH RATE IN DEGREES/S OF THE STAR 48 IN BODY FIXED COORDINATES
      W(3) = 0.0*RAD
C INITIAL ROLL RATE IN DEGREES/S OF THE FREEFLYER IN BODY FIXED
C COORDINATES
      W(4) = 0.5*RAD
C INITIAL YAW RATE IN DEGREES/S OF THE FREEFLYER IN BODY FIXED
C COORDINATES
      W(5) = 0.0*RAD
C INITIAL PITCH RATE IN DEGREES/S OF THE FREEFLYER IN BODY FIXED
C COORDINATES
      W(6) = 0.0*RAD
C INITIAL VELOCITY OF THE STAR 48 IN THE X DIRECTION IN BODY FIXED
C COORDINATES
      VEL(1) = 0.0
C INITIAL VELOCITY OF THE STAR 48 IN THE Y DIRECTION IN BODY FIXED
C COORDINATES
      VEL(2) = 0.0
C INITIAL VELOCITY OF THE STAR 48 IN THE Z DIRECTION IN BODY FIXED
C COORDINATES
      VEL(3) = 0.0
C INITIAL VELOCITY OF THE FREEFLYER IN THE X DIRECTION IN BODY FIXED
C COORDINATES
      VEL(4) = 0.0
C INITIAL VELOCITY OF THE FREEFLYER IN THE Y DIRECTION IN BODY FIXED
C COORDINATES
      VEL(5) = 0.0
C INITIAL VELOCITY OF THE FREEFLYER IN THE Z DIRECTION IN BODY FIXED
C COORDINATES
      VEL(6) = 0.0
C INITIAL EULER ANGLE THETA VALUE FOR THE STAR 48
      ANG(1) = 0.0001 * RAD
C INITIAL EULER ANGLE PHI VALUE FOR THE STAR 48
      ANG(2) = 0.0
C INITIAL EULER ANGLE PSI VALUE FOR THE STAR 48
      ANG(3) = 0.0
C INITIAL EULER ANGLE THETA VALUE FOR THE STAR 48
      ANG(4) = 0.0001 * RAD
C INITIAL EULER ANGLE PHI VALUE FOR THE STAR 48
      ANG(5) = 0.0
C INITIAL EULER ANGLE PSI VALUE FOR THE STAR 48
      ANG(6) = 0.0
```

```
C INITIAL INERTIAL VELOCITY IN THE X DIRECTION FOR THE STAR48
      VELIN(1) = 0.0
C INITIAL INERTIAL VELOCITY IN THE Y DIRECTION FOR THE STAR48
      VELIN(2) = 0.0
C INITIAL INERTIAL VELOCITY IN THE Z DIRECTION FOR THE STAR48
      VELIN(3) = 0.0
C INITIAL INERTIAL VELOCITY IN THE X DIRECTION FOR THE FREEFLYER
      VELIN(4) = 0.0
C INITIAL INERTIAL VELOCITY IN THE Y DIRECTION FOR THE FREEFLYER
      VELIN(5) = 0.0
C INITIAL INERTIAL VELOCITY IN THE Z DIRECTION FOR THE FREEFLYER
      VELIN(6) = 0.0
C INITIAL ANGULAR ROLL RATE FOR THE STAR 48 IN INERTIAL COORDINATES
      WIN(1) = 0.0
C INITIAL ANGULAR YAW RATE FOR THE STAR 48 IN INERTIAL COORDINATES
      WIN(2) = 0.0
C INITIAL ANGULAR PITCH RATE FOR THE STAR 48 IN INERTIAL COORDINATES
      WIN(3) = 0.0
C INITIAL ANGULAR ROLL RATE FOR THE FREEFLYER IN INERTIAL COORDINATES
      WIN(4) = 0.0
C INITIAL ANGULAR YAW RATE FOR THE FREEFLYER IN INERTIAL COORDINATES
      WIN(5) = 0.0
C INITIAL ANGULAR PITCH RATE FOR THE FREEFLYER IN INERTIAL COORDINATES
      WIN(6) = 0.0

C OPEN THE DATA FILES
      OPEN(1,FILE = 'VELI48.DAT')
      OPEN(2,FILE = 'VELIFF.DAT')
      OPEN(3,FILE = 'DISTI48.DAT')
      OPEN(4,FILE = 'DISTIFF.DAT')
      OPEN(5,FILE = 'SEPDIS.DAT')
      OPEN(6,FILE = 'ROTI48.DAT')
      OPEN(7,FILE = 'ROTIFF.DAT')
      OPEN(8,FILE = 'SEPTOT.DAT')
      OPEN(9,FILE = 'SEPVELI.DAT')
      OPEN(10,FILE = 'BODVEL48.DAT')
      OPEN(11,FILE = 'BODVELFF.DAT')
      OPEN(12,FILE = 'BODANG48.DAT')
      OPEN(13,FILE = 'BODANGFF.DAT')
      OPEN(14,FILE = 'ROTBOD48.DAT')
      OPEN(15,FILE = 'ROTBODFF.DAT')
      OPEN(16,FILE = 'INANG48.DAT')
      OPEN(17,FILE = 'INANGFF.DAT')

C CALCULATE THE NUMBER OF STEPS USED IN THE RUNGE KUTTA

      STEP = TTOTAL / DATA(21)  + TSPRING / HSPRING
```

```
C CALL THE RUNGE KUTTA TIME STEP ROUTINE

      DO 1000 N = 1,STEP

C DETERMINE TIME STEP.  IF THE TIME IS LESS THAN THE SPRING TIME CONSTANT
C THEN USE THE SPRING TIME STEP
      PRTVAR = 0.0

      IF (DATA(23) .LE. TSPRING) THEN
        DATA(21) = DATA(24)
      ENDIF

C DETERMINE TIME STEP.  IF THE TIME IS GREATER THAN THE SPRING TIME
C CONSTANT THEN USE THE REGULAR TIME STEP

      IF (DATA(23) .GT. TSPRING) THEN
        DATA(21) = H
      ENDIF

       CALL RUNGE (DATA,NEQ,W,VEL,ANG,WIN,VELIN,DISTIN,ROT,ROTBOD)

      SEPDISX = DISTIN(4) - DISTIN(1)
      SEPDISY = DISTIN(5) - DISTIN(2)
      SEPDISZ = DISTIN(6) - DISTIN(3)
      SEPDIS = SEPDISX

      SEPVELX = VELIN(4) - VELIN(1)
      SEPVELY = VELIN(5) - VELIN(2)
      SEPVELZ = VELIN(6) - VELIN(3)
      IF (SEPDIS .LE. 0) THEN
       SEPDIS = 0.0
      ENDIF

      DATA(27) = SEPDIS

      PRINT*, 'TIME= ',DATA(23)

      TIME = DATA(20) + DATA(23)

      SEPTOT = (SEPDISX**2 + SEPDISY**2 + SEPDISZ**2)**0.5
      SEPVELT = (SEPVELX**2 + SEPVELY**2 + SEPVELZ**2)**0.5

      IF (DATA(21) .LT. 0.1) THEN
        COUNT = 0
      ENDIF

      COUNT = COUNT + 1
       IF (COUNT .EQ. 5) THEN
        WRITE (1,500) TIME, VELIN(1), VELIN(2), VELIN(3)
        WRITE (2,500) TIME, VELIN(4), VELIN(5), VELIN(6)
        WRITE (3,500) TIME, DISTIN(1), DISTIN(2), DISTIN(3)
```

```
          WRITE (4,500) TIME, DISTIN(4), DISTIN(5), DISTIN(6)
          WRITE (5,500) TIME, SEPDISX, SEPDISY, SEPDISZ
          WRITE (8,500) TIME, SEPTOT, SEPVELT
          WRITE (9,500) TIME, SEPVELX, SEPVELY, SEPVELZ
          WRITE (10,500) TIME, VEL(1), VEL(2), VEL(3)
          WRITE (11,500) TIME, VEL(4), VEL(5), VEL(6)
         DO 980 I=1,NEQ
         ROT(I) = ROT(I)/RAD
         W(I) = W(I)/RAD
         ROTBOD(I) = ROTBOD(I)/RAD
         WIN(I) = WIN(I)/RAD
980      CONTINUE
          WRITE (6,500) TIME, ROT(1), ROT(2), ROT(3)
          WRITE (7,500) TIME, ROT(4), ROT(5), ROT(6)
          WRITE (12,500) TIME, W(1), W(2), W(3)
          WRITE (13,500) TIME, W(4), W(5), W(6)
          WRITE (14,500) TIME, ROTBOD(1), ROTBOD(2),ROTBOD(3)
          WRITE (15,500) TIME, ROTBOD(4), ROTBOD(5),ROTBOD(6)
          WRITE (16,500) TIME, WIN(1), WIN(2), WIN(3)
          WRITE (17,500) TIME, WIN(4), WIN(5), WIN(6)
         DO 990 I =1,NEQ
         ROT(I) = ROT(I) * RAD
         W(I) = W(I) * RAD
         ROTBOD(I) = ROTBOD(I) * RAD
         WIN(I) = WIN(I) * RAD
990      CONTINUE

500        FORMAT (1X, 1 F12.1,3 F12.5)

          COUNT = 0
         ENDIF
1000   CONTINUE
      STOP
      END


      SUBROUTINE RUNGE (DATA,NEQ,W,VEL,ANG,WIN,VELIN,DISTIN,ROT,ROTBOD)
       REAL*8 DATA(1:100),W(1:100),F1(1:100),F2(1:100),H,H2,
     C       F3(1:100),F4(1:100),W1(1:100),VEL(1:100),VEL1(1:100),
     C       ANG(1:100),ANG1(1:100),WIN(1:100),VELIN(1:100),
     C       DISTIN(1:100),ROT(1:100),ROTBOD(1:100)
       INTEGER NEQ,I

       H = DATA(21)
       T = DATA(23)
       TEMP = DATA(23)

       H2 = H / 2.0

C W = THE EULER ANGLES AND F1 = DW FOR THE FIRST PASS
```

```
      CALL EULER (W,DATA,F1)
       DO 10 I = 1,NEQ
        W1(I) = W(I) + H2*F1(I)
10      CONTINUE

      T = T + H2
      DATA(23) = T

      CALL EULER (W1,DATA,F2)
       DO 20 I = 1,NEQ
        W1(I) = W(I) + H2*F2(I)
20      CONTINUE

      CALL EULER (W1,DATA,F3)
       DO 30 I = 1,NEQ
        W1(I) = W(I) + H*F3(I)
30      CONTINUE
      T = T + H2
      DATA(23) = T

      CALL EULER (W1,DATA,F4)
       DO 40 I = 1,NEQ
        W(I) = W(I) + (H /6.0) * (F1(I) + 2*F2(I) + 2*F3(I) + F4(I))
40      CONTINUE


C PERFORM RUNGE-KUTTA ON BODY FIXED VELOCITY EQUATIONS

C RESET TIME
      T = TEMP
      DATA(23) = TEMP

      CALL VELOC (VEL,W,DATA,F1)
       DO 50 I = 1,NEQ
        VEL1(I) = VEL(I) + H2*F1(I)
50      CONTINUE

      T = T + H2
      DATA(23) = T

      CALL VELOC (VEL1,W,DATA,F2)
       DO 60 I = 1,NEQ
        VEL1(I) = VEL(I) + H2*F2(I)
60      CONTINUE

      CALL VELOC (VEL1,W,DATA,F3)
       DO 70 I = 1,NEQ
        VEL1(I) = VEL(I) + H*F3(I)
70      CONTINUE
      T = T + H2
      DATA(23) = T
```

```
      CALL VELOC (VEL1,W,DATA,F4)
       DO 80 I = 1,NEQ
        VEL(I) = VEL(I)+ (H /6.0)*(F1(I)+ 2*F2(I)+ 2*F3(I)+ F4(I))
80      CONTINUE

C PERFORM RUNGE-KUTTA ON EULER ANGLE EQUATIONS

C RESET TIME
      T = TEMP
      DATA(23) = TEMP
      ANG1(1) = ANG(1)
      ANG1(4) = ANG(4)

      CALL ANGLE (ANG,W,F1)
       DO 90 I = 1,NEQ
        ANG1(I) = ANG(I) + H2*F1(I)
90      CONTINUE

       T = T + H2
       DATA(23) = T

       CALL ANGLE (ANG1,W,F2)
        DO 100 I = 1,NEQ
         ANG1(I) = ANG(I) + H2*F2(I)
100       CONTINUE

       CALL ANGLE (ANG1,W,F3)
        DO 110 I = 1,NEQ
         ANG1(I) = ANG(I) + H*F3(I)
110       CONTINUE
      T = T + H2
      DATA(23) = T

       CALL ANGLE (ANG1,W,F4)
        DO 120 I = 1,NEQ
         ANG(I) = ANG(I)+ (H /6.0)*(F1(I)+ 2*F2(I)+ 2*F3(I)+ F4(I))
120       CONTINUE

C TRANSFORM THE VELOCITY VECTOR FROM BODY FIXED COORDINATES TO
C INERTIAL COORDINTATES

     CALL TRANS1 (VEL,ANG,VELIN)

C TRANSFORM THE ANGULAR VELOCITY VECTOR FROM BODY FIXED COORDINATES
C TO INERTIAL COORDINATES

      CALL TRANS2 (W,ANG,WIN)
```

```
C CALCULATE THE DISTANCE AND ANGLE IN INERTIAL COORDINATES

      DO 130 I = 1,NEQ
       DISTIN(I) = DISTIN(I) + H*VELIN(I)
       ROT(I) = ROT(I) + H*WIN(I)
       ROTBOD(I) = ROTBOD(I) + H*W(I)
130     CONTINUE
       RETURN
       END

     SUBROUTINE EULER (W,DATA,DW)
      REAL*8 W(1:100),DATA(1:100),DW(1:100),IXX48,IYY48,IZZ48,IXXFF,
   C      IYYFF,IZZFF,GAMMA,D,TMULT,TSEP,T,e,THRUST,MOMX48,MOMY48,
   C      MOMZ48,MOMXFF,MOMYFF,MOMZFF

C EXPAND DATA DECK INTO READABLE TERMS
      IXX48 = DATA(1)
      IYY48 = DATA(2)
      IZZ48 = DATA(3)
      IXXFF = DATA(4)
      IYYFF = DATA(5)
      IZZFF = DATA(6)
      GAMMA = DATA(9)
      D = DATA(10)
      TMULT = DATA(11)
      TSEP = DATA(20)
      T = DATA(23)

C FORCES INVOLVED IN THE MOMENT OF THE STAR 48 IN THE BODY FIXED
C COORDINATES
      e = 2.718281828
C       THRUST = 44.275 * e **(-0.020932*(T+TSEP))
C       THRUST = 58.051 * e **(-0.010880*(T+TSEP))
      THRUST = 107.97 * e **(-0.013271*(T+TSEP))
C       THRUST = 79.449 * e **(-0.015189*(T+TSEP))
C       THRUST = 84.868 * e **(-0.014135*(T+TSEP))
      THRUST = THRUST * TMULT
      DATA(26) = THRUST

C MOMENTS APPLIED TO THE STAR 48 IN BODY FIXED COORDINATES

      MOMX48 = 0.0
      MOMY48 = 0.0
      MOMZ48 = D * THRUST * SIN(GAMMA)

C MOMENTS APPLIED TO THE FREEFLYER IN BODY FIXED COORDINATES

      MOMXFF = 0.0
      MOMYFF = 0.0
      MOMZFF = 0.0
```

```
      DW(1) = (IYY48 - IZZ48) /IXX48 * W(2) * W(3) + (MOMX48/IXX48)
      DW(2) = (IZZ48 - IXX48) /IYY48 * W(3) * W(1) + (MOMY48/IYY48)
      DW(3) = (IXX48 - IYY48) /IZZ48 * W(1) * W(2) + (MOMZ48/IZZ48)
      DW(4) = (IYYFF - IZZFF) /IXXFF * W(5) * W(6) + (MOMXFF/IXXFF)
      DW(5) = (IZZFF - IXXFF) /IYYFF * W(6) * W(4) + (MOMYFF/IYYFF)
      DW(6) = (IXXFF - IYYFF) /IZZFF * W(4) * W(5) + (MOMZFF/IZZFF)

      RETURN
      END

     SUBROUTINE VELOC (VEL,W,DATA,DVEL)
     REAL*8 VEL(1:100),W(1:100),DATA(1:100),DVEL(1:100),GAMMA,
    C      THRUST,MASS48,MASSFF,SEPDIS,CRASH,STROKE,SMULT,FORCE48X,
    C      FORCE48Y,FORCE48Z,FORCEFFX,FORCEFFY,FORCEFFZ,NUMSPR,KS,
    C      FCONN48,FCONNFF,FSPR48,FSPRFF,FTHR48X,FTHR48Y,FTHR48Z,
    C      FTHRFFX,FTHRFFY,FTHRFFZ

C EXPAND DATA DECK INTO READABLE TERMS
      MASS48 = DATA(7)
      MASSFF = DATA(8)
      GAMMA = DATA(9)
      THRUST = DATA(26)
      SEPDIS = DATA(27)
      CRASH = DATA(28)
      STROKE = DATA(15)
      SMULT = DATA(12)
      NUMSPR = DATA(13)
      KS = DATA(14)
      CONDIS = DATA(29)


C CALCULATE THE FORCES ON THE STAR48

      IF (SEPDIS .GT. STROKE) THEN
        CRASH = 1
        DATA(28) = CRASH
      ENDIF

C DETERMINE THE THRUST FORCE

      FTHR48X = THRUST * COS(GAMMA)
      FTHR48Y = -THRUST * SIN(GAMMA)
      FTHR48Z = 0.0

      FTHRFFX = 0.0
      FTHRFFY = 0.0
      FTHRFFZ = 0.0
```

```
C DETERMINE CONNECTOR FORCE

      IF (SEPDIS .LE. CONDIS) THEN
        FCONN48 = DATA(16)
        FCONNFF = DATA(17)
      ENDIF
      IF (SEPDIS .GT. CONDIS .OR. CRASH .EQ. 1) THEN
        FCONN48 = 0.0
        FCONNFF = 0.0
      ENDIF

      DATA(16) = FCONN48
      DATA(17) = FCONNFF

C DETERMINE SPRING FORCE

      IF (SEPDIS .LT. STROKE) THEN
        FSPR48 = -(SMULT*NUMSPR*KS*(STROKE - SEPDIS))
        FSPRFF = -FSPR48
      ENDIF
      IF (SEPDIS .GE. STROKE .OR. CRASH .EQ. 1) THEN
        FSPR48 = 0.0
        FSPRFF = 0.0
      ENDIF

      DATA(30) = FSPR48
      DATA(31) = FSPRFF

C COLLECT FORCING TERMS
      FORCE48X = FTHR48X + FCONN48 + FSPR48
      FORCE48Y = FTHR48Y
      FORCE48Z = FTHR48Z

      FORCEFFX = FTHRFFX + FCONNFF + FSPRFF
      FORCEFFY = FTHRFFY
      FORCEFFZ = FTHRFFZ

C TRANSLATIONAL EQUATIONS OF MOTION

      DVEL(1) = FORCE48X /MASS48+ VEL(2)*W(3) - VEL(3)*W(2)
      DVEL(2) = FORCE48Y /MASS48+ VEL(3)*W(1) - VEL(1)*W(3)
      DVEL(3) = FORCE48Z /MASS48+ VEL(1)*W(2) - VEL(2)*W(1)

      DVEL(4) = FORCEFFX /MASSFF+ VEL(5)*W(6) - VEL(6)*W(5)
      DVEL(5) = FORCEFFY /MASSFF+ VEL(6)*W(4) - VEL(4)*W(6)
      DVEL(6) = FORCEFFZ /MASSFF+ VEL(4)*W(5) - VEL(5)*W(4)

      RETURN
      END
```

```
      SUBROUTINE ANGLE (ANG,W,DANG)
       REAL*8 ANG(1:100),W(1:100),DANG(1:100)

C EVALUATE THE EULER ANGLES

       DANG(1) = W(1)*COS(ANG(3)) - W(2)*SIN(ANG(3))
       DANG(2) = (W(1)*SIN(ANG(3)) + W(2)*COS(ANG(3))) / SIN(ANG(1))
       DANG(3) = W(3) -(W(1)*SIN(ANG(3)) + W(2)*COS(ANG(3)))
     C                          *(COS(ANG(1))/SIN(ANG(1)))


       DANG(4) = W(4)*COS(ANG(6)) - W(5)*SIN(ANG(6))
       DANG(5) = (W(4)*SIN(ANG(6)) + W(5)*COS(ANG(6))) / SIN(ANG(4))
       DANG(6) = W(6) -(W(4)*SIN(ANG(6)) + W(5)*COS(ANG(6)))
     C                          *(COS(ANG(4))/SIN(ANG(4)))

       RETURN
       END

      SUBROUTINE TRANS1 (VEL,ANG,VELIN)
       REAL*8 VEL(1:100),ANG(1:100),VELIN(1:100)

C TRANSFORM THE BODY FIXED VELOCITY VECTOR INTO THE INERTIAL
C COORDINATE SYSTEM

       VELIN(1) = VEL(1) * (COS(ANG(3))*COS(ANG(2)) - COS(ANG(1))*
     C                          SIN(ANG(3))*SIN(ANG(2)))
     C         + VEL(2) * (-SIN(ANG(3))*COS(ANG(2)) - COS(ANG(1))*
     C                          COS(ANG(3))*SIN(ANG(2)))
     C         + VEL(3) * (SIN(ANG(1))*SIN(ANG(2)))
       VELIN(2) = VEL(1) * (COS(ANG(3))*SIN(ANG(2)) + COS(ANG(1))*
     C                          SIN(ANG(3))*COS(ANG(2)))
     C         + VEL(2) * (-SIN(ANG(3))*SIN(ANG(2)) + COS(ANG(1))*
     C                          COS(ANG(3))*COS(ANG(2)))
     C         + VEL(3) * (-SIN(ANG(1))*COS(ANG(2)))
       VELIN(3) = VEL(1) * (SIN(ANG(1))*SIN(ANG(3)))
     C         + VEL(2) * (SIN(ANG(1))*COS(ANG(3)))
     C         + VEL(3) * (COS(ANG(1)))


       VELIN(4) = VEL(4) * (COS(ANG(6))*COS(ANG(5)) - COS(ANG(4))*
     C                          SIN(ANG(6))*SIN(ANG(5)))
     C         + VEL(5) * (-SIN(ANG(6))*COS(ANG(5)) - COS(ANG(4))*
     C                          COS(ANG(6))*SIN(ANG(5)))
     C         + VEL(6) * (SIN(ANG(4))*SIN(ANG(5)))
       VELIN(5) = VEL(4) * (COS(ANG(6))*SIN(ANG(5)) + COS(ANG(4))*
     C                          SIN(ANG(6))*COS(ANG(5)))
     C         + VEL(5) * (-SIN(ANG(6))*SIN(ANG(5)) + COS(ANG(4))*
     C                          COS(ANG(6))*COS(ANG(5)))
     C         + VEL(6) * (-SIN(ANG(4))*COS(ANG(5)))
```

```
      VELIN(6) = VEL(4) * (SIN(ANG(4))*SIN(ANG(6)))
     C         + VEL(5) * (SIN(ANG(4))*COS(ANG(6)))
     C         + VEL(6) * (COS(ANG(4)))

      RETURN
      END

      SUBROUTINE TRANS2 (W,ANG,WIN)
      REAL*8 W(1:100),ANG(1:100),WIN(1:100)

C TRANSFORM THE BODY FIXED ANGLULAR VELOCITY VECTOR INTO THE INERTIAL
C COORDINATE SYSTEM

      WIN(1) = W(1) * (COS(ANG(3))*COS(ANG(2)) - COS(ANG(1))*
     C                           SIN(ANG(3))*SIN(ANG(2)))
     C         + W(2) * (-SIN(ANG(3))*COS(ANG(2)) - COS(ANG(1))*
     C                           COS(ANG(3))*SIN(ANG(2)))
     C         + W(3) * (SIN(ANG(1))*SIN(ANG(2)))
      WIN(2) = W(1) * (COS(ANG(3))*SIN(ANG(2)) + COS(ANG(1))*
     C                           SIN(ANG(3))*COS(ANG(2)))
     C         + W(2) * (-SIN(ANG(3))*SIN(ANG(2)) + COS(ANG(1))*
     C                           COS(ANG(3))*COS(ANG(2)))
     C         + W(3) * (-SIN(ANG(1))*COS(ANG(2)))
      WIN(3) = W(1) * (SIN(ANG(1))*SIN(ANG(3)))
     C         + W(2) * (SIN(ANG(1))*COS(ANG(3)))
     C         + W(3) * (COS(ANG(1)))

      WIN(4) = W(4) * (COS(ANG(6))*COS(ANG(5)) - COS(ANG(4))*
     C                           SIN(ANG(6))*SIN(ANG(5)))
     C         + W(5) * (-SIN(ANG(6))*COS(ANG(5)) - COS(ANG(4))*
     C                           COS(ANG(6))*SIN(ANG(5)))
     C         + W(6) * (SIN(ANG(4))*SIN(ANG(5)))
      WIN(5) = W(4) * (COS(ANG(6))*SIN(ANG(5)) + COS(ANG(4))*
     C                           SIN(ANG(6))*COS(ANG(5)))
     C         + W(5) * (-SIN(ANG(6))*SIN(ANG(5)) + COS(ANG(4))*
     C                           COS(ANG(6))*COS(ANG(5)))
     C         + W(6) * (-SIN(ANG(4))*COS(ANG(5)))
      WIN(6) = W(4) * (SIN(ANG(4))*SIN(ANG(6)))
     C         + W(5) * (SIN(ANG(4))*COS(ANG(6)))
     C         + W(6) * (COS(ANG(4)))

      RETURN
      END
```

Vita

Kevin Micheal Fuller was born in Hamilton, New York on April 20, 1968. He spent his entire high school years in Hamilton and graduated from Hamilton Central High School in June, 1986. That following September he attended The State University of New York at Geneseo where he pursued a 3/2 Engineering Program offered to qualified students. In 1989, he transferred to Syracuse University and in May, 1991 he received the degree of Bachelor of Science in Aerospace Engineering from Syracuse University. Upon completion of this engineering curriculum, The State University of New York at Geneseo also presented him with the degree of Bachelor of Arts in Physics in 1991.

After teaching young adults for a year at Space Camp in Huntsville, Alabama, Mr. Fuller returned to School at the University of Tennessee Space Institute in Tullahoma, Tennessee. In May, 1994, he received his Master of Science degree in Aerospace Engineering from the University of Tennessee. He is currently employed at the Center for Space Transportation and Applied Research (CSTAR) in Tullahoma, and he plans to obtain a position in Aerospace Engineering in the commercial market place in the near future.